Faculdade de Engenharia da Universidade do Porto

U. PORTO

FEUP **FACULDADE DE ENGENHARIA**
UNIVERSIDADE DO PORTO

Design of an optimal controller with load compensation for transport in an industrial extrusion line

Bruno Filipe Ferreira Brito

Dissertation prepared under the
Master in Electrical and Computers Engineering
Major Automation

Supervisor: Prof. Dr. Adriano Silva Carvalho
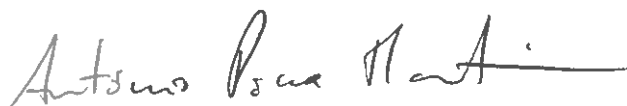Co-supervisor: Eng.º José Pedro Silva

September 2013

A Dissertação intitulada

"Design of an Optimal Controller With Load Compensation for Transport in a Industrial Extrusion Line"

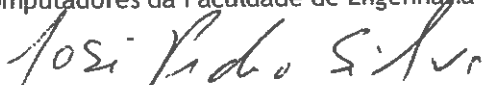foi aprovada em provas realizadas em 10-10-2013

o júri

Presidente Professor Doutor António José de Pina Martins
Professor Auxiliar do Departamento de Engenharia Eletrotécnica e de Computadores
da Faculdade de Engenharia da Universidade do Porto

Professora Doutora Maria Teresa Duarte Barroca Delgado Outeiro
Professora Adjunta do Departamento de Engenharia Eletrotécnica Industrial do
Instituto Politécnico de Coimbra - Instituto Superior de Engenharia

Professor Doutor Adriano da Silva Carvalho
Professor Associado do Departamento de Engenharia Eletrotécnica e de
Computadores da Faculdade de Engenharia da Universidade do Porto

Engenheiro José Pedro Silva
Engenheiro da Continental Mabor

O autor declara que a presente dissertação (ou relatório de projeto) é da sua exclusiva autoria e foi escrita sem qualquer apoio externo não explicitamente autorizado. Os resultados, ideias, parágrafos, ou outros extratos tomados de ou inspirados em trabalhos de outros autores, e demais referências bibliográficas usadas, são corretamente citados.

Autor - Bruno Filipe Ferreira de Brito

Faculdade de Engenharia da Universidade do Porto

"A brother may not be a friend but a friend will always be a brother"
Benjamin Franklin

Resumo

Nos dias que correm, a competição ao nível industrial assume um carácter mundial, centrando-se na conquista de novos mercados. Este clima de competição é visível inclusivamente entre as filiais da mesma companhia uma vez que todas querem produzir mais, melhor e com menor custo. Investindo, para isso, no desenvolvimento do produto e nas suas linhas produção. Portanto, uma linha de produção é como um processo em constante mudança e evolução tecnológica, no sentido da automatização do processo, de garantir a qualidade do produto e obter o menor custo de produção. Este necessita ainda de se adaptar aos requisitos do produto.

Apesar de todas as máquinas na Continental Mabor trabalharem acima da velocidade máxima indicada pelos fabricantes ainda existem sistemas rudimentares e que começam a apresentar bastante imprecisão para as velocidades elevadas de trabalho.

Deste modo, esta dissertação inicia-se com o estudo do processo e de todos os componentes do sistema, de forma a se poderem conhecer os factores limitadores da produção existentes.

Após isto é desenvolvido um modelo matemático da linha, sendo posteriormente validado com dados retirados do processo. Este modelo é usado tanto para identificar os factores limitantes da linha assim como também para poder estimar sua a capacidade de produção e, como outros estudos que poderão ser feitos a partir do mesmo. Este modelo tem como objectivo final avaliar se o novo sistema de transporte desenvolvido também nesta dissertação é realmente capaz de aumentar a capacidade de produção actual.

O motivo pelo qual é desenvolvido um novo sistema para o controlo do motor de transporte na máquina de corte é o facto de esta ser actualmente o bottleneck da linha de produção.

É assim desenvolvido um controlo inovador que permite controlar o binário, a velocidade e a posição do motor. Este apresenta também compensação de carga no controlo de velocidade através de um EKF que permite estimar a carga aplicada ao motor e é também usado para que o motor se mantenha estável na posição final. Além de tudo isto é desenvolvido um algoritmo que permite um transporte óptimo e adaptável às condições físicas, podendo-se limitar a aceleração e desaceleração de modo a evitar o deslize do material mas garantindo da mesma forma um transporte óptimo para as condições em que não ocorre deslizamento. Por outro lado garante também elevada precisão devido ao uso de um controlador linear que minimiza uma função de custo que tem em conta o quadrado do erro de posição e da utilização de uma estrutura modificada de um controlador de binário

baseada de modo a obter-se uma menor ondulação do binário do motor para elevados tempos de ciclo de processamento.

Este ganho de precisão e velocidade podem representar uma enorme vantagem para uma empresa que é capaz de produzir actualmente 55000 pneus diários, permitindo aumentar a sua capacidade de produção de pisos para pneus mudando apenas o método de controlo.

Abstract

Nowadays, the competition at the industrial level takes on a global nature, focusing on new markets. This climate of competition is visible even between branches of the same company, as they all want to produce more, better and at lower cost, which is something that needs investment both in product development and production lines. This highly active area of work requires for the production line to be in a process of constant change and technological evolution towards automation of the process, to ensure product quality and achieve the lowest production cost, going hand in hand with the requirements of the product.

Although all machines in Continental Mabor work above the maximum speed indicated by the manufacturers, there are still sub-optimal systems because these high velocities often amount to a significant process inaccuracy.

Thus, this paper begins with the study of the process and all components of the system to be able to meet with the existing production limiting factors.

The next stage is to develop a mathematical model of the line, and subsequently validate it comparing information from software algorithm simulation with data from the process. This model is used to identify the factors limiting the line as well as to be able to estimate its production capacity, and, other studies which may be created from this robust simulation tool. The model aims to evaluate if the new transport system, also developed in this dissertation, is actually able to increase the current production capacity.

The reason to have been developed a new system to control the motor for the material transport in the cutting machine is the fact that this is currently the bottleneck of the production line.

Allowing for more innovative control to be implemented, which handles specifically with: the torque, speed and position of the motor. Also providing load compensation in the speed control via an Extended Kalman Filter that estimates the load applied to the engine, and is also used for the engine to guarantee that it remains stable.

Another benefit of this algorithm is that it allows an adaptive transportation and optimal physical conditions, being able to limit the acceleration and deceleration, preventing slippage of the material but ensuring optimal transportation for the present conditions. Moreover ensuring high precision due to the use of a linear controller, that minimizes a cost function which takes into account the square of the position error and the use of a modified structure of a torque controller, so as to obtain low torque ripple for high cycle processing times.

This gain in accuracy and speed can be a huge advantage for a company that is currently capable of producing 55,000 tires daily, allowing to increase its production capacity of tire floors with the simple change of the control method.

Acknowledgments

To my teacher and supervisor Adriano Carvalho for all the advices, reliability and responsiveness, but mainly for all the insightful conversations which made me take a step forward;

To my co-supervisor Eng. José Pedro Silva that was always available to help and for believing in my work which made me grow in the enterprise;

To my teammates of Continental Mabor S.A. for all the help and fellowship provided especially to Eng. Joaquim Ascenção for all the motivation and encouragement;

To my father who is a role-model, to my mother and my sisters for all the unconditional help and for supporting my studies;

Those friends who were at my side during the implementation and writing process whose insight was very helpful, especially to Manuel Sampaio;

To family Sá, To Tiago Sá for all the shared knowledge and talks that triggered in me the interest in motor control and to André Sá to make me appreciate the simple things in life;

To all my friends in particular Vitor Domingos that always makes me laugh and Luciano Sousa never got tired of listening to me;

To Murad Gurbanov, to Simone Fischi and Massimiliano Rosetti that shared with me one of the best moments in my life;

To my friend Tiago Caetano, who always gave me a hand to get up and not let me give up when I wanted;

Finally to FEUP and Continental Mabor S.A. for providing me the opportunity of carrying out this dissertation in business environment with such good conditions.

Contents

List of Figures

List of Tables

Abbreviations and Symbols

Abbreviations (alphabetical order)

AC	Alternating Current
ADC	Analog-to-Digital Converter
CAN	Campus Area Network
CMSIS	Cortex Microcontroller Software Interface Standard
DAC	Digital-to-Analog Converter
DC	Direct Current
DSD	Delta Sigma Demodulator
DSP	Digital Signal Processor
DTC	Direct Torque Control
EKF	Extended Kalman Filter
FEUP	Faculty of Engineering of the University of Porto
FFT	Fast Fourier Transform
FOC	Field Oriented Control
FPGA	Field Programmable Gate Array
HMI	Human Machine Interface
IGBT	Insulated Gate Bipolar Transistor
LQR	Linear Quadratic Regulator
LSB	Least Significant Bit
MCU	Micro Controller Unit
MIMO	Multiple Input Multiple Output
MIMO	Multiple Input Multiple Output
MISO	Multiple Input Single Output
MPC	Model Predictive Control
MSc	Master of Science
PFC	Power Factor Correction
PI	Proportional Integrative
PID	Proportional Integrative Derivative
PM	Permanent Magnet

PWM	Pulse Width Modulation
RMS	Root Mean Square
RPM	Rotation Per Minute
S.A.	Sociedade Anónima
SPWM	Sinusoidal Pulse Width Modulation
SVM	Space Vector Modulation
TCU	Temperature Control Unit
TDM	Time Division Multiplexing
TUE	Total Unadjusted Error

Symbols List

T	Tension on the material
H	Horizontal tension on the material
d	Derivative operator
w	Linear Density
l	Half-length of the chain
s	Laplace transform
$L(k)$	Tread Length at instant k
V_{input}	Input speed
V_{output}	Output speed
Δt	Time step
k_{relax}	Relax Constant
$k_{cooling}$	Cooling Constant
L_{zone}	Length of the Zone
V_{line}	Line Speed
T_{Cut}	Cut Time
$L_{Take\_Off\_Roll}$	Take-Off-Roll zone length
$L(k)_{Take\_Off\_Roll}$	Length of the material inside the Take-Off-Roll zone at instant k
$V_{Shrinkage}$	Shrinkage zone speed
$L_{Shrinkage}$	Shrinkage zone length
$L(k)_{Shrinkage}$	Length of the material inside the Shrinkage zone at instant k
$L_{Incline}$	Incline zone length
$L(k)_{Incline}$	Length of the material inside the Incline zone at instant k
$V_{incline}$	Incline zone speed
$L(k)_{Cooling1}$	Length of the material inside the Cooling zone 1 at instant k
$L_{Cooling1}$	Cooling zone 1 length
$V_{Cooling}$	Cooling zone speed
$L(k)_{Cooling1}$	Length of the material inside the Cooling zone 1 at instant k
$L(k)_{Cooling2}$	Length of the material inside the Cooling zone 2 at instant k

$L_{Cooling2}$	Cooling zone 2 length
$L(k)_{Cooling3}$	Length of the material inside the Cooling zone 3 at instant k
$L_{Cooling3}$	Cooling zone 3 length
$L(k)_{Decline}$	Length of the material inside the decline zone at instant k
$L_{Decline}$	Decline zone length
$V_{Decline}$	Decline zone speed
$L(k)_{Loop}$	Length of the material inside the loop zone at instant k
L_{Loop}	Loop zone length
$V_{Transport}$	Transport conveyor speed
h	Minimum distance of the catenary to the floor
ω_e	Rotor Electric Angular Speed
ω_r	Rotor angular speed
p	Number of Poles
i_u, i_v and i_w	u, v and w phase currents
i_α	α-axis current component
i_β	β-axis current component
θ_e	Rotor Electric Position
V_s	Stator Voltage
V_d	Direct-axis stator voltage
V_q	Quadrature-axis stator voltage
r_s	Stator phase resistance
I_s	Stator current vector
λ_s	Air-gap flux vector
λ_q	Quadrature-axis flux component
λ_d	Direct-axis flux component
λ_{pm}	Permanent magnet flux
L_d	Direct-axis inductance
L_q	Quadrature-axis inductance
T_e	Electromagnetic torque
J	Moment of Inertia
B	Friction coefficient
T_L	Load torque
$V_{control}$	Amplitude of the control signal
V_{tri}	Amplitude of the triangular wave
m_a	Amplitude modulation index
m_f	Frequency modulation index
$f_{control}$	Frequency of the control signal
V_{DC}	Bus-DC voltage
T_s	Sample time

$\Delta\delta$	Torque angle increment
J	Cost function
P	Solution of the Ricatti equation
w_k	Process noise
v_k	Observation noise
Q_k	Process noise covariance matrix
R_k	Observation noise covariance matrix
S_k	Innovation covariance matrix
K_k	Kalman gain
H	Observation matrix
ω_0	Initial rotor speed
θ_0	Initial rotor position
T_{brake}	Torque brake
f_s	Carrier signal frequency
$\alpha - \beta$	Fixed reference frame
d-q	Rotating reference frame
$V_{a,b,c}$	a,b,c phase voltage
V_{ref}	Voltage vector reference
$\theta_{\alpha-\beta}$	Voltage angle in $\alpha - \beta$ reference frame
γ_s	Stator flux position
δ	Torque angle
λ_{s_ref}	Reference flux stator amplitude
γ_{s_ref}	Control angle
V_{α_ref}	α-axis voltage reference
V_{β_ref}	β-axis voltage reference
x_k	State vector
u_k	Input vector
z_k	Observation vector
$f(x_{k-1}, u_{k-1})$	State estimation function
$h(x_k)$	Measurement estimation function
F_k	Jacobian process matrix
H_k	Jacobian observation matrix
$P_{k|k-1}$	Estimated process covariance matrix
$P_{k|k}$	Corrected process covariance matrix
y_k	Observation error
$x_{k|k-1}$	Predicted/Estimated state vector
$x_{k|k}$	Corrected state vector
A_{x_k}	Estimation state matrix
I	Identity matrix

A	State matrix
B	Input matrix
K	LQR gain
Q	Process cost matrix
R	Output cost matrix
C	Output matrix
D	Feedforward matrix
d	Input disturbance
v	Output disturbance
t_{stop}	Stop time
RPM_{200}	Rotation speed of the simple extruder of 200mm of diameter in rpm
RPM_{150}	Rotation speed of the simple extruder of 150mm of diameter in rpm
RPM_{90}	Rotation speed of the simple extruder of 90mm of diameter in rpm
$P_{average}$	Average perimeter
$d_{average}$	Average diameter
d_{screw}	Screw diameter
$d_{interior}$	Interior screw diameter
$A_{n\_section}$	Area of the normal section
$d_{interior\_lead}$	Interior distance of the lead
d_{out_lead}	Outside distance of the lead
$h_{n\_section}$	Height of the normal section
V_{lead}	Volume of the lead
A_{die}	Area of the die

Chapter 1

Introduction

1.1. The Project

This Dissertation is related to the internship in Continental Mabor within the ContiMaster prize, offered to the best student that finish the 4th year of the Master in Chemical, Industrial, Mechanics and Electronic Engineering, being developed in the Faculty of Engineering of the University of Porto (FEUP), within the MSc in Electrical and Computer Engineering providing the opportunity to develop a final project in the faculty.

The initial propose of the internship was to do the dissertation in the ambit of the project, "Upgrade of the Extrusion Line", which had as principal objectives the knowledge about the extrusion process and systems related to it, a survey of the actual electronic and mechanical components of the line and finally from the comparison of different solutions offered by different enterprises the choice of the new components.

However with the knowledge of the process and the real working conditions, was identified an high variation on the cutting length in the actual cutting system, not only related to the actual mechanical conditions that can be improved, but also the algorithm used to move the tread material to the cut position, leading with material out of tolerance.

In this way was proposed to develop a new drive system, using the position of the material as control variable and not the line speed of production as it is the actual system. The new drive system should be based in the state of art of the motors control, with the application of the most modern control techniques and using a low-cost microcontroller. Despite the technological upgrade project was being developed during the internship and at same time were developed new solutions for other projects, as for example a new programming algorithm for tread detection using Siemens Step 7, they are outside of the ambit of this Dissertation, being all this document about the development of a new algorithm to control the final position of the material in the cutting system.

1.2. Company Presentation

1.2.1. The Company: Continental AG

In October 8 of 1871 Continental-Caoutchouc- und Gutta-Percha Compagnie is founded in Hanover as a joint stock company. Manufacturing at the main factory in Vahrenwalder Street includes soft rubber products, rubberized fabrics, solid tires for carriages and bicycles.

Later in 1892 Continental is the first German company to manufacture pneumatic tires for bicycles and in 1898 has started the production of automobile pneumatic tires without tread pattern starts in Hanover-Vahrenwald.

But the big step was coming and in 1904 Continental presents the world's first automobile tire with a patterned tread.

In 2001, Continental acquired the DaimlerChryler's automotive electronics which is now part of the Continental Automotive systems. Later in 2004 Phoenix AG joined also the group and in 2006 the automotive electronics unit of Motorola in 2006.

In 2007 Continental acquires Siemens VDO Automotive AG and advances to among the top five suppliers in the automotive industry worldwide, at the same time boosting its market position in Europe, North America and Asia. Continental is structured in six divisions:

- *Chassis & Safety*
- *Powertrain*
- *Interior*
- *Passenger car & Light Truck Tires*
- *Commercial Vehicle Tires*
- *ContiTech*

The group is specialist in the production of breaking systems, dynamic vehicle control, power transmission technologies, electronic systems and sensors. Continental has approximately 150 000 collaborators, divided between 36 countries in about 200 different locations.

1.2.2. Continental Mabor

A joint venture is set up together with the Portuguese company Mabor for the production of tires in Lousado in 1989/1990. 1993 sees complete takeover of the tire activities and of a factory producing textile cord.

Mabor stands for "Manufatura Nacional de Borracha" and was the first factory of pneumatics in Portugal. It started its process in 1946 with the assistance of General Tire.

In July of 1999, it started a great restructuration program that transformed all the old installations of Mabor in the one of the most modern 21 units from Continental. Starting from a 5000 tires a day production, it developed to 21 000 in 1996. Currently Continental - Mabor has the capacity of an average of 44 000 tires a day therefore being one of the factories with better productivity index.

Finally in 2012 Mabor receives the Quality Prize of the Continental group, being the first producing tires for the group Porsche.

Initially only producing Mabor brand tires, nowadays, the spectrum of the company is much larger not just in brand but in sizes and types. Almost all of the production is meant for exportation, and more than half of this is absorbed by the substitution market, and the rest is distributed through assembly lines.

Continental - Mabor has a total area of 204 140 square meters and about 1600 collaborators.

1.3. Motivation

Henry Ford, in 1913, was the creator of the first assembly line in series production vehicles [2]. The purpose of creating these lines was to increase production in the shortest time possible and at the lowest cost.

Thus, automated production lines represent a fundamental choice in production systems where high production volumes and constant quality assurance must be guaranteed [1].

Nowadays, the competition is not just between industries, it is also between companies of the same group, being the competition and source for continuous technological changing in order to improve and also arrive to the optimal solutions in the production.

An extrusion line is a complex and extensive system, composed by many different subsystems with many different technologies. So the technological upgrade of one extrusion line represents a big chance to meet old technologies that are present in the industry, such as automata, drives, motors, etc., and also an occasion to know the state of art of the industrial communications, automation and measurements system with high precision in the industrial environment.

Even though that from the comparison of many different solutions offered by many companies, with most recent technology is obtained the best solution, sometimes the best solutions are specially designed for the applications, reflecting advantages that general solutions presented in the market cannot achieve.

Upon analysis of the process comes to the conclusion that only the replacement of the traction system in the transport conveyor for new servo-motors and automata Siemens would just guarantee the same behaviour, obtaining in this way the same performance and precision.

Represents in this way an opportunity to develop a dedicated solution for the transport system in the cutting machine, representing an enormous opportunity to understand and learn new control techniques, power electronics, motor control, microcontrollers programming, etc. and its application in the industrial level.

Not only the domain of all these themes but also represents the chance to create a new product, with high value for the enterprise represented in the increase of the production with high quality and lower waste of the produced material. Furthermore the designed solution can also attract the interest of other companies that belong to the group with the positive results obtained in Mabor.

The proposed project aims to use new modern control methods and its application in the industry with known potential which should increase the speed and precision of the system whose domain will certainly be an asset for future projects.

1.4. Objectives

After few months of formation and work on the extrusion line, was identified a high variance in the cutting-length system, that results in high percentage of material put of tolerance and so high production costs for the enterprise. To solve that this year has started the technological upgrade of the production line, having as main objectives the reduction of the power consumption, the implementation of the PROFINET communication, reduce the cost of the maintenance and to reduce the risks of failure. Despite the technological upgrade plan for the all extrusion line, it only consists for the cutting system in replacement of the obsolete electronic components, keeping the actual cutting algorithm and mechanical structure. Besides the problem with sliding of the material, the current algorithm, which relies upon the line speed where the final position is controlled by a hysteresis controller using the mechanical brake, also adds error to the final cutting position.

In order to achieve higher precision, according with the specified tolerances of the production and also higher speed, was launched the challenge to develop a new control system of the transport conveyor.

Firstly was proposed to develop a model of the extrusion line. It is necessary to know if the actual system is already optimized in terms of the speed production or if is possible to improve it. The results should be compared with the real system to validate the model.

On the other side the developed mathematical representation of the line should be used considering the new drive system, in order to simulate the new algorithm developed and to get valid conclusions about the new control system in the line performance.

At the industrial level the implementation of a new system should always ensure the complete operation of the actual system for the case of failure the new system, so the first requirement is that the controller should be able to control the speed of the traction motor. The acceleration of the motor and deceleration should also be controlled with the objective of avoiding the sliding of the material. Finally it is meant to develop a new algorithm based in the material position being necessary to control the position of the motor.

In order to achieve the main goal of developing a new control for the transport system and the system modelling the main objectives are:

1. Modelling the extrusion line;
2. Validation of the model with the system;
3. Design the drive system using a new the control architecture;
4. Simulation of the model of the production line;
5. Simulation of the model considering the new controller for moving treads;
6. Implementation of the designed control in lab environment;

1.5. Document Structure

This document is divided in 7 chapters. Due to the nature of this project that consists in the development of a new control system which has no academic predefined structure, the presented structure will be different from the canonical form as it follows the steps that were taken during the development in order to better understand its final design and components. Each contains several subsections according to the subjects mentioned.

Chapter 2 introduces and shows an overview of extrusion process and the line components as form of framework.

Chapter 3 presents a mathematical model of the extrusion system and its validation with the real system.

Chapter 4 refers to the motor modelling, modulation methods and the fundamental component of the control system, the torque controller.

Chapter 5 revolves the position and speed controller and the development of a new optimal control scheme.

Chapter 6 reports the implementation of the controller, a modified scheme of the torque controller and finally the system validation and final simulation.

Chapter 7 presents an overview of the project; final conclusions are made as some suggestions about future possible developments.

Table 1.1 Document Structure

Chapter	Title
1	Introduction
2	System Overview
3	System Modelling
4	Motor Control
5	Control of the transport conveyor
6	System Validation and Implementation
7	Conclusions

Chapter 2

System Overview

In this chapter it is intended to summarize the processes and the components inherent to a production line fully automated, which make part of the extrusion process. A generic way without going into technical details at the process level because is not part of the framework of this dissertation. Each component of the line will be discussed in more detail later, so here it is just referred its main role in the process.

2.1. Basic Concepts

The extrusion is a fabrication technique, included in the forming operations. It consists in the moulding of a viscous thermoplastic under pressure through a die. Mechanical screws pressure the melted rubber and form a continuous charge of viscous fluid. The solidification of the extruded material is achieved by blowers, water spray or diving the material under the water. This technique is mainly used for producing continuous lengths of material with constant cross-sectional [1]. In this case the cross-section is defined by the die, as it is possible to observe in the next figure.
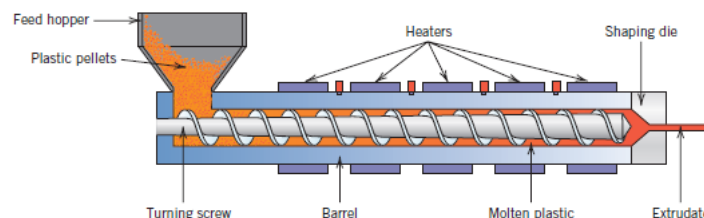
Figure 1 Basic Model of an Extruder

The die basically consists in the shape of the orifice, that the rubber will be forced to pass through, containing the profile of the tread.

There are three types of the extrusion line in the tire production, sidewall, tread and in some cases, a kind of combined line, since that is able for the production of both tread and sidewall. It also can be characterized as duplex, triplex or quadruplex line, depending on the number of extruders. It is also important to refer, that each extruder can have different diameter, according with surface area of the orifice, the die. The treads for tires have different structures, being composed mainly of a base, cover and one or two wings, being represented in figure 2.
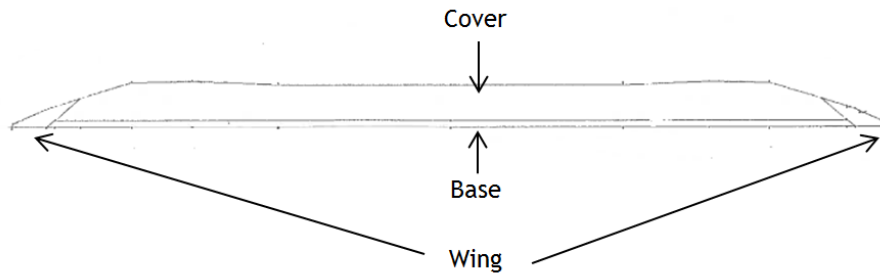
Figure 2 Structure elements of the tread

As it is referred in this case the extruders are composed with more than one simple extruder, after the material passes through the die it is forced, on the extruder head, to pass through another die, that give the desired profile to the material, joining the material of each extruder.

For each type of tire, there is a different receipt and in every receipt is defined all the variables of the process, as the temperature of every component of the extruder, the speed of the motor that will pressure the rubber, the pressure for each extruder, etc.

2.2. Description of the production process

The E03 extrusion line that will be the main topic of this dissertation is a triplex extrusion line. So it is composed for a 90mm, 150mm and 200mm extruder. It is also a combined line because it is prepared to produce treads and side-wall, although it is mainly used for tread production.
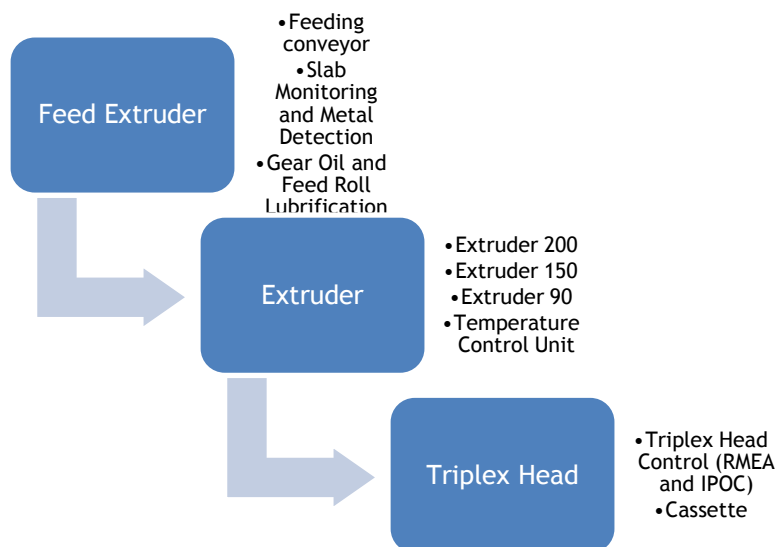
Figure 3 Extruder Composition

The process begins with the compound feeding of the extruder process. Each feeder is composed principally by a feeding conveyor and a metal detector. The rubber can contain metal pieces, which represents a high hazard to the extruder. It can damage seriously the screw, that would represent the stop of the line for a long time and so a high cost to the enterprise.

Specifically for the E03 extrusion line the produced treads for tires are composed of a wing, a base and cover, existing one extruder for each component. That is why in the case of the E03 extrusion line there is a triplex extruder.

Each part of the extruder must have a temperature defined by the receipt which is guaranteed by Temperature Control Unit (TCU).

In the triplex head the screw pushes the material to pass through the die, getting the desired profile. It is important to refer, that the screw speed is controlled by RMEA. It basically consists in a fuzzy logic system that according to the weight per length and width defined in recipe it accelerates or decelerates the screw. Beyond to control the rotation speed of each extruder, it also controls the line speed value, ensuring the continuous flow of the material from the extruders to the line. There is also another control system named IPOC, belonging to the structure of the RMEA and that indicates to the operator when one recipe is finish and he can start with the production of the next recipe. The main function of this program is to avoid the mixture of different compounds inside the extruder for different recipes.
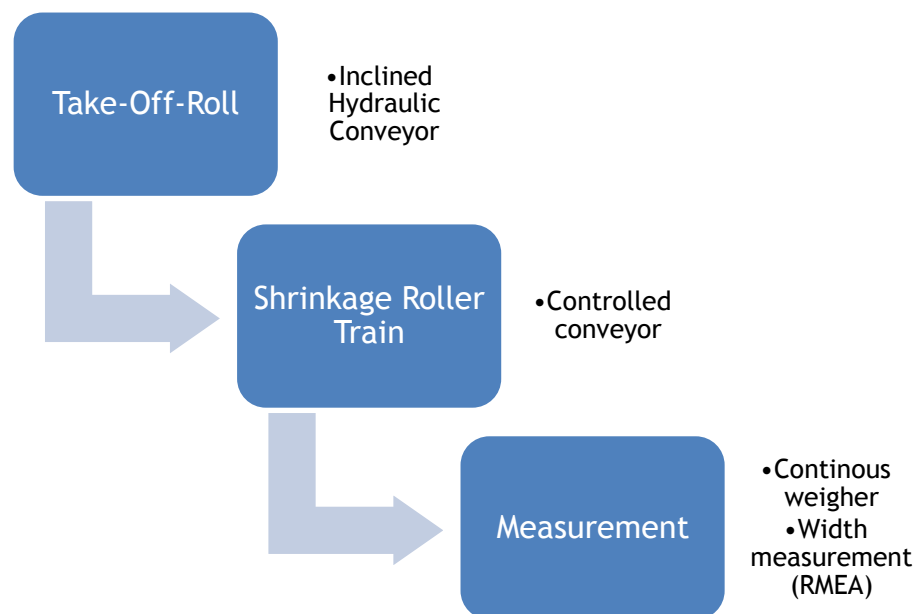
Figure 4 First three main components of the line after the extrusion

The material flows continuously from the triplex head and is retracted by the take-off-roll, starting its long path along the process. It should avoid that the material expands or shrink in next phases, it is necessary to eliminate all the tensions that exist inside the material. That is why after the material is retracted. There is a group of cylinders, rolling with different angular speed to relax and eliminate all tensions inside the material. This is the shrinkage roller train.

The speeds of all the conveyors situated after the take-off-roll are controlled using mechanical dancers. This dancer measure the existing tension on the material between two conveyor, increasing or decreasing the speed of the next conveyor, avoiding the break or the stock of material in some positions of the line.

To control the head of the extruder, and verify the properties, it is necessary to measure online the weight per length and the width. The width is measured resorting from the image processing of the RMEA system and through the weight per length using a continuous balance.

Marking Device
- Group of paints
- Laserjet

Cooling tread
- Inclined Conveyor
- Cooling Conveyor
- Water Tanks
- Blower
- Declined Conveyor

Cutting tread
- Cutting Machine (Spirka)
- Encoder
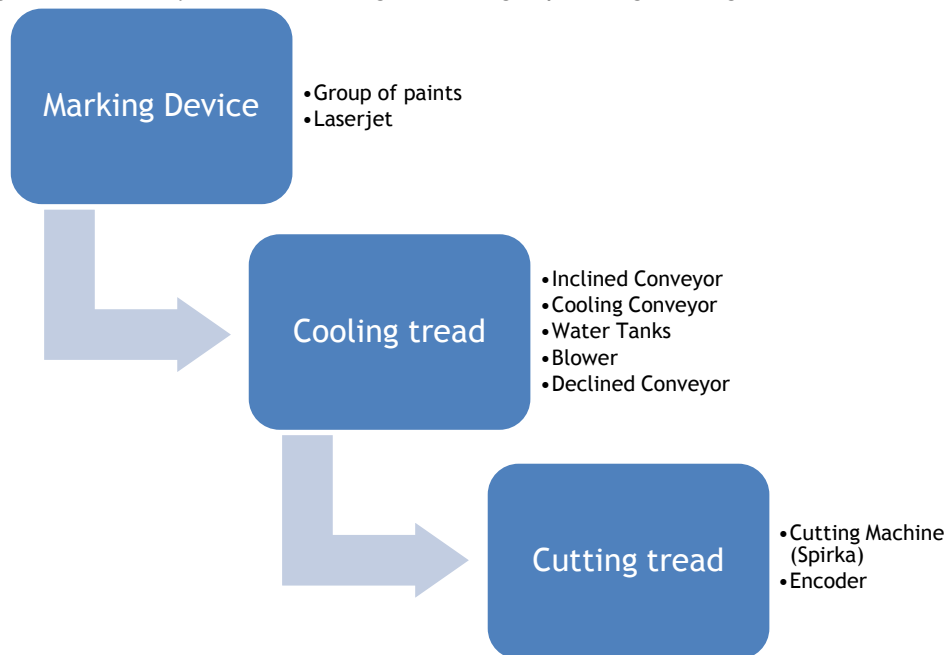
Figure 5 Further components of the line

Consequently, the material needs to be identified with a marking device. The marking process basically consists in a continuous paint of lines with different colours. The number of lines and its colours consists in a code that will identify later the recipe of that material, existing installed one vision system that checks the right colour and position of the stripes, considering the material out of tolerance if the stripes are not correct. There is also a printing device, consisting in a laser jet that prints a reference on the surface of the material as its flowing.

The next step is the solidification of the material. So, the material is moved to the superior level of the extrusion line, where are situated the water tanks. The tread flow is bathed in water, moving underwater during three paths of water tanks. In the end, to remove the water from the material, there are a series of blowers and, after it, the material goes down again to the cutting machine.

The cutting process is composed by the loop and the cutting machine. The cutting machine has a transport conveyor and a transversal motor with the knife for cut. During the cut the material is stopped in the transport conveyor and before that the line continues to produce material. So the loop, situated before the transport conveyor has the function to accumulate material while the tread is cut. After the cut, the transport conveyor has to move more material to the cut position removing material from the loop.
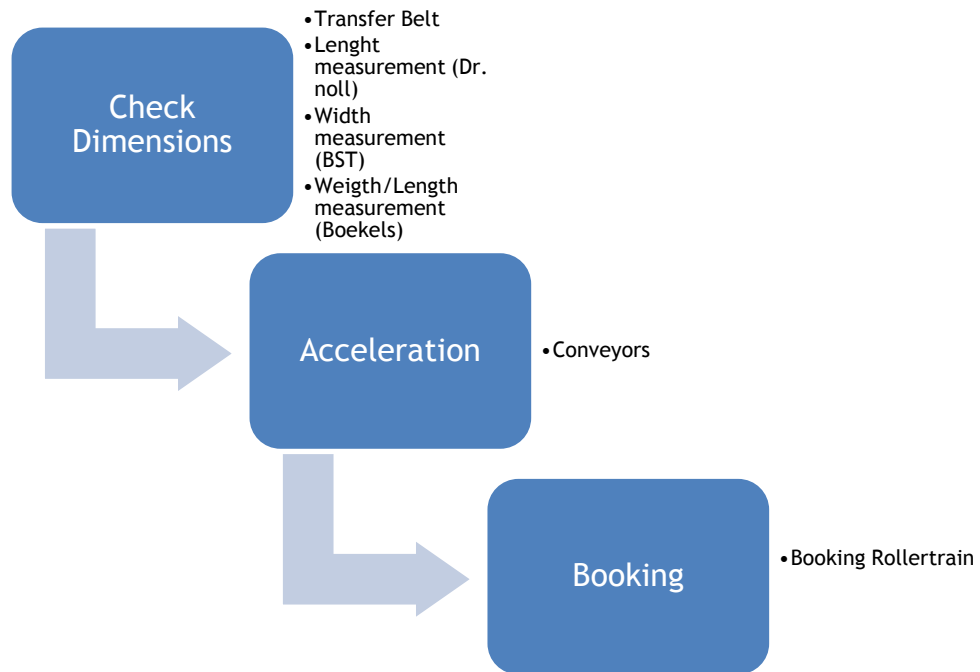
Figure 6 Final divisions of the production line

To conclude, it is important to retain that it must be checked the length, the width and the continuous weight to ensure the material features defined in the recipe. If the measurements are inside the range of the tolerance values, the material is accelerated and retracted by an automatic system, the booking roller train. If is not, the booking does not retract the material and it will follow till be removed by an operator. The material that is not in good condition can still be reutilized and it is still used again in the mixing process.

2.3. System breakdown

A system breakdown is a structuring method based on system and product decompositions, creating a system architecture for better analysis and understanding [2].

Because all the production line represents a very complex and extensive system, to understand all involved components it is presented a system breakdown structure of all this process.

In a first approach, of all system, the whole system can be divided in three principle components:

✓ The mechanical process as the transport, cutting process;
✓ The control of the process;
✓ The power systems.
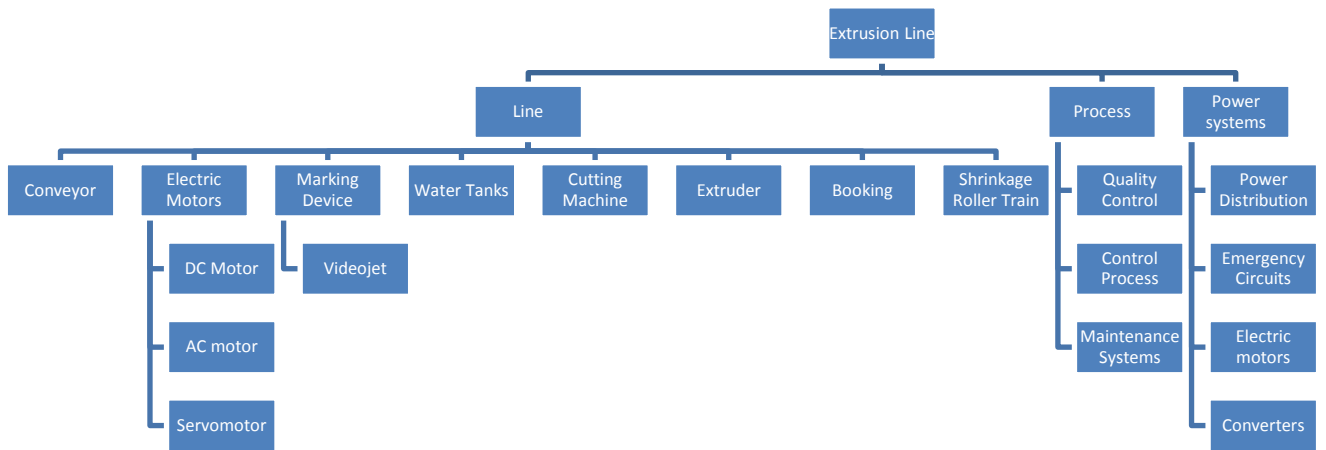
Figure 7 System breakdown of the extrusion line

At the second level and at the control process level, there are since the drivers to the motors, the automatons, the interfaces for the user until the communication system.
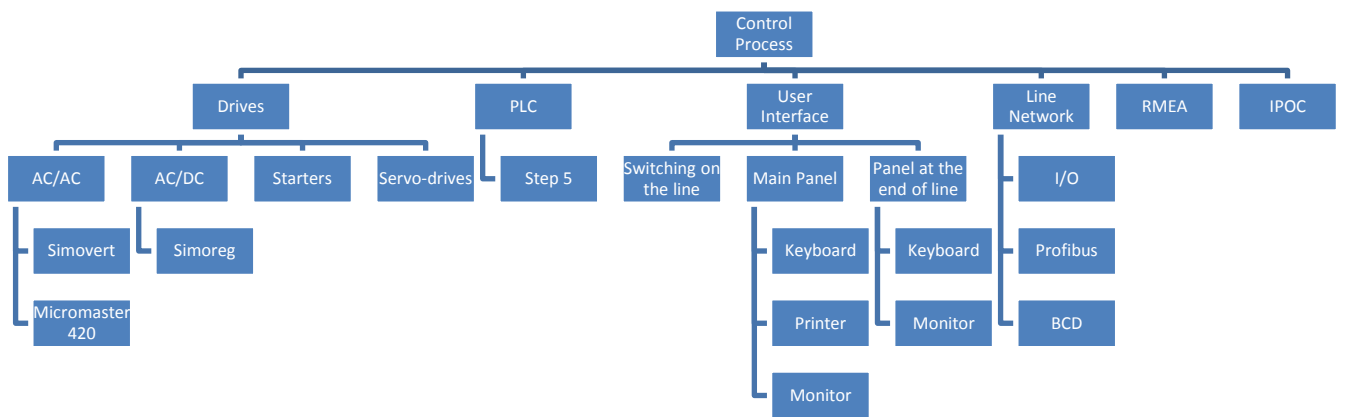
Figure 8 System Breakdown of the control process

In quality guarantee field, there is since the metal detection on the feeder extruder till the measurement system, which checks if all the dimensions and profiles of the product are in agreement with the recipe that is being produced at that moment.
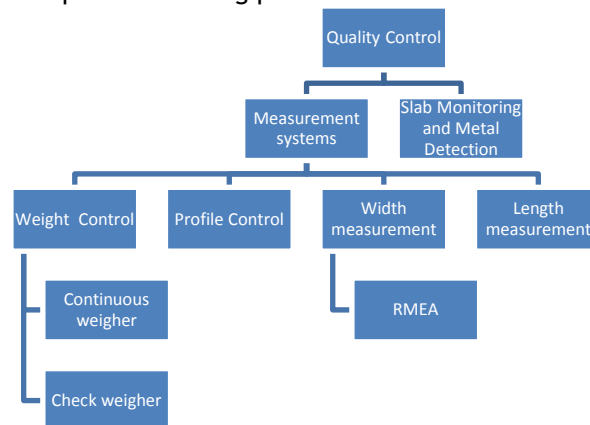
Figure 9 System Breakdown of the quality control

Finally, the maintenance system is responsible for all mechanical lubrication, control temperature, etc. On the other hand there is the power system responsible for all power distribution as represented in the figure 10 and 11.
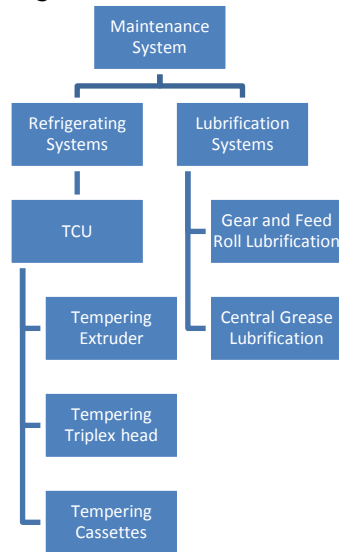
Figure 10 System Breakdown of the maintenance system
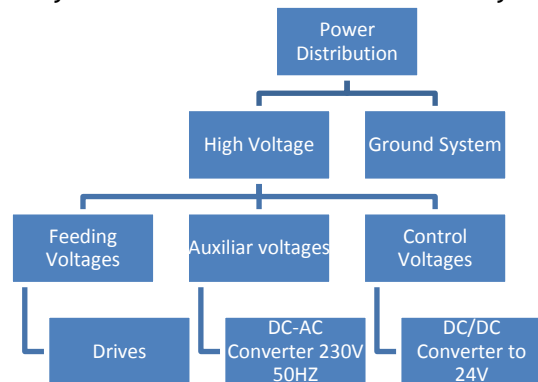
Figure 11 System Breakdown of the power distribution

Chapter 3

System Modelling

3.1. Introduction

In order to analyse the actual performance of extrusion line, to find what is the bottleneck and what should be done to increase the speed production, is developed a mathematical model to simulate the actual state of operation. With a good model will be possible to also evaluate its performance and stability if some change is done in order to increase the speed of the production. So in this chapter each division of the production line will be modelled, being used data obtained from the normal operation of the line to validate the model. In this way can be found a simplified model of the extruder, of the each division of the line and finally of the cut system.

3.2. The catenary equation

The natural curve that a suspended chain supported only at its ends takes in the space is represented by the catenary equation 3.2.5. It was first studied by Robert Hooke in 1670 and this equation was developed by Leibniz, Huygens and Johann Bernoulli in 1691.

Assuming a uniform chain with linear density w in a uniform gravitational field, the weight is about uniformly distributed.
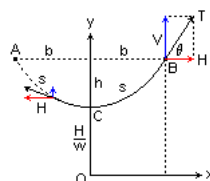
Figure 12 Force diagram in a suspended uniform chain

Where T represents the tension on the material, H the horizontal component of the tension cause by the weight of the material and s the half-length of the chain.

Consider the equilibrium of an infinitesimal length of chain, in a xy reference frame, we have

$$ds^2 = dx^2 + dy^2 \tag{3.2.1}$$

and that,

$$w * ds = H * y'' \tag{3.2.2}$$

From this we get the differential equation for the curve:

$$w * \sqrt{1 + y'^2} = H * y''$$

(3.2.3)

This is a separable first order equation in respect to y'. Integrating in order to y' and defining $a = \frac{H}{w}$ it results

$$y' = \sinh \frac{x}{a}$$

(3.2.4)

Integrating a second time it gives:

$$y = a * \cosh \frac{x}{a}$$

(3.2.5)

This is the catenary curve. In order to the geometrical parameters of the chain we have that

(3.2.6)

$$\frac{ds}{dx} = \sqrt{1 + \frac{dy^2}{dx}} \Leftrightarrow \frac{ds}{dx} = \sqrt{1 + \sinh \frac{x^2}{a}} = \cosh \frac{x}{a}$$

Applying a simple integration in order to x it gives

$$s = a * \sinh \frac{x}{a}$$

(3.2.7)

3.3. The cutting tread system

Before to explain the cutting system it is important to understand what is the Loop and the main rule in the cutting system.

When the material is stopped to begin the cut of the tread, all the flow of material before the cutting system cannot be stopped in order to guarantee a continuous production. So the material was accumulated in the Loop. There is on the Loop an open space between the decline conveyor and the transport conveyor of the cutting system. The material is accumulated here and because it is suspended in the extremes of both conveyors making a catenary curve, as represented in the next picture.
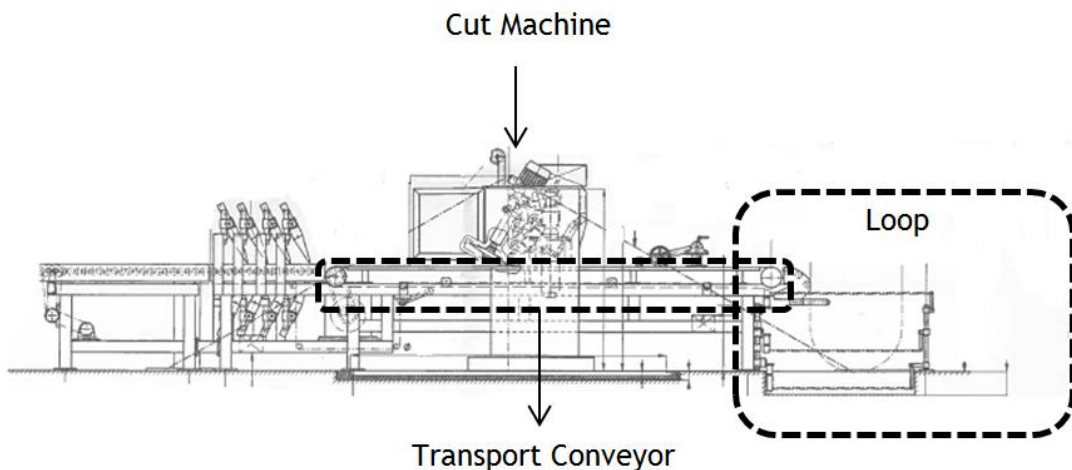
Figure 13 Schematic of the cutting machine

Now it is possible to explain the actual algorithm of the control system. There are two main phases:

1. The transport phase: in this phase the material is moved until the length after the blade is smaller than the desired cut-length;
2. The cut phase: when the transport conveyor is stopped in order to cut the material with a blade. In this phase the material is accumulated in the Loop.

During the transport phase, the transport conveyor has two defined speeds according with the position of the material in the loop.

According with the figure 14, if the material is under the position *h1* there is enough accumulated material on the Loop. So the transport conveyor speed is 1.5 times faster than the speed of the decline conveyor.

If the material is above the position *h1* the transport conveyor speed is the same as the decline conveyor in order to keep on the continuous flow of the material. Otherwise the material would be tensioned and the continuous chain of material would break. If the material passes through the position *h2* the line stops because there is too much material in the Loop and the cut-machine is not faster enough to answer to all this debit of material.
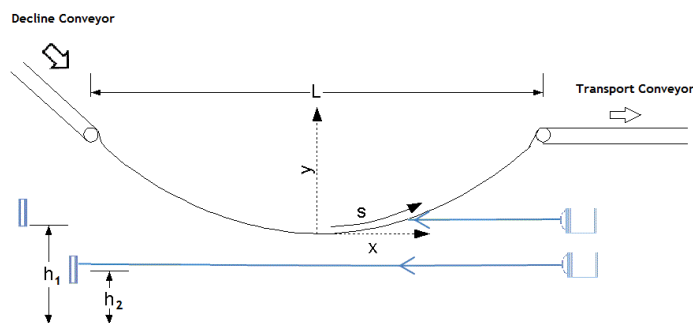
Figure 14 Schematic of the loop

When the length of the material after the blade is near of the desired length value it is applied a mechanical brake to stop the material transport. The instant when the mechanical brake is applied is adjusted according with the average error of the cutting length. If the material is too long the mechanical brake will be applied in advance. Otherwise, if it is too short it will be applied delayed.

3.3.1. Problem Identification

The actual cutting system is the main problem present in all the extrusion lines. There is a big variance present in the cutting length which leads to a high number of rejected treads. So it is necessary to produce a higher total number of treads in order to get the desired number of good treads. This leads to the increase the costs of production and an efficiency reducing.

There are mechanical problems in the cutting machine such as:

✓ Drift of the material during the brake;
✓ The error introduced by the gear-box resolution;
✓ Variable time delay for breaking;

The variable time delay will introduce variations in the final position of the tread. On other hand the movement system is a speed controller and does not have in account the position of the tread. So when the tread is arriving at the final position it is applied the full brake, which sometimes can exceed the maximum friction introducing overshoot in the final position. As a result of this overshoot, the motor is not able to come back and the final position will be wrong, then cutting length of the material.

This problem can be solved if:

✓ The maximum applied brake is dimensioned according with the maximum friction;
✓ If the controller is a position controller without overshoot the desired position instead of the speed controller;
✓ The position controller has a low approach speed;
✓ The brake is applied by the motor, reducing the variance in the time brake;
✓ If the intensity of the brake could be controlled.

All this aspects will be taken in account during the development of new control system for the transport conveyor.

3.4. Mathematical model of the production line

The production of treads for tires trough extrusion is a continuous production process. The system can be modelled as a Multiple Input Single Output (MISO) system, where the inputs are the RPMs of each extruder and the output the number of treads, as represented in the next picture.
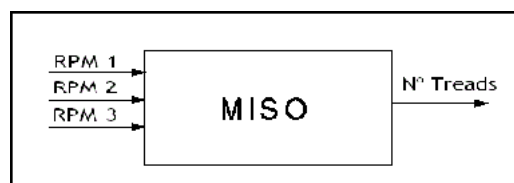
Figure 15 Inputs and outputs of the system

First it is important to refer that on the topological level the production line is represented as a continuous flow of material that reaches different zones of the line while the conveyors are moving. On the picture below is presented the topological structure of the actual extrusion line and it is identified each zone.
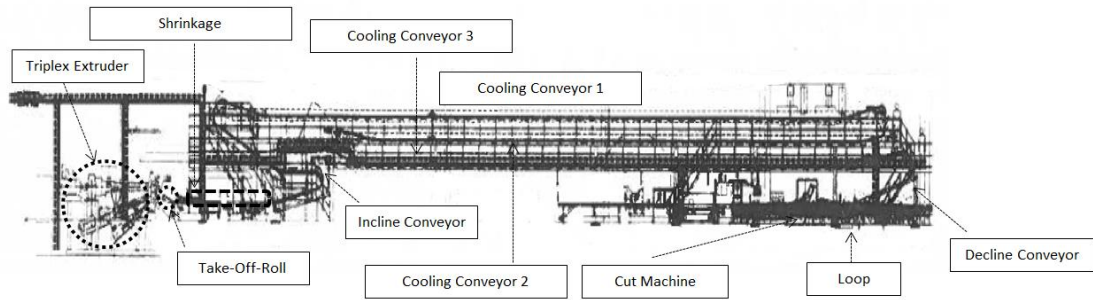
Figure 16 Location of the different zones of the extrusion line

On the other side this system exhibits both continuous and discrete dynamic behaviour, representing the continuous flow of the material the continuous behaviour and the cut-machine the discrete.

The main question that appeared during the development of this model was which variable should be used in order to represent the tread? Should it be the volume, the height or the length? Once is the length of material present in the loop that defines the minimum height and so the speed of the transport conveyor, is the length of the material that defines the quantity of material present in the line and finally because what defines the cycle time of the cut machine is the length of each piece, the variable that will be used to model the system is the length in meters.

3.4.1. Extruder Model

The materials used for tread production are thermoplastic, meaning that can be deformed with the increase of the temperature. In this way is it used the hot extrusion process as the process for moulding the material with the desired shape. As referred before usually for tread production the extruders are composed with more than one simple extruder, being the material of each extruder forced in the extruder head to pass through a die, giving origin to the final structure of the tire tread.

The main objective of this model is to determine the rotation speed that each extruder should rotate in order to secure the continuous flow of the material according to the defined line speed of the product that has been produced and from that analyse how the actual structure of extruders limit the production speed.

The developed mathematical model consider that in steady state, and neglecting all the dynamics effects of the rubber, that each extruder is independent of the other existing one function which relates the rotation speed of each extruder to the material debit to the line, as presented in equation 3.4.1.1. In this way the equations developed consider a single extruder with single screw to be modelled.

$$\begin{bmatrix} RPM_{200} \\ RPM_{150} \\ RPM_{90} \end{bmatrix} = F(V_{line}) \qquad (3.4.1.1)$$

The screw in the fundamental component of the extruder, being the quality and capacity of production of the extruder related to its design. The extruder is divided in three sections or barrel zones: feeding, mixing and metering section, identified in the next picture.
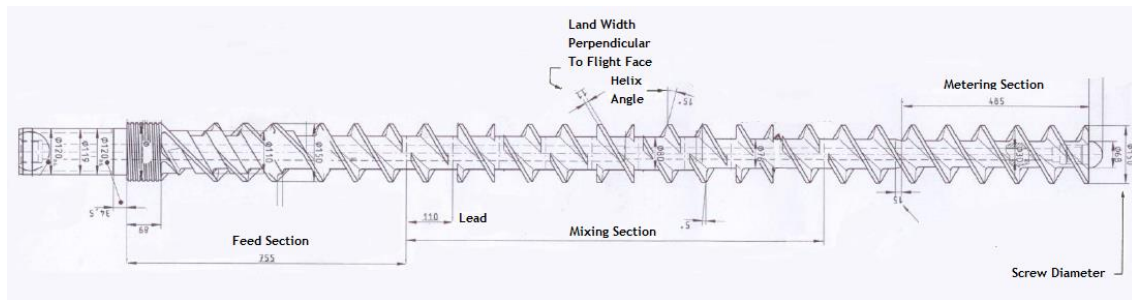
Figure 17 Metering Screw

The compounds are inserted in the feed section that with the screw rotation will flow inside the extruder. In the mixing section the pressure and the high temperature gives origin to a uniform melt, being possible, in this zone, to insert pins on the barrel to achieve a more homogenous melt.

The main idea of the model is to determine the debit of the extruder, volume per second, assuming that the material inside the extruder is already compressed and will not suffer volume changes during its displacement along the screw. Every rotation of the screw results in a volume displacement of material equivalent to the volume of one lead, because it is being modelled a screw with constant lead. The mechanical draw of the screw from an extruder of 150mm can be found in appendix II and generic model of the screw with constant lead and diameter is presented in picture 18.
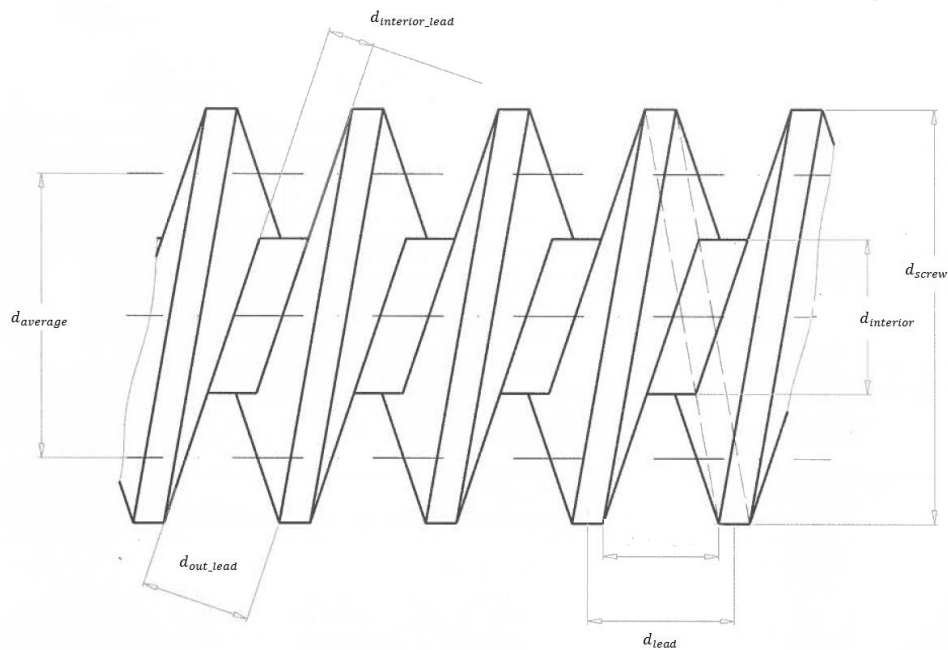
Figure 18 Extruder screw with constant lead and diameter

The average rotation perimeter and diameter are given by the followed expressions respectively.

$$Perimeter_{average} = \pi * Diameter_{average} \qquad (3.4.1.2)$$

$$Diameter_{average} = \frac{(d_{interior} + d_{screw})}{2} \qquad (3.4.1.3)$$

The area of the normal section with free space is given in equation 3.4.1.4.

$$A_{n\_section} = \frac{(d_{screw} - d_{interior})}{2} * \frac{(d_{interior\_lead} + d_{out\_lead})}{2} \qquad (3.4.1.4)$$

Finally the height of this section in presented in equation 3.4.1.5 and the volume in 3.4.1.6 which results from the product of the nominal section area with the height of this section.

$$h_{n\_section} = \sqrt{Perimeter_{average}{}^2 + d_{lead}{}^2} \qquad (3.4.1.5)$$

$$V_{lead} = A_{n\_section} * h_{n\_section} \qquad (3.4.1.6)$$

The debit of the extruder is defined as the product of the rotation speed with the volume of the lead, being the speed of the material the quotient of the debit with the area of the die where the material is extruded, as presented in equations 3.4.1.7.

$$V_{line} = \frac{V_{lead} * RPM_{extruder}}{A_{die}} \qquad (3.4.1.7)$$

This means that, neglecting the dynamic effects of the rubber, in steady state, the speed of the material is proportional to one constant, function of the dimensions of the single extruder, defined as the volume of the lead. On the other hand is proportional and inversely proportional of two variables, the rotation speed of the screw and the area of the die respectively.

Actually, the rotation speed defined in the production parameters of each receipt is obtained by experience of the operator and with several tests until the produced material has the desired characteristics. This model can be used to determine an approximation of the speeds values, simplifying the process. On the other side it can also be used for better parameterization of the IPOC program.

Although the application and precision of this model is limited since it just consider the mechanical dimensions of the extruder and die, and do not consider the dynamics effects of the rubber, which in same aspects can take relevance.

3.4.2. The line model

Each system will be modelled as a flux of material, where the material comes in and out with a defined speed. During the development of the production line model it is considered that the extruders are able produce the necessary debit of material, in order to guarantee the continuous flow of material according with the line speed. When the total length of the material reaches the length of the zone, the exceeded length should be added to the next zone ensuring a continuous flow of material. This flux is modelled with the speed in which the material comes in and out of each zone of the line. In this model it is assumed that the extruder are have to the necessary debit of material according to the line speed and ensuring the continuous flow of material.

Having $L(k)$ as the tread length present in each zone at the instant k, at the next instant $k + 1$ the length will be

$$L(K + 1) = L(k) + (V_{input} - V_{output}) * \Delta t \qquad (3.4.2.1)$$

where V_{input} and V_{output} are the input and output of the material speed in each zone, respectively.

One important fact is that on the shrinkage zone and in the cooling, the input speed is slower than the output of the zone before. This happens because, as it was explained before, the material shrinks and so the flux of the material in terms of length is smaller. On the other hand, the material becomes denser, but this fact is not important for this model. The same happens when the rubber goes inside the cooling tank and it is cooled, the material also shrinks.

This decrease of speed are modelled with the creation of two constant: the relax constant, k_{relax}, and cooling constant, $k_{cooling}$.

A finite state machine was used as mathematic model, representing each state a zone of the production line and the condition transitions are modelled as

$$L(k + 1) > L_{zone} \tag{3.4.2.2}$$

The only discrete part is after the cutting machine where the continuous flow of rubber is transformed in individual parts that will make part of the tire as final product.

Here there are two states where the tread is moving: in one with 1.5 times the line speed and in the other with the line speed. There is also another state where the tread is stopped at the blade position. In the first two states, the length of material in the loop at each time step is in the first case described by:

$$L(K + 1) = L(k) - 0.5 * V_{line} * \Delta t \tag{3.4.2.3}$$

In the second case is constant.

$$L(K + 1) = L(k) + (V_{line} - V_{line}) * \Delta t = L(k) \tag{3.4.2.4}$$

The conditions transitions are according with the position h as represented in the next picture.
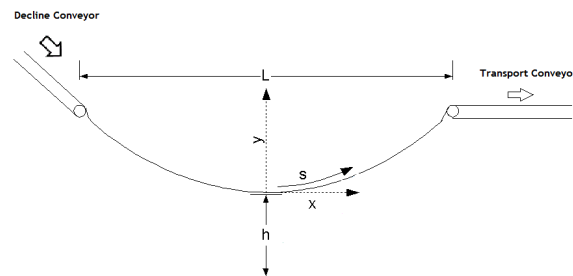
Figure 19 Curve of the material on the loop

The conveyors are spaced by the distance L, and because the tread is suspended in the extremes of both conveyors, the curve that it describes is defined by the catenary equation 3.4.2.5, presented below, where s is half of the total length.

$$s = h * \sinh \frac{L}{2 * h} \tag{3.4.2.5}$$

At each infinitesimal time instant, it is possible to consider a stationary curve and the length of the tread constant in each instant. With this it is just necessary to solve the above equation at each time instant in order to get the height h that will be the transition condition. Because this is a non-linear equation and to simplify the computational cost was developed an Matlab script that calculates for each instant the minimum distance to the floor, h, the corresponding tread length that is on the Loop, being the values saved on a

vector. During the simulation it is just necessary to search on the vector the corresponding length, $L(k + 1)$, the corresponding minimum distance. The loop simulation is presented in the next figure.
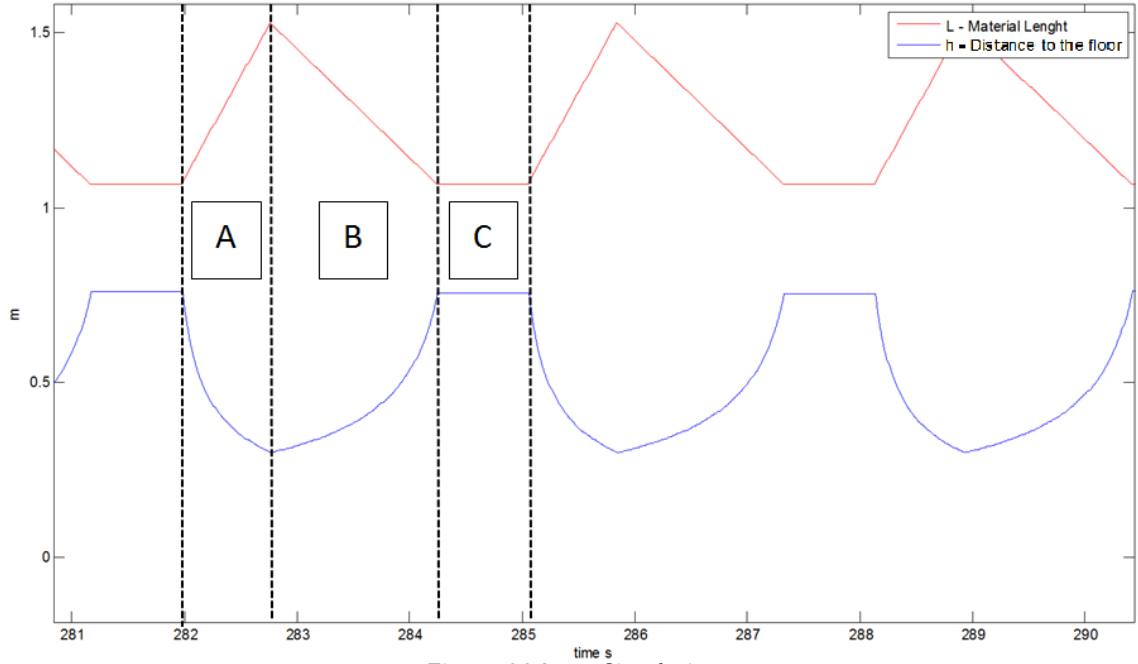
Figure 20 Loop Simulation

As presented in the figure 20 h represents the vertical distance of the catenary curve that the material does to the floor and L the quantity of material, in meters, that is inside the loop. Observing the figure 20 there are three delimited zones: A, B, and C. In zone A the transport conveyor is stopped in order to start a transversal cut in the material, during 0.8 s. As expected because the line do not stops in order to execute the cut, the material is accumulated in the loop, so L grows proportional to the line speed and the height decreases. After the cut the transport conveyor starts to move, pushing material from the loop at one speed 1.5 times the line speed, increasing again the height and decreasing the material on the loop. Finally when the height reach 0.75 m from the floor, the transport conveyor speed is set to be equal to the line speed so the material in the loop stays constant and the same happens to the distance to the floor.

The final equations system for each zone is presented next.

1. Take-Off-Roll Model Equations

$$\begin{cases} L(k+1)_{Take\_Off\_Roll} = L(k) + V_{line} * \Delta t; \; for \; L(k+1)_{Take\_Off\_Roll} < L_{Take\_Off\_Roll} \\ L(k+1)_{Take\_Off\_Roll} = L(k) + \left(V_{line} - V_{Shrinkage}/k_{Shrinkage}\right) * \Delta t \; for \; L(k+1)_{Take\_Off\_Roll} > L_{Take\_Off\_Roll} \end{cases}$$ (3.

2. Shrinkage Model Equations

$$\begin{cases} L(k+1)_{Shrinkage} = 0 \; for \; L(k+1)_{Take\_Off\_Roll} < L_{Take\_Off\_Roll} \\ L(k+1)_{Shrinkage} = L(k)_{Shrinkage} + V_{Shrinkage} * \Delta t \; for \; L(k+1)_{Shrinkage} < L_{Shrinkage} \\ L(k+1)_{Shrinkage} = L(k)_{Shrinkage} + \left(V_{Shrinkage} - V_{incline}\right) * \Delta t \; for \; L(k+1)_{Shrinkage} > L_{Shrinkage} \end{cases}$$ (3.

3. Incline Conveyor Equations

$$\begin{cases} L(k+1)_{Incline} = 0 \; for \; L(k+1)_{Shrinkage} < L_{Shrinkage} \\ L(k+1)_{Incline} = L(k)_{Incline} + V_{incline} * \Delta t \; for \; L(k+1)_{Incline} < L_{Incline} \\ L(k+1)_{Incline} = L(k)_{Incline} + \left(V_{incline} - V_{Colling1} * k_{Cooling}\right) * \Delta t \; for \; L(k+1)_{Incline} > L_{Incline} \end{cases} \quad (3.4.2.8)$$

4. Cooling 1 Equations

$$\begin{cases} L(k+1)_{Cooling1} = 0 \; for \; L(k+1)_{Incline} < L_{Incline} \\ L(k+1)_{Cooling1} = L(k)_{Cooling1} + V_{Cooling} * \Delta t \; for \; L(k+1)_{Cooling1} < L_{Cooling1} \\ L(k+1)_{Cooling1} = L(k)_{Cooling1} \; for \; L(k+1)_{Cooling1} > L_{Cooling1} \end{cases} \quad (3.4.2.9)$$

5. Cooling 2 Equations

$$\begin{cases} L(k+1)_{Cooling2} = 0 \; for \; L(k+1)_{Cooling1} < L_{Cooling1} \\ L(k+1)_{Cooling2} = L(k)_{Cooling2} + V_{Cooling} * \Delta t \; for \; L(k+1)_{Cooling2} < L_{Cooling2} \\ L(k+1)_{Cooling2} = L(k)_{Cooling2} \; for \; L(k+1)_{Cooling2} > L_{Cooling2} \end{cases} \quad (3.4.2.10)$$

6. Cooling 3 Equations

$$\begin{cases} L(k+1)_{Cooling3} = 0 \; for \; L(k+1)_{Cooling2} < L_{Cooling2} \\ L(k+1)_{Cooling1} = L(k)_{Cooling3} + V_{Cooling} * \Delta t \; for \; L(k+1)_{Cooling3} < L_{Cooling3} \\ L(k+1)_{Cooling3} = L(k)_{Cooling3} \; for \; L(k+1)_{Cooling3} > L_{Cooling3} \end{cases} \quad (3.4.2.11)$$

7. Decline Conveyor Equations

$$\begin{cases} L(k+1)_{Decline} = 0 \; for \; L(k+1)_{Decline} < L_{Decline} \\ L(k+1)_{Decline} = L(k)_{Decline} + V_{Decline} * \Delta t \; for \; L(k+1)_{Cooling1} < L_{Cooling1} \\ L(k+1)_{Decline} = L(k)_{Cooling1} \; for \; L(k+1)_{Cooling1} > L_{Cooling1} \end{cases} \quad (3.4.2.12)$$

8. Loop Equations

$$\begin{cases} L(k+1)_{Loop} = 0 \; for \; L(k+1)_{Decline} < L_{Decline} \\ L(k+1)_{Loop} = L(k)_{Loop} + \quad V_{Decline} * \Delta t \; for \; L(k+1)_{Decline} > L_{Decline} \; \cap \; L_{Loop} < L \\ L(k+1)_{Loop} = L(k)_{Loop} + \left(\quad V_{Decline} - V_{Transport} \right) * \Delta t \; for \; L_{Loop} > L \end{cases} \quad (3.4.2.13)$$

9. Speed Transport Equations

$$\begin{cases} V_{Transport} = 0 \; if \; L_{Transport\_Conveyor} = L_{Cut} \; \cap \; t < T_{Cut} \\ V_{Transport} = 1.5 * V_{Decline} \; if \; h < h1 \\ V_{Transport} = V_{Decline} \; if \; h > h1 \end{cases} \quad (3.4.2.14)$$

3.4.3. Conclusion

It is possible to conclude from the equations presented above that, in order to guarantee the stability of the production, the line speed between the conveyors should be the same in the case of the material do not suffer any physical modification. If the material shrinks, the speed should be proportionally reduced by the same factor.

Finally, in the case of the cutting machine, the average flux of the transport conveyor should be the same as on the Loop to ensure that the average length of material inside the Loop is the same as the taken out by the transport conveyor.

3.5. Model Simulation and Validation

For model simulation was also developed a Matlab script, for faster computation and also to have available all the simulation data. To validate the mathematical model of the extrusion line where simulated four different recipe using the production parameters, such as the speed line, the desired cutting length, the shrinkage gain, was measured the cutting time, T_{Cut} , and also the length of each zone. For comparison where measured the next production times:

- ✓ The arriving time of the continuous flow of material at each zone of the production line;
- ✓ The transport time;
- ✓ The average production time of 10 treads.

The results are presented in the next table:

Table 2 Comparison of simulation data with real data from the production line

Receipt nº	410147	Simulated	Error	410484	Simulated	Error	410684	Simulated	Error
Line Speed m/min		34			37			28	
Shrinkage %	-3	-3	0	-2	-2		-2	-2	0
Cut time sec.				0,8					
Tread Length m	1,749	1,749	0	1786	1786	0	2.048	2.048	0
Take-off time sec.	0	0	0				0	0	0
Incline time sec.	14	12,1	0,4	0	0	0	19	14,6	0,96
T_cooling1 sec.	30	25,4	1,9	13	12	0	38	30,57	4,4
T_cooling2 sec.	125	123	4,6	103	101	1	156	150,6	7,43
T_cooling3 sec.	200	203,5	2	176	175	2	250	249,81	5,4
Decline time sec.	274	284	-3,5	248	249	1	353	349,05	0,19
Loop time sec.	283	293	-10	255	256,8	-1	354	360	3,95
Transport time sec.	2,5	2,5	-10	2,15	2,2	-1,8	4	3,94	-6
Time of 10 treads sec.	32,5	32,3	0	30,5	30,03	-0,05	47,4	48,34	0,06

3.6. Conclusions

A mathematical model of the extruder and also about the production line has been developed.

The obtained results from the mathematical model are really close to the measured results, concluding that this model can be used to evaluate the performance of the new control design. It is also possible to quantify these performance results in production number that can be translated in possible earnings for the enterprise.

But not only, but also it is possible to estimate for a new receipt the time of production and the capability of production of this extrusion line.

Chapter 4

Motor Control

This chapter is discussed about the chosen motor control method, being approached the motor model, modulation methods and finally the chosen motor control strategy. The simulations will be performed using PSIM which is a circuit simulation tool that allows easy power circuit and control design [3]. The simulation motor parameters are from the EMRAX 228 which was the motor used to perform the implementation tests of the final controller design.

4.1. The Synchronous Machine

4.1.1. Introduction

The Permanent Magnet motors (PM) are generally used in high performance drives like industrial robot arms, servo-motors and machine tools, as the example of the Siemens servo-motors, as the robot arm of ABB that moves real heavy coils used in Continental Mabor due to their advantages as high power density, high torque, high efficiency, free maintenance and occupy less space because the space that they need for magnetization is smaller [4].

Despite the range of applications of this kind of motor has increased, it is mainly applied in the servo-systems[5], because when comparing with the induction motor there is not slippage which means higher precision in the position control.

4.1.2. The Permanent Magnet motor mathematical model

A simplified model of the PM motor can be obtained with the d-q transformation, which transforms stationary symmetrical alternated variables in continuous ones using a rotating reference frame. This is possible because the d-q frame is rotational with an angular speed with the same value of the electrical speed, $\omega_e = p * \omega_r$, such that p is the number of pole pairs and ω_r the mechanical rotor speed.

In the d-q reference frame theory, the mathematical model of the PM can be obtained considering the rotor flux fixed to the d axis, and so there is not any rotor flux on the q

axis[6]. On the q axis there is the stator flux induced by the stator current and the flux linkages that is leading by 90 electrical degrees[7]. It is important to refer that in this model the motor core losses and flux variations with the temperature are negligible.

On the next picture a representation of this axis model can be found.
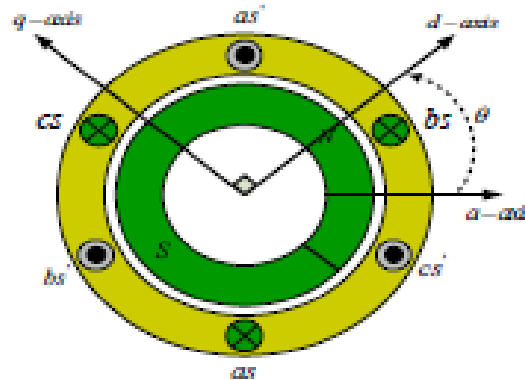
Figure 21 d-q axis representation retired from [6].

The derivation of the d-q frame starts with the assumption that PM is a three-phase balanced machine, so the voltage and current phase are lagged 120° from each other.

The three phases are projected into a two axis referential $\alpha - \beta$ through the Clarke-Transformation. If we look to the next three equations of the Clarke transform, it is possible to identify in the third equation the assumption of an balanced current machine, where the sum of the three currents is zero, such that i_a, i_b and i_c are the three phases. The first to equations are just the projection of each current vector in the reference frame $\alpha - \beta$, where i_α and i_β are the currents in the new referential.

$$\begin{cases} i_{\alpha = i_a} \\ i_\beta = \dfrac{1}{\sqrt{3}} * i_a + \dfrac{2}{\sqrt{3}} * i_b \\ i_a + i_b + i_c = 0 \end{cases}$$ (4.1.2.1)

There is also a Clarke inverse transform that will be very useful for the motor control, to convert the references of the controller into real quantities to be applied in the motor.

$$\begin{cases} i_a = i_\alpha \\ i_b = -\dfrac{1}{2} * i_\alpha + \dfrac{\sqrt{3}}{2} * i_\beta \\ i_c = -\dfrac{1}{2} * i_\alpha - \dfrac{\sqrt{3}}{2} * i_\beta \end{cases}$$ (4.1.2.2)

After the conversion of the three phase system into two phases it is necessary to project the two vectors of the fixes referential $\alpha - \beta$ on the synchronous rotating frame d-q. In this way all the variables will be constant in steady state. This is known as the Park transform.

$$\begin{cases} i_d = \dfrac{2}{3} * \left(\cos \theta_e * i_\alpha + \sin \theta_e * i_\beta \right) \\ i_q = \dfrac{2}{3} * \left(-\sin \theta_e * i_\alpha + \cos \theta_e * i_\beta \right) \end{cases}$$ (4.1.2.3)

On the next pictures i_a, i_b and i_c are represented as i_u, i_v and i_w. A summary of this transformations represented in both axis frame can be found on the figure 22.
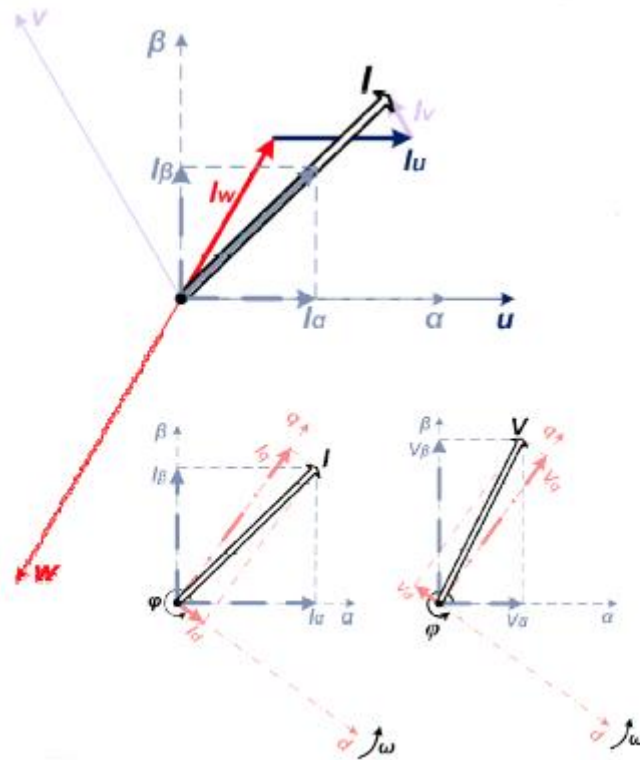
Figure 22 Summary of Transformations retired from [8]

Concluding the Clarke transformation is used to remove the redundancy of the tree phase system. The Park transform provides a synchronous rotating frame, so the currents and voltages are stationary in the d-q reference frame. In this way all the units referenced to this frame will be constant in steady state, bringing some huge advantages to the calculus and making easier the control of the PM motor. In figure 23 is represented the application of both transformations.
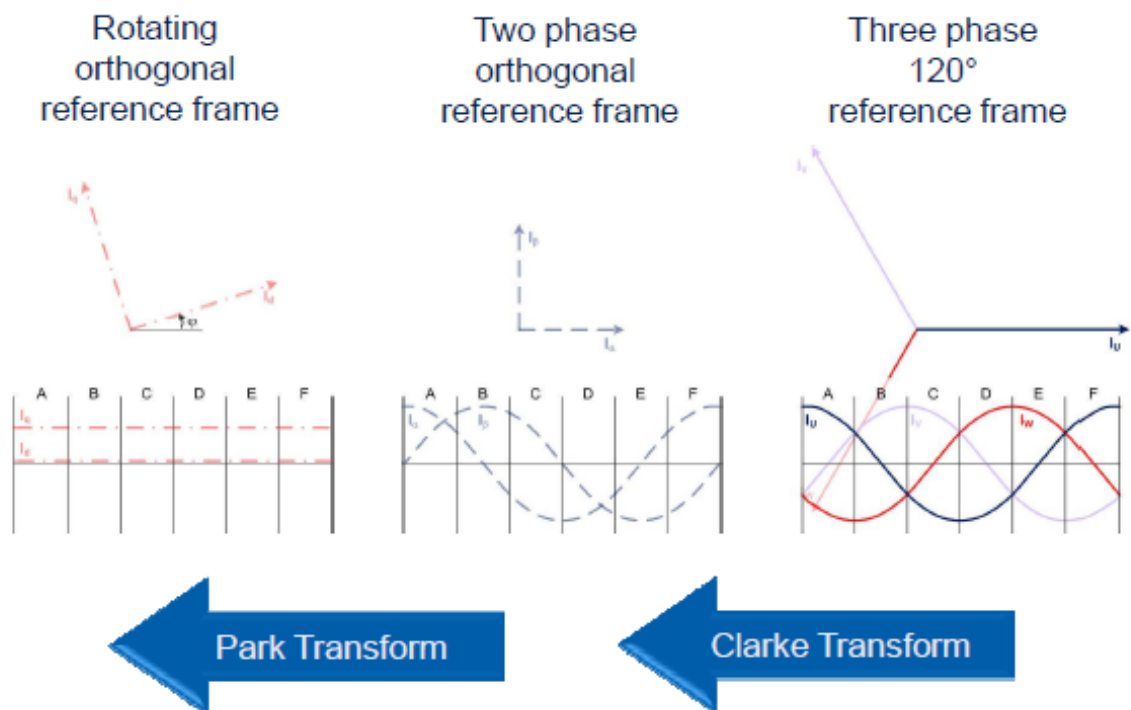
Figure 23 Stationary and Rotating Reference Frames retired from [8]

Using the d-q frame as reference, it is possible to convert the stator voltage V_s, into V_d and V_q components as represented in the next equation.

$$V_s = r_s * I_s + \frac{d\lambda_s}{dt} + jw_e\lambda_s \Rightarrow \begin{cases} V_d = r_s * I_d + \dfrac{d\lambda_d}{dt} - w_e\lambda_q \\ V_q = r_s * I_q + \dfrac{d\lambda_q}{dt} + w_e\lambda_d \end{cases} \qquad (4.1.2.4)$$

Where r_s is the stator phase resistance, I_s is the stator current, $\frac{d\lambda_s}{dt}$ the differential stator flux and λ_s the stator flux. The same occurs on the flux components. As it was referred, all the rotor flux is fixed to the d axis, and the only components of the flux in the q axis is due to the flux linkage resulting in the next equations.

$$\begin{cases} \lambda_d = L_d i_d + \lambda_{pm} \\ \lambda_q = L_q i_q \end{cases} \qquad (4.1.2.5)$$

with L_d and L_q as the stator inductance related to the d-q axis.

Considering that the permeability of high flux density permanent magnet is approximately the same of the air, L_d is define as the stator inductance when the rotor is aligned with the permanent magnets, being known as *direct axis inductance*. By rotating the magnets 90 electrical degrees to the position where L_d is measured, the stator flux will be aligned with the iron of the rotor and so the inductance measured, is known as *quadrature axis inductance*. This results in the next equivalent circuit of the PM motor.
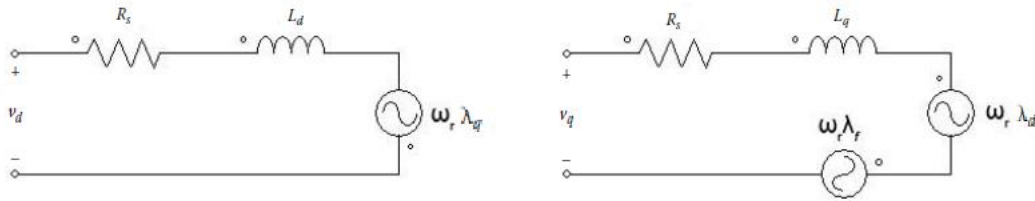
Figure 24 Electrical representation circuits of the PM motor model using d-q frame, edited from [7]

Now, it is possible to define the electromagnetic torque expression as function of the flux and currents on the d-q axis. The electromagnetic torque is given by

$$T_e = \frac{3}{2} * p * (\lambda_d * i_q - \lambda_q * i_d) \qquad (4.1.2.6)$$

Looking at the expression presented above, it is possible to conclude that the produced torque is directly proportional to the flux along the d axis and the stator current in quadrature i_q. On the other hand the component of the flux aligned with the iron of the rotor λ_q is against the produced torque as the direct current. So, i_q is essentially the torque producer component and i_d the flux producer.

Furthermore the electromagnetic torque results from the cross product between flux and the current vector, as shown in the expression below.

$$T_e = \frac{3}{2} * p * (I_s \times \lambda_s) \Leftrightarrow \frac{3}{2} * p|I_s||\lambda_s| \sin\theta_{T_e} \qquad (4.1.2.7)$$

In the equation 4.1.2.7 I_s is the stator current vector that creates the rotating field and λ_s the flux vector, resultant of the permanent magnet flux and the induced flux by the

current in the stator. Finally θ_{T_e} is the torque angle that will be discussed later in adopted control method of the motor.

By the replacement of the flux linkages in terms of the inductances and currents, yields

$$T_e = \frac{3}{2} * p * (\lambda_{pm} * i_q + (L_d - L_q) * i_q * i_d) \tag{4.1.2.8}$$

From the d-q reference frame we have

$$\begin{cases} i_q = |i_s| \sin \delta \\ i_d = |i_s| \cos \delta \end{cases} \tag{4.1.2.9}$$

Since δ is constant for a given load torque, the d and q currents are also constant in the rotor reference frame[9].

Substituting this equation into the expression 4.1.2.8 the torque is given by:

$$T_e = \frac{3}{2} * p * (\frac{1}{2}(L_d - L_q) * i_s^2 \sin 2\delta + \lambda_{pm} * i_s * \sin \delta) \tag{4.1.2.10}$$

Finally the mechanical equation of the motor is on 4.1.2.11.

$$T_e - T_L = J \frac{dw_r}{dt} + Bw_r \tag{4.1.2.11}$$

Where T_L is the load torque, J the moment of inertia, B the friction coefficient and w_r the rotor speed [10].

In this sub-chapter was presented a resumed analysis of the PM motor, explaining the main characteristics of this type of motors. It is also presented both Park and Clarke transformations that are necessary for the development of the control method of the motor.

In the end a mathematical model of the PMSM is presented, based on the d-q reference axis, allowing the knowledge of the flux and torque expressions for the PMSM, where the equation 4.1.2.10 will be discussed later since all the control method starts from it.

4.2. The inverter and modulation methods

4.2.1. Introduction

Considering the propose of this project, which is design of a new traction control system to the transport conveyor of the cutting machine, being necessary to feed the motor in a controlled way, such that the both transient and steady state are controlled. To achieve that it is necessary to use an inverter or DC-AC converter, which generates from a DC supply an controlled AC supply with an determined amplitude and frequency[11].

In this chapter will be presented the basic topology of a 3 phase full-bridge inverter and also the modulation methods that generate the command signals necessary to control the inverter and generate a controlled output, in magnitude and frequency.

4.2.2. Sinusoidal PWM (SPWM)

Sinusoidal Pulse Width Modulation is a widely used modulation technique in the power converters control. The main reasons are the simplicity of control, implementation and good power quality although the high frequency switching losses associated[7].

The Sinusoidal PWM, as the name refers consists basically in a sinusoidal control signal with the desired frequency $V_{control}$, usually known as modulation signal, that is compared with a triangular waveform, known as carrier wave, V_{tri}. The carrier signal usually has a constant frequency (f_s) since this frequency will determine the switching frequency. The control signal is used to modulate the switch duty ratio, in others words, to control the time that is applied on the motor V_d or zero voltage[11]. This method is presented in the following picture.
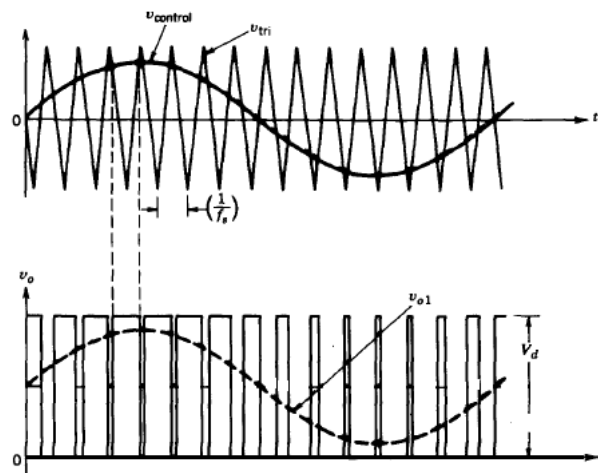
Figure 25 Pulse Width Modulation edited from [11]

There are two important concepts that are important to define: modulation index m_a, that is the relation between the amplitude of the control signal and the amplitude of the carrier wave. And frequency index m_f that is the relation between the frequency of the carrier wave and the control signal.

$$m_a = \frac{V_{control}}{V_{tri}}$$

(4.2.2.1)

$$m_f = \frac{f_s}{f_{control}}$$

(4.2.2.2)

where $f_{control}$ is the frequency of the control signal. It is pretended to control a 3-phase inverter, so there is a control signal for each phase and each control signal should be lagged 120 electrical degrees. The peak amplitude of the fundamental voltage is given by the next expression.

$$V_{o1} = m_a * \frac{V_{DC}}{2}$$

(4.2.2.3)

The frequency index will determine the frequency of the first harmonic accompanied by four side harmonics at $m_f \pm 2$ and $m_f \pm 4$, but in three-phase inverter only harmonics in line-to-line are of concern[7]. Once the harmonics in the output on any leg of the inverter is identical, some of the harmonics are eliminated in line-to-line voltage. Considering for

example, m_f odd and multiple of 3 and that the phase difference in the harmonics output is $120m_f$ degrees between the line harmonics, this results in a phase difference multiple of 360 degrees. As a consequence the line harmonics is supressed in line-to-line voltage.
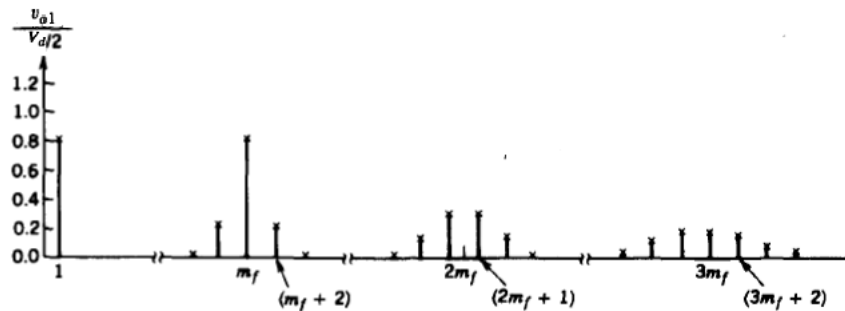
Figure 26 Harmonics edited from [11]

Because the harmonics in the output of each arm of the inverter are identical, so if it is considered only the harmonics at m_f frequency and it is multiples, the phase difference between the harmonics will be also multiple of 120 electrical degrees. So, if m_f is odd the phase difference would be zero and this problem is solved in composed line-to-line voltages, where m_f should be chosen odd to eliminate the harmonic content introduced by the inverter.

PWM can be also unipolar or bipolar, depending on the power supply. It has just positive polarity in the first case and positive and negative in the second one[11].

The simulation of SPWM method was implemented in PSIM and the block scheme is presented in the next picture and the simulation parameters can be found in Table 3.
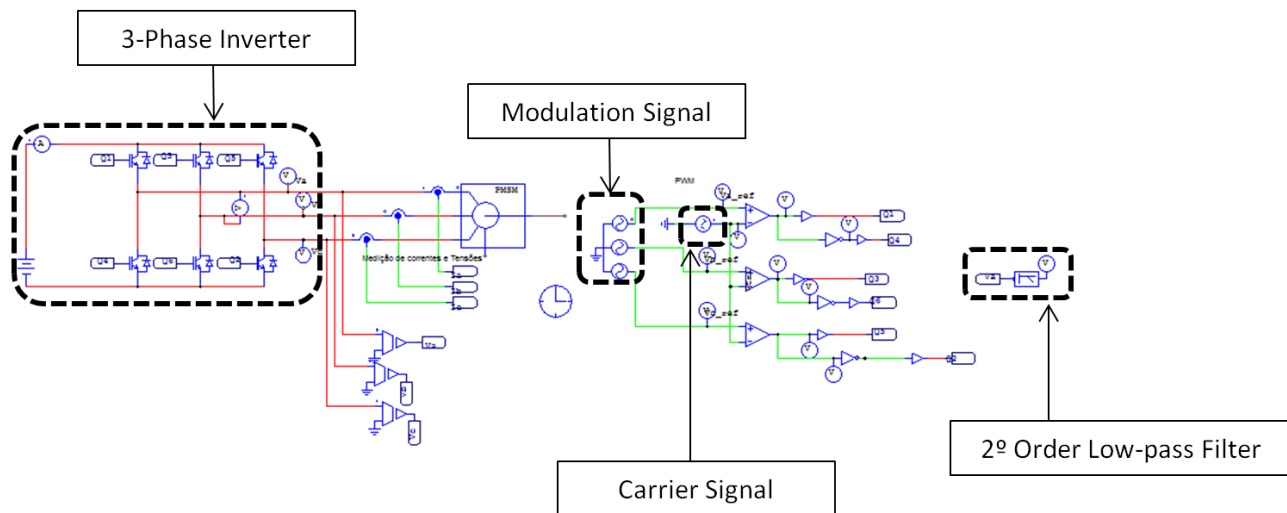
Figure 27 Block scheme of the PWM simulation

Table 3 Simulation Parameters

DC Bus Voltage	400 V
Frequency Carrier Wave	10 kHz
Frequency Modulator Signal	60 Hz
Frequency Low-Pass Filter	600 Hz
Line-Line RMS	122.4745 V

The simulation results are presented next:
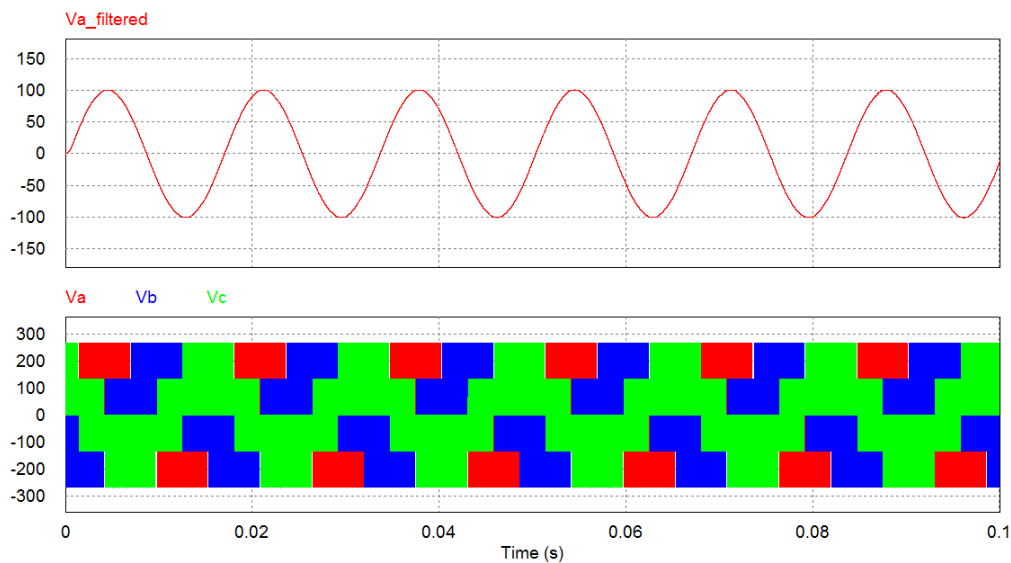
Figure 28 Top plot fundamental harmonic of the generated voltage and in bottom plot three-phase voltages.

In order to check the fundamental component of V_a and verify peak amplitude value, it was applied an second-order filter at 600hz, one decade after the fundamental frequency of V_a. The filtered signal is represented in the first graphic, on the second one are the phase voltage resulting from the commutation of the inverter.

Through the application of the FFT to the simulation results presented in figure 28 can be obtained the harmonic content of each signal. The results are presented in the figure 29.
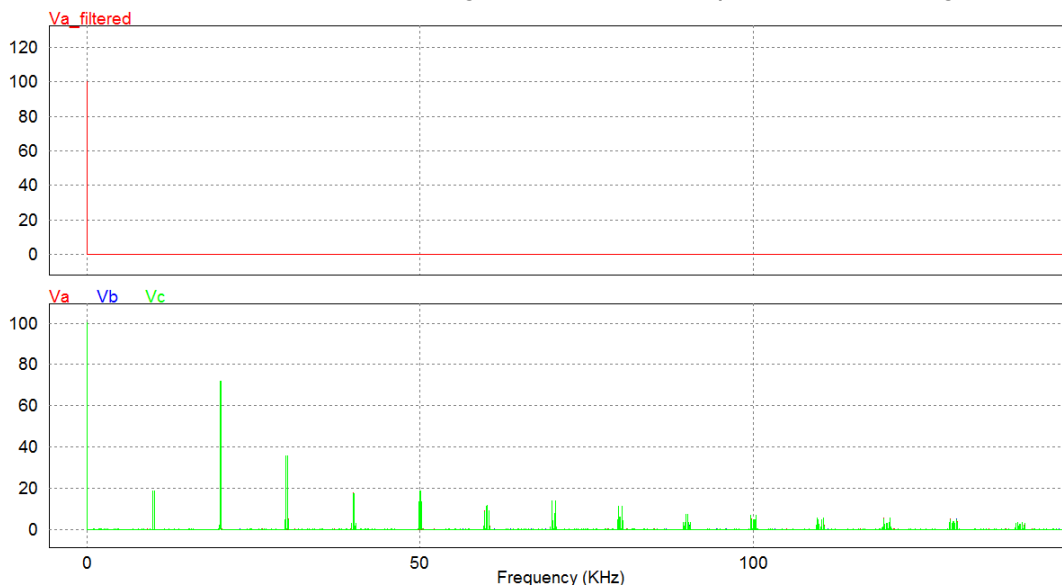
Figure 29 FFT of the fundamental harmonic of the generated voltage and in bottom plot three-phase voltages.

Looking at the simulation results, on the second plot it is possible to observe that at 60Hz is located the fundamental harmonic, which is the frequency of the modulator signal. The harmonics content is located at frequencies multiples of the frequency of the carrier wave as expected. In the first plot if presented the harmonic content of the signal filtered by

the low-pass filter at 600Hz, ensuring that under the carrier signal frequency there is only the modulator signal.

4.2.3. Space Vector Modulation (SVM)

Space Vector Modulation (SVM) became a standard for the switching scheme for the control of the power converters [12]. In contrast to Sinusoidal Pulse Width Modulation (SPWM), which control the three phases separately, in SVM, the 3-phase quantities are treated as components of one vector, the vector of the stator voltage

$$\vec{V_S} = \frac{2}{3} * \left(V_a + V_b e^{-j\frac{2}{3}\pi t} + V_c e^{j\frac{2}{3}\pi t} \right) \tag{4.2.2.4}$$

Where V_a, V_b and V_c are the phase voltages. Basically it is pretended to impose one reference vector

$$\vec{V}_{ref} = |V_{ref}| e^{j\theta_{\alpha-\beta}} \tag{4.2.2.5}$$

With

$$|V_{ref}| = \sqrt{V^2{}_\alpha + V^2{}_\beta} \tag{4.2.2.6}$$

And

$$\theta_{\alpha-\beta} = \tan^{-1} \frac{V_\beta}{V_\alpha} \tag{4.2.2.7}$$

Rotating in space at speed ω_e, so V_{ref} can be obtained by two adjacent vectors as represented in the next picture.
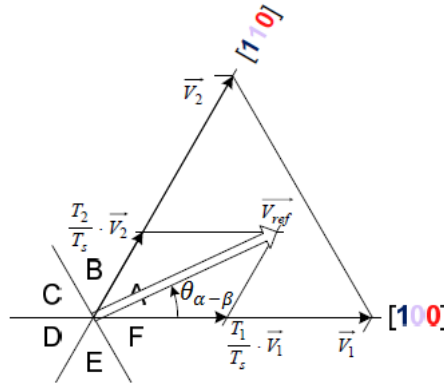
Figure 30 Reference vector approximation edited from [8]

The electrical angle is divided in sectors. Therefore according with the electrical position V_{ref} is obtained as combination of two different active vectors and two passive vectors. In the next picture it is possible to observe a representation of the space vector, with the sectors definitions and the active vectors in each sector.
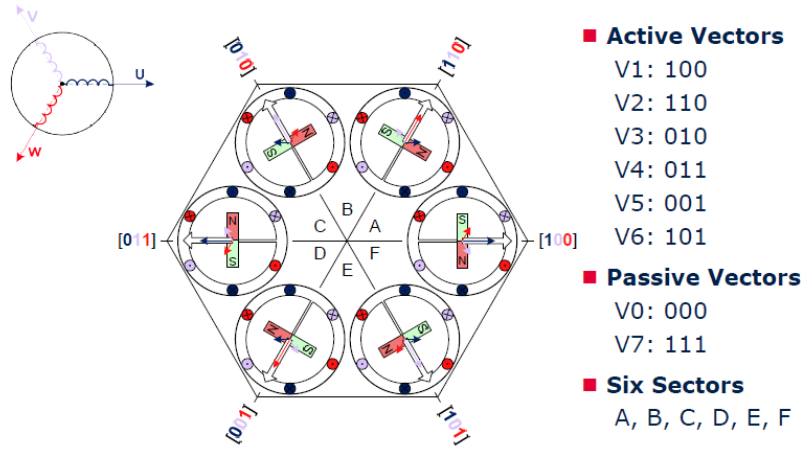
Figure 31 Space vector diagram retired from [8]

And so the time that each arm will be active is defined by the projection of the voltage reference vector in the active and passive vectors that belong on the corresponding sector, the time calculations are given in the next two expressions.

$$T_1 = \frac{\sqrt{3} * T_s * |V_{ref}|}{V_{DC}} * \sin(\frac{\pi}{3} - \theta_{ref})$$ (4.2.2.8)

$$T_2 = \frac{\sqrt{3} * T_s * |V_{ref}|}{V_{DC}} * \sin(\theta_{ref})$$ (4.2.2.9)

where V_{DC} is the voltage of the DC power supply, T_s the period and θ_{ref} the electrical position relative to the sector. The time resulting from the passive vectors is defined as

$$T_0 = T_s - T_1 - T_2$$ (4.2.2.10)

The next stage of the algorithm is to generate a switching signal for each gate, with the expected time for each vector during one period. To produce this, it is generated a triangular wave with a period T_s, amplitude $\frac{T_s}{2}$. Comparing the time values with the amplitude of the triangular wave is generated the pulse with the width necessary to implement the expected sequence. The algorithm is represented in the next picture.
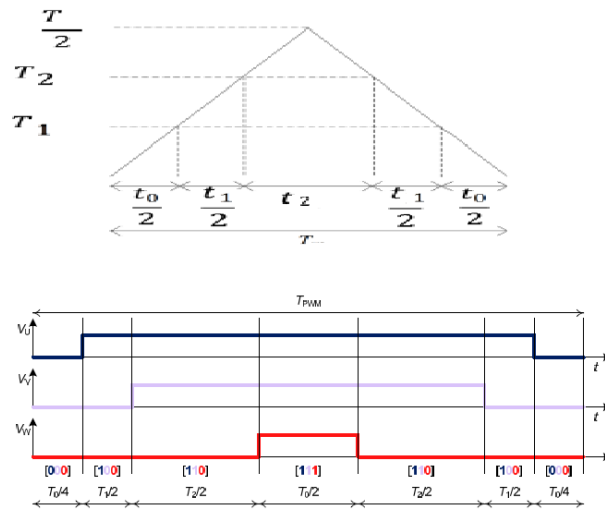
Figure 32 Seven segment SVM scheme with two passive vectors

The algorithm that uses the two passive vectors is known as seven segments, there is also an algorithm of SVM with 5 segments where the passive vectors are not used.

Concluding the main advantages of SVM is the minimization of the necessary number of switches during the time T_s, also reduces the harmonic distortion in the line, is designed for three phase electrical machines since it describes the machine in both steady and transient state and allows approximately a 15% increment of modulation index when comparing with SPWM. The implementation of SVM was developed using a C block of PSIM. The simulation parameters are presented in the next table.

Table 4 Simulation parameters of SVM

DC Bus Voltage	400 V
T_s	100 us
Frequency Reference Signal	60 Hz
Frequency Low-Pass Filter	600 Hz
Phase Voltage Reference	100 V

Then it is presented the block scheme and also the simulation results.
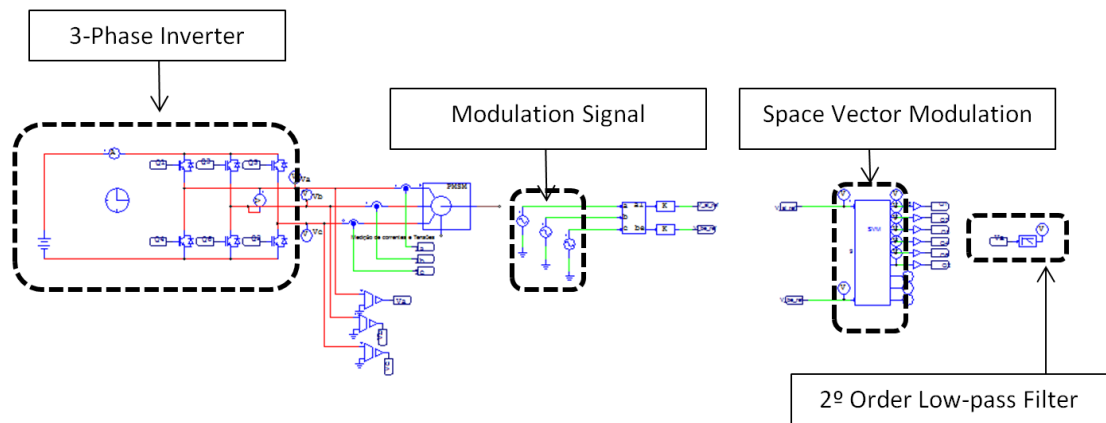
Figure 33 SVM simulation block scheme
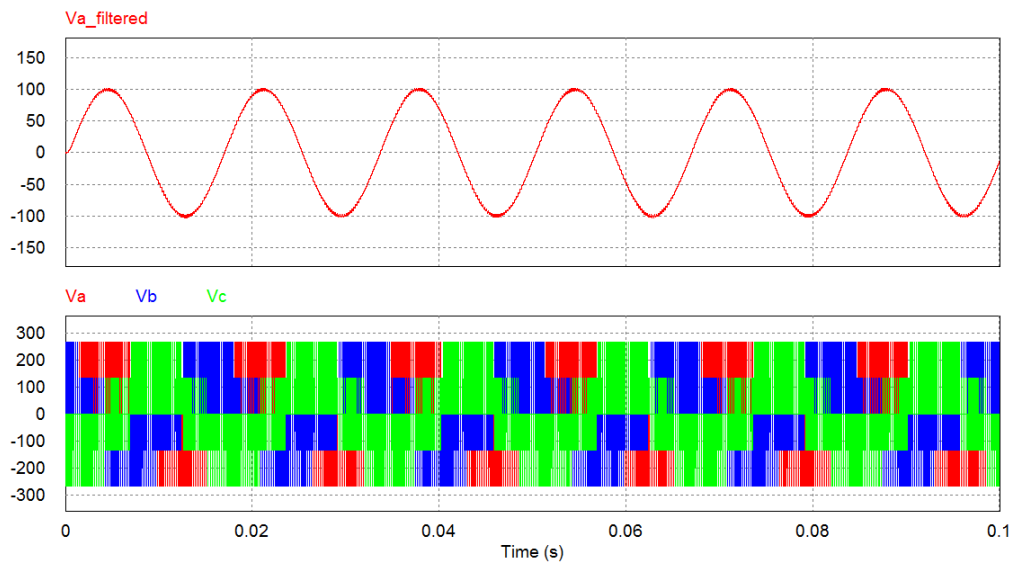
Figure 34 Top plot fundamental harmonic of the generated voltage and in bottom plot three-phase voltages with SVM

The same procedure that was applied in the SPWM simulation to verify the results was also applied to the SVM results. On the first plot it is presented the filtered signal, being the phase-voltage has the excepted amplitude. On the second one the three phase voltages without filter.

In order to analyse the harmonic content of the line is presented the FFT of the generated phase voltages.
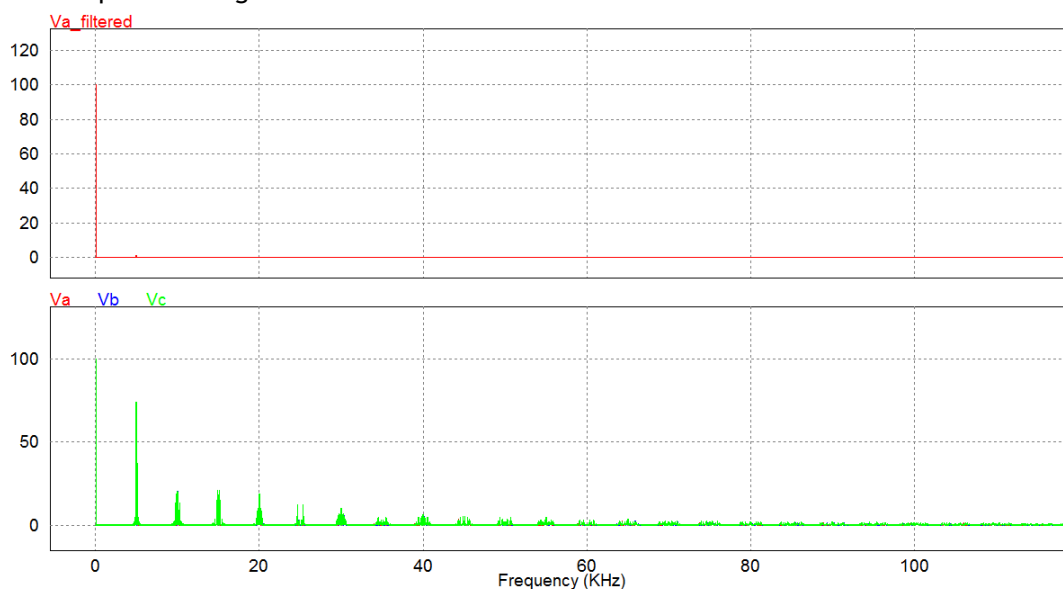
Figure 35 FFT of the signals presented in the figure 31

4.2.4. Conclusion

Looking at the simulation results and comparing the second plot of the figure 28 with the same plot of the figure 34 is possible to conclude there are less commutations, from the contrast of the figures, meaning that SVM minimizes the necessary number of switches during the time T_s. From the FFT, that the harmonic content at higher frequency of the fundamental is bigger in figure 29 in comparison with the harmonic content presented if figure 35 and so SVM also minimizes the harmonic distortion in the line. Concluding SVM is advantageous, since it is designed for three phase electrical machines and it describes the machine in both steady and transient state, allowing also approximately a 15% increment of modulation index when comparing with PWM, in overmodulation [13].

4.3. Direct Torque Control Method (DTC)

4.3.1. Introduction

Until now it was shown that if the torque applied to the motor is controlled it is possible to control both speed and position. It is here where the fundament of all this control design method starts. In spite of the motor control can be performed in different forms, they can be gathered in two main groups: vector and scalar control[14]. On the second group the most used is V/f constant method that just allows the speed control of the motor, but without feedback and so without controlling the transient state of the motor.

Considering the final application of this system, the motor will be almost working in transient state because for each tread, it has to move to one final position to cut the tread

 with the desired length and so it has to start, move to one position and stop without pass through the required position. So it is mandatory to control the transient state of the motor and have a control of the torque with the minimum overshoot for a high precision positioning. To verify this requirement the vector control is adopted.

4.3.2. Brief comparison between FOC & DTC

The Field Oriented Control (FOC) and Direct Torque Control (DTC) method have been invented in 70's and 80's respectively[15]. The main difference between them is the principle of operation, despite the fact that both FOC and DTC are strategies that allow the torque and flux of the motor to be controlled independently[7]. The strategy control of FOC passes through in two current control loops and controlling both i_d and i_q on each loop it controls both torque and flux of the motor. In fact the decoupled control of flux and torque allows a control in dynamic regime comparable to that of DC motors. Moreover the control range of the torque produced extends the entire region of engine speed, even when it is stopped or in regeneration mode [16].

However this method requires a thorough knowledge of the physical parameters of the engine due to the estimation of the rotor flux, as well as the two controllers tuning PI's corresponding to it may prove difficult and laborious. A scheme of the control is present on the next picture.
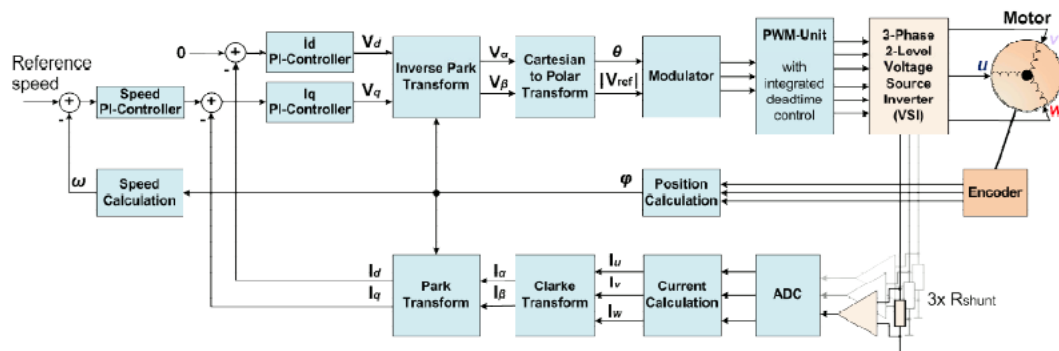
Figure 36 FOC scheme retired from [8]

On the other side in DTC both torque and flux are estimated, using the motor model equations, existing different topologies according with the used modulation method.

It is referred in the literature that DTC has better dynamic response [7],[15] and besides that it just needs one PI controller, becoming least heavy the computation and also the tuning of the parameters.

The most common DTC scheme is based on hysteresis having the advantages over conventional rotor oriented control include the elimination of the d-q current control loops, coordinate transformation and voltage modulator. On the other hand, among the well-known disadvantages of the hysteresis are:
- ✓ variable switching frequency;
- ✓ current and torque distortion caused by sector changes;
- ✓ high sampling frequency needed for digital implementation;
- ✓ implementation of hysteresis comparators;

The application of a voltage modulator can solve the above difficulties [17]. Moreover DTC has small ripple in the torque response control and, using a constant flux reference and with the same value of the permanent magnets flux it is possible to protect the motor of the demagnetization.

According to this DTC with a voltage modulator application was the chosen as torque control method that will be the central part of all control system.

4.3.3. Direct Torque Controller

In this section it will be presented the main part of the controller design. Later it will be presented a control scheme that using the applied torque in the motor as a command signal, being in this way able to control the position and speed of the motor. In this way the torque control is determinant in the control performance.

The Direct Torque Control method was investigated first by Takahashi and Noguchi for induction machines but this concept can also be applied to synchronous machines. As it was referred before, this method is different from the conventional ones, where toque is controlled by the currents loop in d-q reference frame. Even though the conventional scheme of DTC uses hysteresis controllers that allow the elimination of coordinate transformations and voltage modulator, being easier for implementation, it has some disadvantages referred in the section 4.3.2 and also the need of measurement the three phase currents are necessary [14].
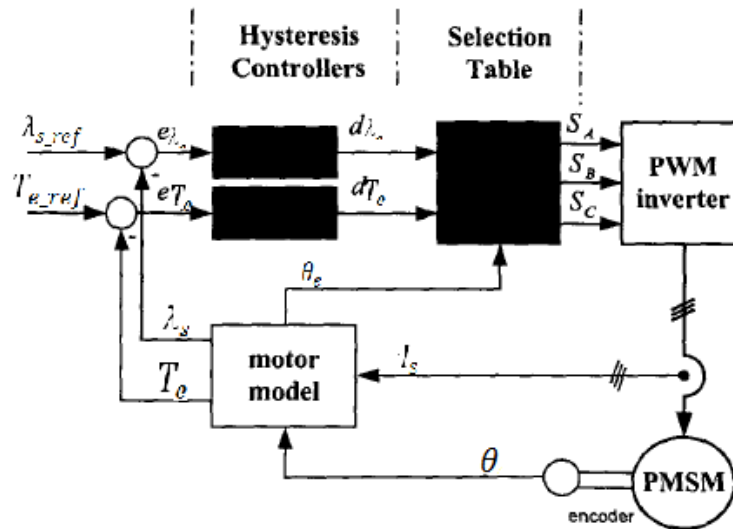
Figure 37 Direct Torque Controller with hysteresis, edited from[14]

The adopted scheme was proposed by Dariusz Swierczyiski and Marian P. Kamierkowski, where the selection table is replaced by a voltage modulator eliminating all the problems referenced above. The developed scheme can be found in the next picture.
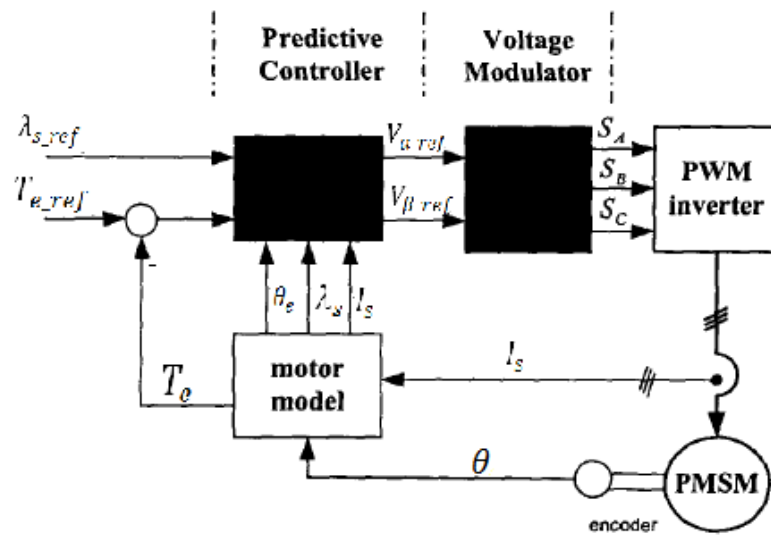
Figure 38 Direct Torque Controller scheme, edited from [17]

Predictive controller receives a flux reference and the torque error. The torque error is determined based on the torque estimation formula and the reference that is pretended to impose in the motor.

The predictive controller based on the flux estimation and its position. It calculates the stator voltage reference vector $|V_{ref}|e^{-j\gamma ref}$ that imposes the desired torque. Stator voltages and flux given in the d-q reference frame are presented in the next expressions.

$$\begin{cases} V_d = r_s * i_d + \dfrac{d\lambda_d}{dt} - p * \omega * \lambda_q \\ V_q = r_s * i_q + \dfrac{d\lambda_q}{dt} - p * \omega * \lambda_d \\ \lambda_d = L_d i_d + \lambda_{pm} \\ \lambda_q = L_q i_q \end{cases}$$

(4.3.3.1)

Overlapping the $\alpha - \beta$ and d-q referential frames it is possible to draw vector flux diagram presented in the figure 39.
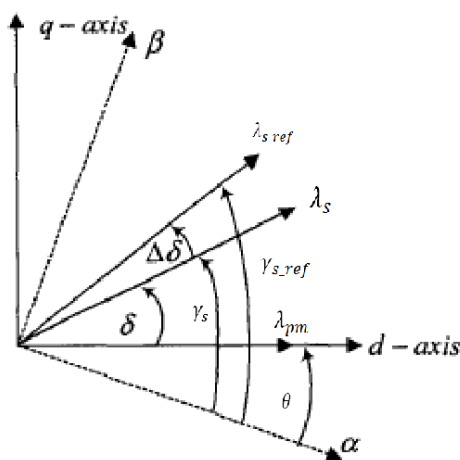
Figure 39 Flux diagram, edited from [7]

Knowing that θ_e is the electrical position, which relates the orientation of the $\alpha - \beta$ to the d-q frame, where λ_s is the actual stator flux vector and γ_s is defined as presented in euqation 4.3.3.2.

$$\gamma_s = \tan^{-1}\frac{\lambda_\beta}{\lambda_\alpha} \qquad\qquad (4.3.3.2)$$

In relation in the d-q frame λ_s makes an δ angle that is the actual torque angle of the motor, when the stator resistance is neglected. In the next equation is presented an expression of the electromagnetic torque function of δ:

$$T_e = \frac{3}{2} * p * (\frac{1}{2}(L_d - L_q) * i_s^2 \sin 2\delta + \lambda_{pm} * i_s * \sin \delta) \qquad (4.3.3.3)$$

From this equation it is conclusive that controlling the torque angle it is possible to control the electromagnetic torque applied to the motor. Looking at the vector diagram in order to change δ it is just necessary to change the position of the stator flux using a stator voltage as PWM or SVM.

During the transient operation of the motor δ will change making that the stator and rotor flux rotate with different speed. But in steady state, δ is constant and corresponds to the load torque. In the next picture it is presented the scheme of the predictive controller.
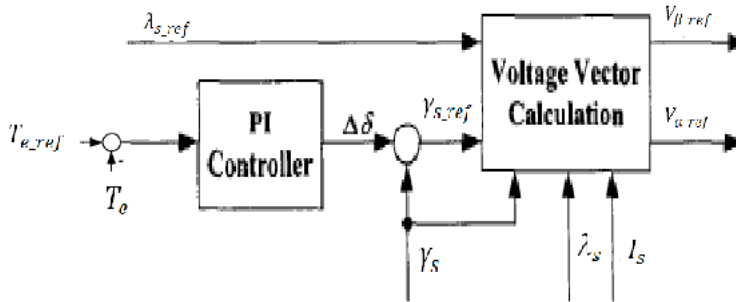
Figure 40 Predictive controller, edited from [17]

So the predictive controller based on the actual position of the flux will calculate which voltages V_α and V_β that should be applied to the stator in order to change the torque angle until the actual electromagnetic torque does not equalizes the torque reference.

The torque angle increment $\Delta\delta$ is result of the PI controller that has as input the torque error, making the increment torque angle proportional to the torque error and so minimizing this last one.

So the voltage modulator just has to apply V_α and V_β such that the vector flux in the stator has module λ_{s_ref} and γ_{s_ref} angle.

Using the fixed reference frame $\alpha - \beta$ the stator voltage is given by:

$$\begin{cases} V_\alpha = r_s * I_\alpha + \dfrac{d\lambda_\alpha}{dt} \\ V_\beta = r_s * I_\beta + \dfrac{d\lambda_\beta}{dt} \end{cases} \qquad\qquad (4.3.3.4)$$

Discretizing the equation with a sample time T_s the flux derivate is replaced by differences between the actual flux and flux reference over the sample time, resulting in the next equation:

$$
\begin{cases}
V_{\alpha\_ref} = r_s * I_\alpha + \dfrac{\lambda_{Sref} * \cos\gamma_{s\_ref} - \lambda_s * \cos\gamma_s}{T_s} \\[3mm]
V_{\beta\_ref} = r_s * I_\beta + \dfrac{\lambda_{Sref} * \sin\gamma_{s\_ref} - \lambda_s * \sin\gamma_s}{T_s}
\end{cases}
\qquad (4.3.3.5)
$$

In this section will be presented the first results obtained from the designed controller, the parameters of the motor simulation are presented in the next table, it will also be this motor that will be used for implementation and test of the designed control.

Table 5 Motor EMRAX 228 Parameters

DC Bus Voltage	400 V
Stator Resistance	18 mΩ
d-axis Inductance	0.180 mH
q-axis Inductance	0.175 mH
Rotor flux	53 mWb
N° Poles	20

The resulting power and control block scheme can be observed in the next picture and the used simulation sample time was 1us and for the SVM was used a sample time of 100 us.
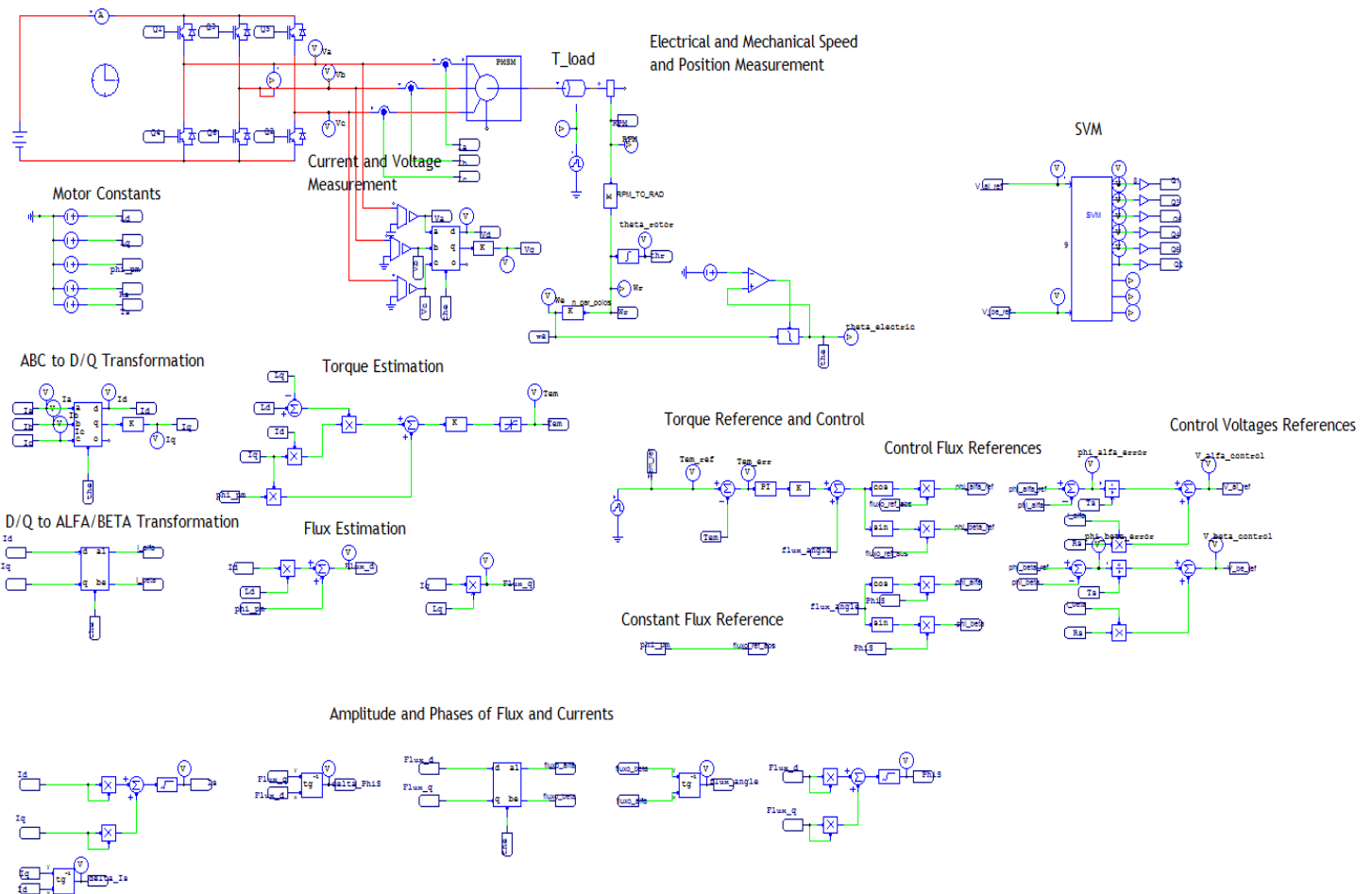
Figure 41 DTC simulation block scheme

This analysis is intended to test:
1. Response to a step;
2. Response to a ramp;
3. Regenerative brake (negative torque reference);
4. Torque load variation influence in the torque response;
5. Application of initial load;
6. Maximum torque overshoot.

From this analysis it will be possible to conclude if the torque controller satisfies the necessary criteria to be applied in the final design. The next picture presents the first simulation results.
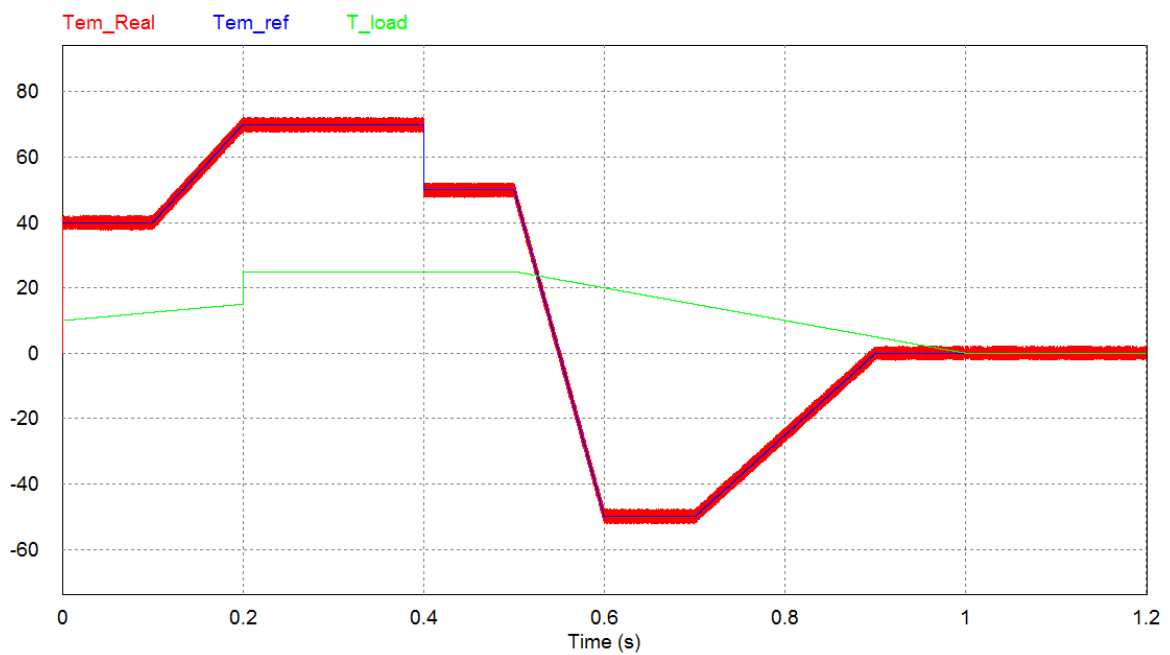
Figure 42 Torque response of the DTC with SVM

In the picture above, the red curve represents the real torque of the motor, with blue the torque reference given to the controller and with green load torque. At the initial instant the controller is able to answer perfectly to a step of 40Nm with an initial load of 10Nm. The answer to ramp references is also good as it is possible to observe from the time intervals [0.1; 0.2] s and at [0.5; 0.6]. In the first case the load is changing and keeps constant in the second time intervals. In both cases the reference is tracked with no influence of the load torque. To conclude at 0.6s it is given a reference of -50Nm being the performance the same as in the other cases. The next picture shows with more detail the time interval [0.2; 0.3] to evaluate the torque ripple.
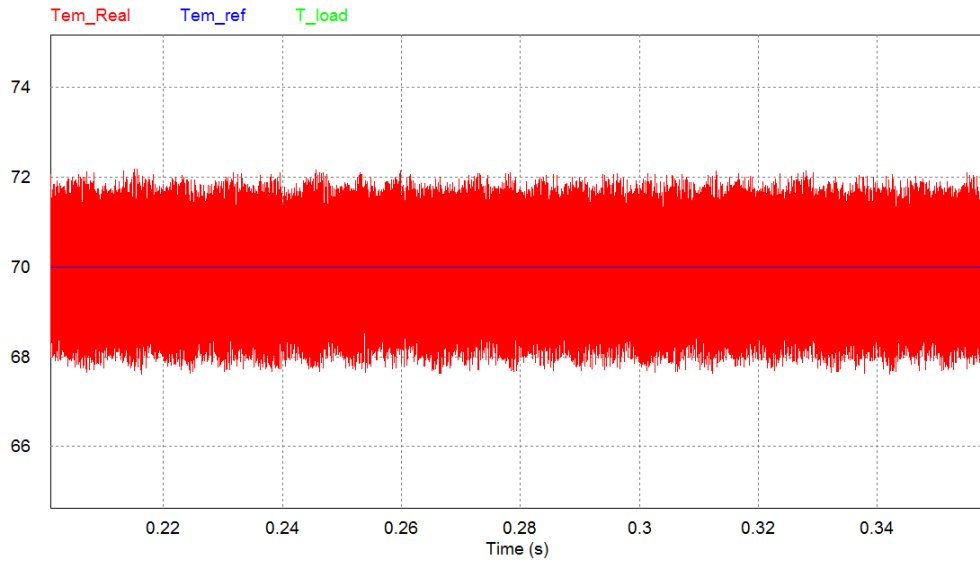
Figure 43 Torque ripple of DTC with SVM simulation result

It is clear that at low and high torque references the torque ripple is about 4Nm of amplitude. This torque ripple will increase as the speed increases being the motor near to instability. In this application the motor will be almost working in transient regimes and at low-speeds this is a problem that does not need to be evaluated. In the case to be necessary to control the torque ripple according with the motor speed two main actions should be done:

1. PI controller parameters should be adjusted according with the speed;
2. Decrease the limit of the torque reference as the speed increase;
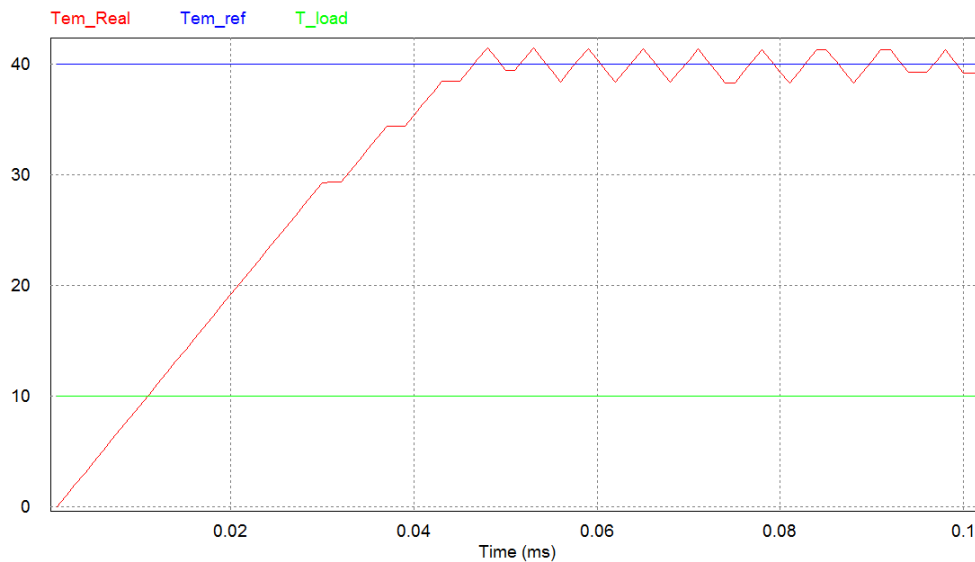
Figure 44 Settling time of DTC-SVM simulation result

This simulation result consists in a zooming of the initial instant. From this it is possible to conclude that the controller just needs around 50us to apply in the motor 40Nm even with an initial load of 10Nm.

Till now was been analysed only the torque response, but there are important characteristics to check. Because this control method is working with a constant flux reference, it should be verified if the flux in air-gap is constant and with the same value of the permanent magnets flux.
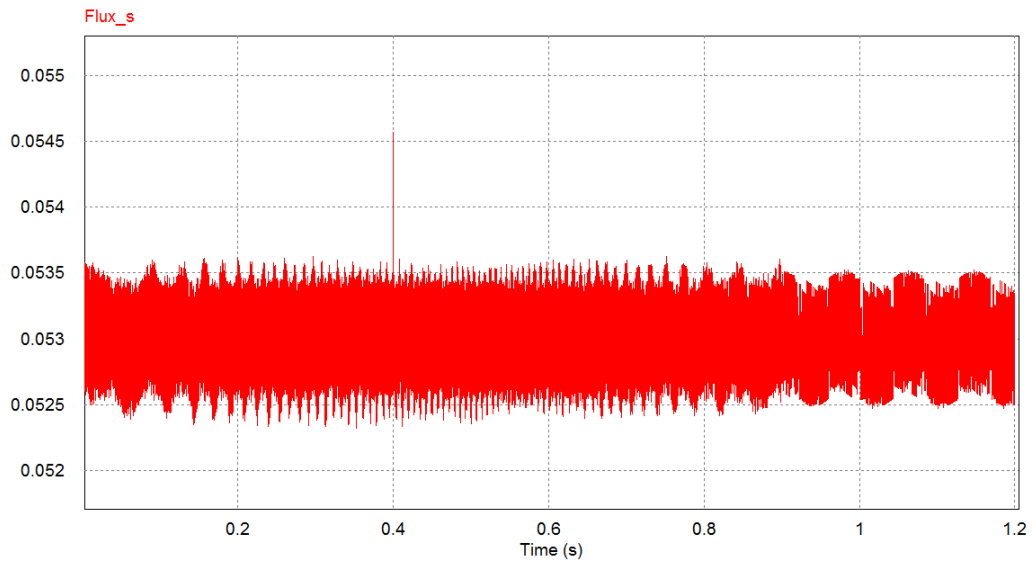
Figure 45Stator flux simulation result

As the simulation result shows, the flux is kept around the flux reference of 53mWb and does not vary more than 1mWb. With this the magnetization of the motor is kept constant protecting the motor from demagnetization.

Since the control reference voltages are given in the $\alpha - \beta$ reference frame, through the inverse of the Clarke Transform, it is possible to convert it in three phase reference voltage

to be applied in a PWM block scheme as presented in the sub-chapter 4.1.2. Using the same control as the presented for DTC-SVM and just replacing the SVM for the PWM, the obtained results are now presented. To be possible the comparison between the modulation methods results, the applied torque references and flux were the same for both methods. The simulation step was the same and the carrier frequency was 10 kHz.
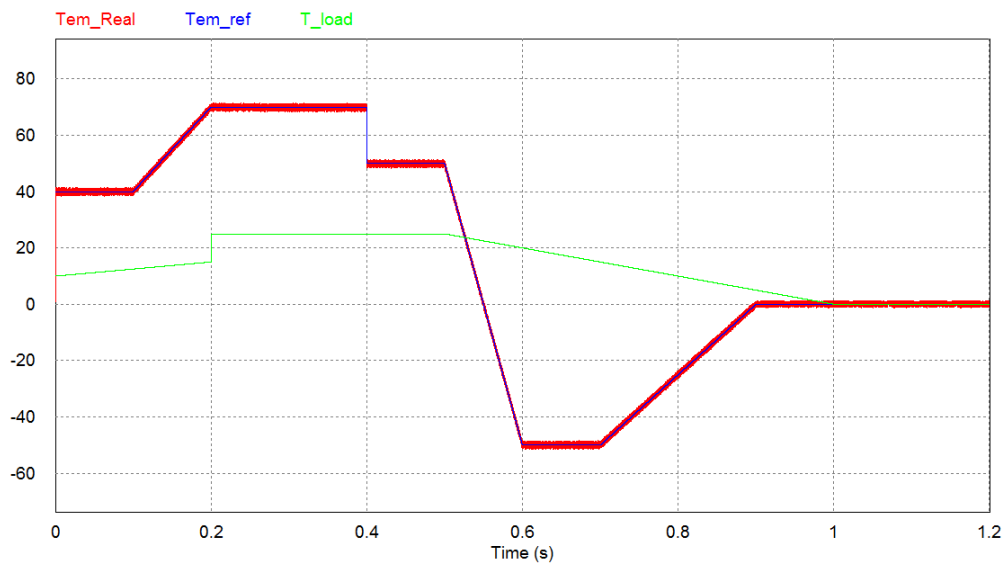
Figure 46 Torque response with DTC-SPWM simulation result
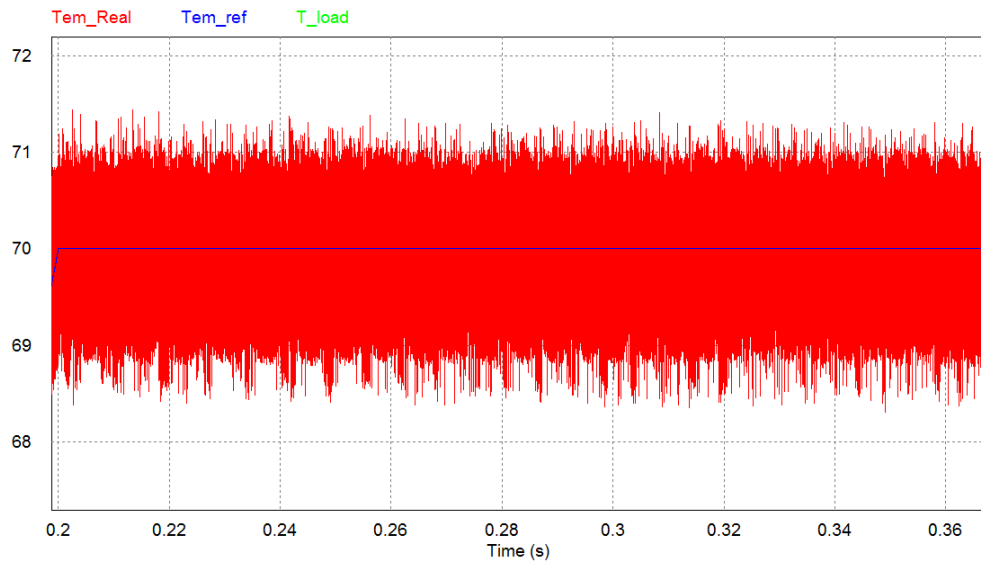
Figure 47 Torque ripple of DTC with SPWM simulation result
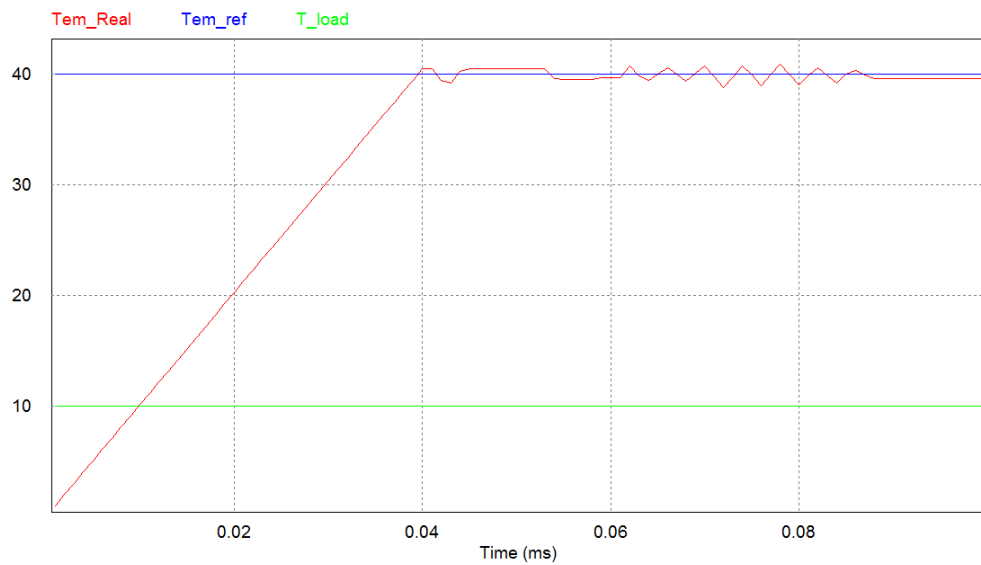
Figure 48 Settling time of DTC-SPWM simulation result

From the first simulation plot it is just possible to conclude that with both modulation methods are able to track the same torque references, but the first to important conclusions from this comparison is that the torque ripple is approximately half of the obtained with the SVM, as can be found in the second simulation plot. Also the step response time is inferior.

4.3.4. Conclusion

In this section it was presented the requirements that the design of the torque controller should fulfil. Through the comparison between two possible methods for torque control, FOC and DTC, it was concluded that for this application DTC is more suitable since it presents a better torque control which represents of the main requirements of the controller.

Based on the literature was presented a DTC-SVM scheme that was successfully implemented in the simulation environment. From the simulation results were verified the necessary performance requirements, such that torque ripple, no variation of the torque with the variation of the load, etc. In every test DTC-SVM has obtained good results so it can be used as the fundamental part final control design. The DTC-SVM method taken from the literature was adapted for the application of the SPWM as modulation method.

The same simulations were realized with this modified method and it was possible to get an even better performance with SPWM however the SVM still be able of discussion and simulation during the next steps of the control design.

Chapter 5

Control of the transport conveyor

5.1. Introduction

The new controller design should take in account the operation conditions to achieve better performance and also precision. It is important to control the acceleration and deceleration of the transport conveyor to avoid the drift of the tread that will lead errors in the cutting length. To have higher precision on the cutting machine, the position of the transport conveyor should be controlled. Lastly to guarantee the actual mode of operation of the transport conveyor it is necessary to control the speed, because has was explained before the actual cutting system consists basically in to impose some predefined speeds in the transport conveyor according with the position of the loop.

Therefore it is necessary to develop a drive that allows full control of the motor. The drive should control the electromagnetic torque in order to control the acceleration and deceleration, the speed and the position.

In this section will be discussed the optimal control problem but just in steady state, because what is pretended it is to design a controller that minimizes the final error of the transport system. The topic of time-varying optimal control could be also topic of discussion in order to optimize also the transient control regime, but another technique to optimize it will be presented, which allows a non-varying gain of the controller having a smaller computational cost.

5.2. Linear Quadratic Regulator

The problem of optimally tracking a reference has been received growing attention for precision applications due to its wide practical applications, such as the industrial robots, low power consumption as the industrial heaters [18].

Designed for Multiple Input Multiple Output (MIMO) systems, the optimal control methods allow the designer to determine an control law that minimizes a cost function J [19]. According with the chosen cost function the results can be just partially optimal.

In fact, for infinite time problem, the constant gain is optimal and it is called linear quadratic regulator[19]. There are several methods to find the value of K, such as solving the Ricatti equation or, the eigenvector decomposition but they will not be discussed here because it is not the objective of this project.

Using an feedback control law defined as

$$u = -Kx \tag{5.2.1.1}$$

For a given discrete system

$$x_{k+1} = A * x_k + Bu_k \tag{5.2.1.1}$$

The objective is to find an u_k so that a cost function defined in 5.2.1.2 is minimized.

$$J = \frac{1}{2}\sum_{k=0}^{\infty}[x_k^T * Q * x_k + u_k^T * R * u_k] \tag{5.2.1.2}$$

Q and R should be positive definite matrix and the pair (A, B) has to be stabilizable.
The value of K will be given by

$$K = (R + PB)^{-1}B^T PA \tag{5.2.1.3}$$

Where P is the unique positive definite solution of the Riccati equation

$$P = Q + A^T(P - PB(R + PB)^{-1}B^T P)A \tag{5.2.1.4}$$

Note that in order to get the solution it is necessary to iterate the Riccati equation until it converges.

5.2.1. Control Strategy

The control strategy is based on directly controlling the torque that is applied to the rotor. It is possible from the mechanical equation to predict dynamic and steady state behaviour. So the idea is firstly to build a state space model of the mechanical behaviour of the system and analyse the controllability, just after that it is possible to design a controller for the system. For analysis the mechanical equation of the motor is

$$T_{em} - T_L = J * \frac{d\omega_r}{dt} + B * \omega_r \tag{5.2.1.5}$$

where T_{em} is the electromagnetic torque, T_L the load, J the moment of inertia and B is the friction coefficient.

It is possible to build a state space model of the rotor movement, where the state is composed by the motor position θ and the angular speed ω_r.

$$x = \begin{bmatrix} \theta_r \\ \omega_r \end{bmatrix} \qquad \dot{x} = \begin{bmatrix} \omega_r \\ \dfrac{d\omega_r}{dt} \end{bmatrix} \qquad A = \begin{bmatrix} 0 & 1 \\ 0 & -\dfrac{B}{J} \end{bmatrix} \qquad B = \begin{bmatrix} 0 \\ \dfrac{1}{J} \end{bmatrix} \tag{5.2.1.6}$$

Using an incremental encoder to measure the position and the speed we have,

$$C = \begin{bmatrix} 1 & 1 \end{bmatrix} \qquad\qquad D = 0 \tag{5.2.1.7}$$

Now it is necessary to verify if the system is controllable or not. Introducing the state space model in Matlab and to calculate the controllability matrix the result was

$$Con = \begin{bmatrix} 0 & \frac{1}{J} \\ \frac{1}{J} & -\frac{B}{J^2} \end{bmatrix} \text{ and } rank(Con) = 2 \text{ for } J \in R \qquad (5.2.1.8)$$

So the controllability matrix is always non-singular, meaning that it is possible to control both states, the position and the speed of the motor, having as command the electromagnetic torque.

$$u = \begin{bmatrix} 0 \\ T_{em} \end{bmatrix} \qquad (5.2.1.9)$$

The discussion about the choice of the controller should be determined by the system requirements, so, in this case, because the necessity of high precision of the control position, the developed controller should:

    ✓   Minimize the position error;

    ✓   Have no overshoot;

    ✓   Minimum transportation time.

As was explained before, the LQR minimizes a cost function, in this case the cost function will be dependent on the position error e_θ and the speed error, e_{ω_r}, to satisfy the high precision requirement in steady state.

$$J = \begin{bmatrix} \theta_r \\ \omega_r \end{bmatrix} Q \lfloor \theta_r \quad \omega_r \rfloor + \begin{bmatrix} 0 \\ T_{em} \end{bmatrix} R \lfloor 0 \quad T_{em} \rfloor \qquad (5.2.1.10)$$

Adjusting the Q and R matrix it is possible adjust the transport time, however it is important to refer the speed of the system is always limited by the maximum torque of the motor and the maximum torque applicable to the tread imposed by the friction. Otherwise the tread can drift and the position error will not be controlled.
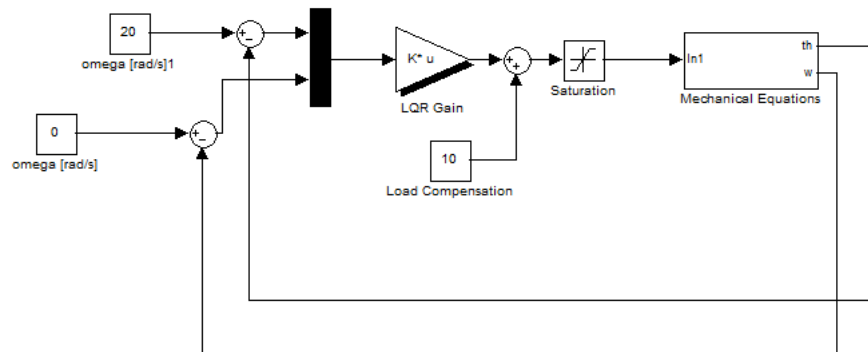
Figure 49 Simulink block scheme for simulation of the mechanical model controlled by the LQR

On the picture presented above it is presented the Simulink scheme used to simulate the theoretical system dynamics with the LQR controller. Was developed a Matlab scrip for easy determination of the gain K while the matrix Q and R were being adjusted. So the first simulations were done in Simulink with the theoretical model of the system. The maximum torque limitations of the motor are simulated through the saturation block that limits the reference torque from the LQR. The results can be observed on the next pictures for a position reference of 20 rad, speed reference of 0 rad/s and a torque load of 10Nm and with the torque reference saturation limit of 50Nm.
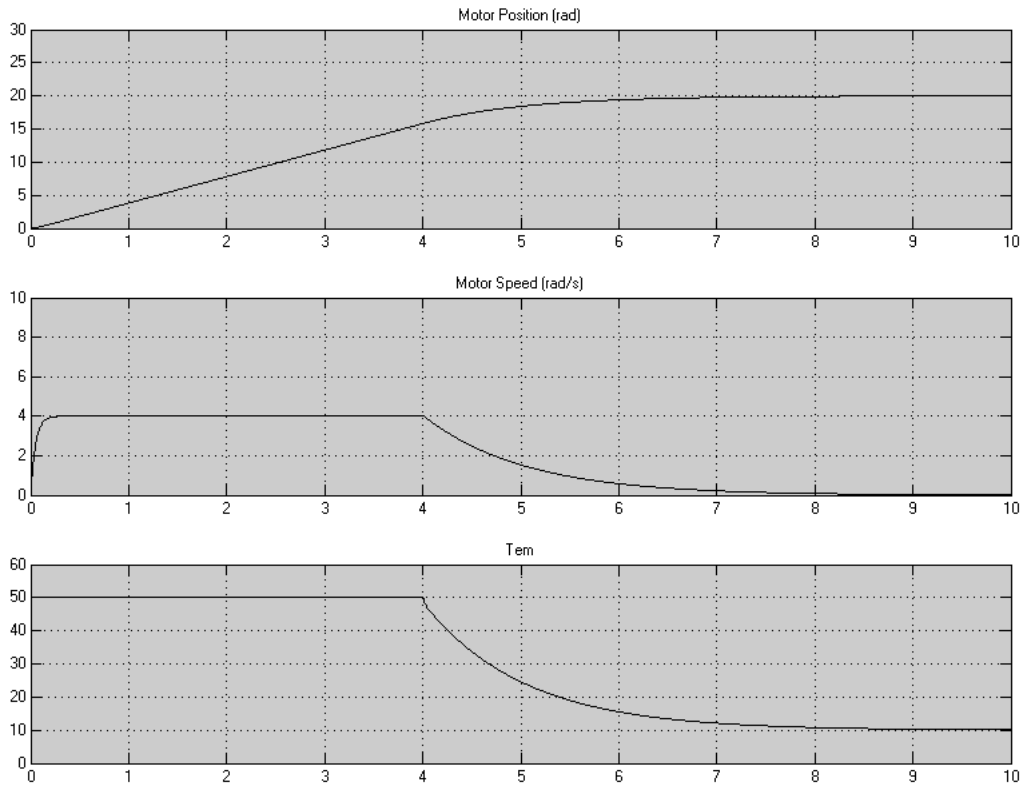
Figure 50 Simulation Results for $\theta = 20$ and $\omega = 0$ reference with a load of 10Nm. In the first picture is simulated the position control and in the second the speed control.

The next step was the integration of the LQR with the DTC in the PSIM simulation. This simulation was developed using a C code block of PSIM for each component of the controller resulting in the next block scheme. The fact that the simulation was developed using C code an advantage for later implementation.
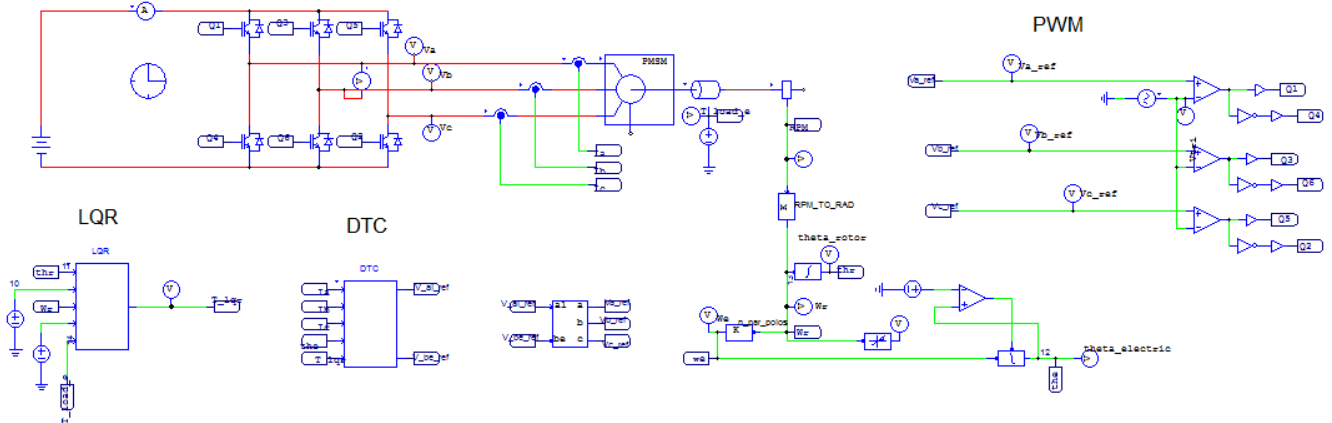
Figure 51 Position control block scheme implemented in PSIM

For now it will be considered that the load torque is known, being this value added to the torque reference from the LQR to compensate the system. To procedure the validations of the LQR were performed two simulations. Firstly was simulated the position control, to do it was given a position reference of 20 rad and a null speed reference, so the rotor has to stop in this position. Furthermore was simulated the speed control, but to do it, it is necessary to give also the desired speed reference and use as position reference the feedback position from the encoder. In this way the position error is always zero and do not take place in torque reference generated by the LQR, just the speed error is taken in account.
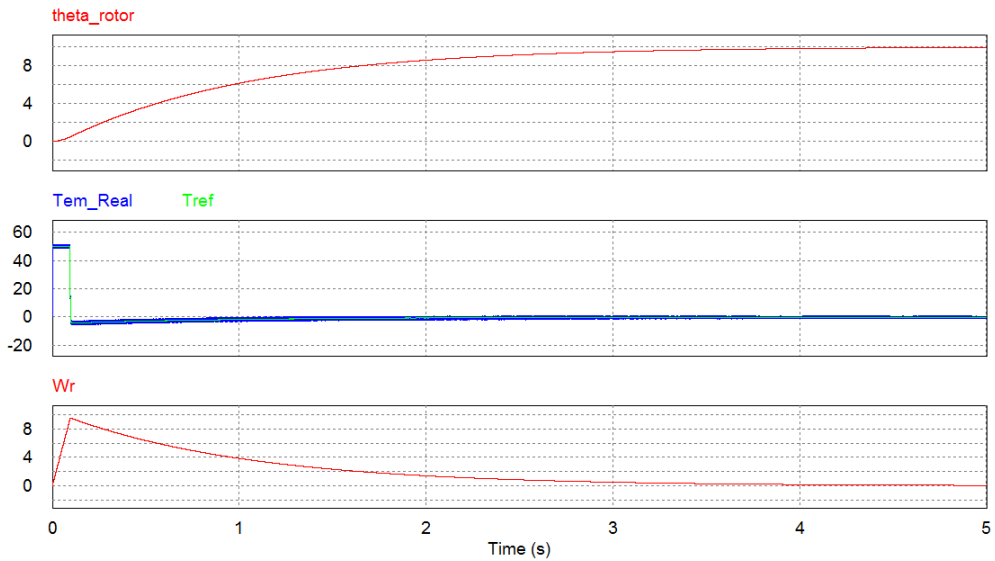
Figure 52 Position control simulation results for a position reference of 10 rad.

The first conclusion that can be taken is that the system is able to control the rotor position. However the settling time is too long. Looking at the torque reference generated by the LQR it is possible to see that the controller just actuate during a short time period. It just accelerates the rotor the necessary that when it stops to accelerate, the rotor will be decelerated by the inertial and it will stop at reference position.

In the speed control simulation was used a speed reference of 10 rad/s and using the same load torque of 10 Nm as before.
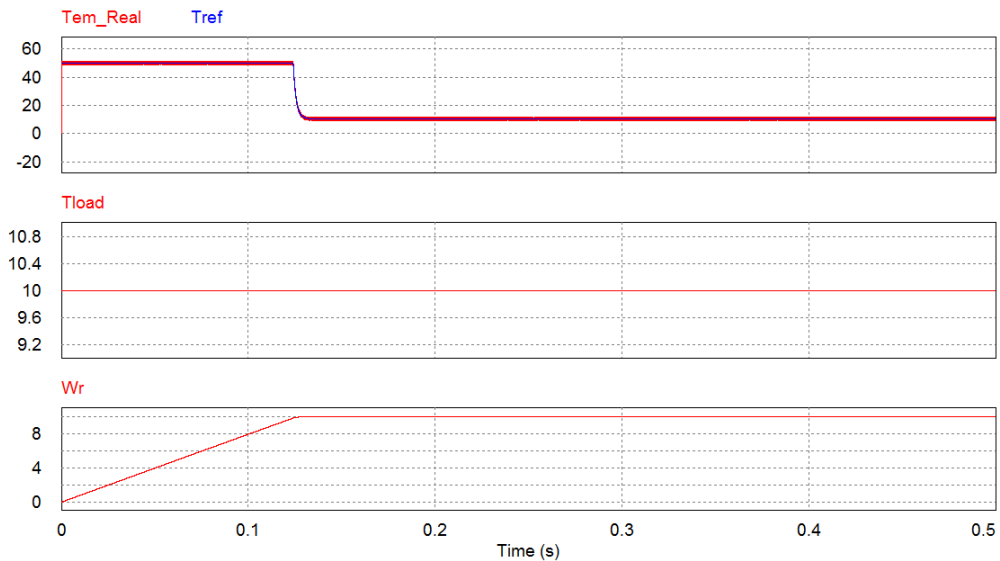
Figure 53 Speed control with LQR for a speed reference of 10 rad/s

As speed controller the LQR has good performance, no overshoot and null error in steady state.

Until now was assumed that the load is known. However it is important to test the condition where the controller does not know the load value, to ensure that the position control is not affected. The result, where the load torque is added to the torque reference generated by the LQR, is on figure 54.
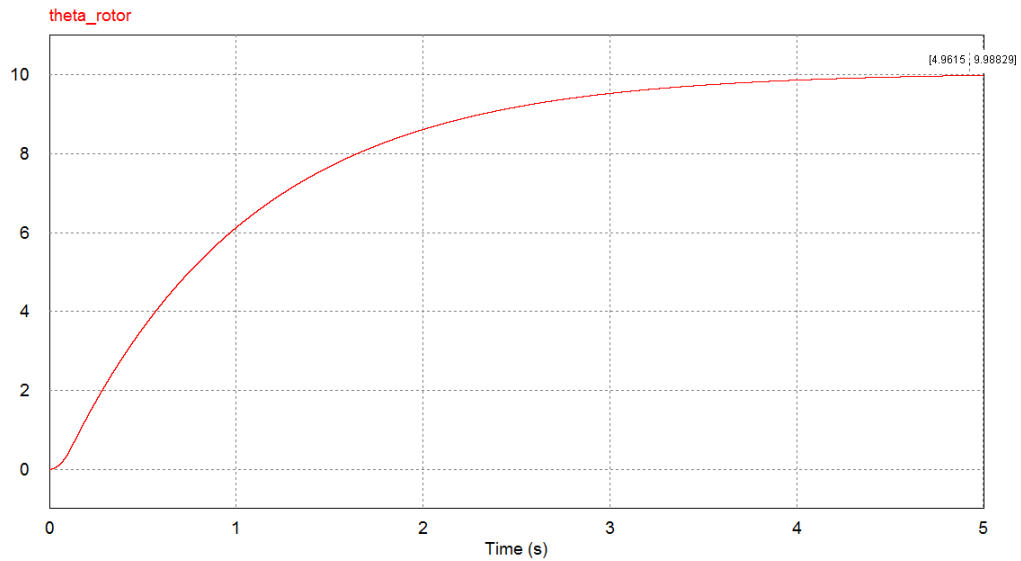
Figure 54 Position control with load compensation

In order to conclude if the load compensation has effect in steady state position error, it was performed the same simulation but without compensate it. The results can be found in figure 55.
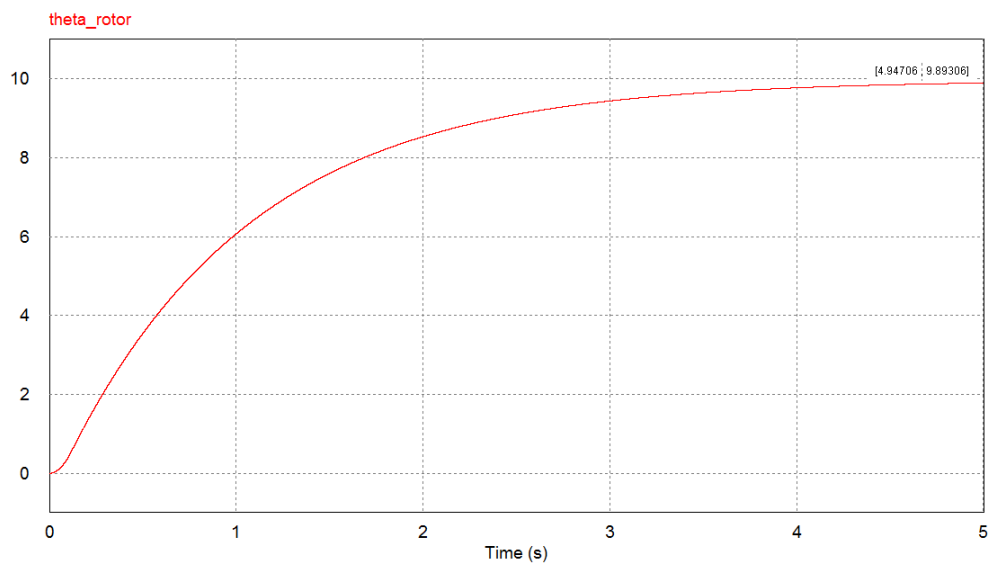
Figure 55 Position control without load compensation

The final rotor position of the rotor is 9.893rad for a position reference of 10rad, which represents an error of approximately 10%. When comparing with the result presented in the figure 54, for the same time instant the rotor position is 9.988rad which represents an error about 1%, 10 times smaller. It is clear from this last two simulation results that the fact that if the load is unknown will introduce a steady state and constant error that it is not eliminated by the LQR. The error introduced by the non-compensation of the load is proportional to the time of movement, and so bigger for larger positions references. This happens because the load torque compensation is an acceleration increment of the rotor resulting in an increase of the final position proportional to the square of this acceleration.

5.2.2. Conclusions

The LQR controller allows both position and speed control, minimizing the square of the error position and error speed, being in advantage when comparing with linear controllers as the example of the Proportional Integrative Derivative controller (PID). It also allows controlling the position and speed without overshoot.

Nonetheless the position control is not time optimal. Looking to the output of the controller, the generated torque reference is always positive and it means that the capacity to brake is not used.

The optimized way to move from one point to another is to accelerate the maximum as possible and start braking at exact instant that we are going to stop at desired final position. Because LQR is a linear controller, it only generates negative torque references after the rotor passes through the position reference, this means that the transportation time can be optimized if the controller uses the capability to brake, minimizing the transportation time and also allowing power regeneration, reducing the power consumption.

However it was observed that if the load is not compensated, the controller is not able to eliminate the steady state position error.

5.3. Load Estimator

5.3.1. Introduction

Till now the developed control topology is able to control all the state variables of the PM motor, however, as it was concluded in the last section, the steady state error in the control position is larger if the load is not compensated, which can be unacceptable for the end of the application. So it is mandatory to know the load that is applied to the motor. It can be measured trough the load sensors application or by estimation. With the estimation the costs of the application can be reduced, since the load sensors are expensive [20]. On the other hand, the sensor measurements can failure and are affected by the noise. Because of this and more reasons that are topic of later discussion, it was proposed to develop a load estimator to solve the permanent error in the control position.

5.3.2. The Extended Kalman Filter

The Kalman filter was developed by Rudolph Kalman in 1960. In spite of originally developed for use in spacecraft navigation, the Kalman filter turns out to be used in many different applications[21]. Based on the state space model equations of the process, the Kalman filter is able to estimate the state variables from a certain measurements, which can be operated when the dynamic system is disturbed by Gaussian noise[22].

Also known as Linear Quadratic Estimator is an algorithm that uses a series of measurements, affected by Gaussian noise that produces statistical optimal estimations of unknown variables.

Because the Kalman filter was developed for linear systems, the Extended Kalman Filter (EKF) is a nonlinear version of the Kalman filter. The EKF linearizes all nonlinear transformations and substitutes the linear transformations of the Kalman filter by Jacobian matrices, maintaining the computational cost and efficiency[23].

In this way the state transition and observation model can be non-linear functions, defined at each instant k as:

$$\begin{cases} x_k = f(x_{k-1}, u_{k-1}) + w_{k-1} \\ \quad\quad z_k = h(x_k) + v_k \end{cases} \tag{5.3.2.1}$$

Where w_k and v_k are the process and observation noises which are both assumed to be Gaussian with zero mean and with covariance Q_k and R_k respectively.

The EKF is a recursive algorithm and is divided with three main parts:

    I.   Prediction
    II.   Observation
    III.   Correction

The function $f(x_{k-1}, u_{k-1})$ is used to compute the predictive state and $h(x_k)$ the predictive measurement. To compute the predictive covariance matrix by the fact that the system is non-linear, it is necessary to compute the Jacobian of each matrix.

$$F_k = \frac{df}{dx_k}(x_k, u_k) \tag{5.3.2.2}$$

$$H_k = \frac{dh}{dx_k}(x_k, u_k) \tag{5.3.2.3}$$

In equation 5.3.2.2 and 5.3.2.3 are defined the Jacobian process and observation covariance matrix, respectively, correspondingly the Kalman filter algorithm is the followed.

Prediction

State estimation

$$x_{k|k-1} = f\left(x_{k-1|k-1}, u_{k-1}\right) \tag{5.3.2.4}$$

Covariance estimation

$$P_{k|k-1} = F_{k-1}P_{k-1|k-1}F^T_{k-1} + Q_{k-1} \tag{5.3.2.5}$$

Observation

Measurements from the sensors

$$z_k = h(x_k) + v_k \tag{5.3.2.6}$$

Correction

Innovation or estimated measurement error

$$y_k = z_k - h\left(x_{k|k-1}\right) \tag{5.3.2.7}$$

Innovation covariance

$$S_k = H_k P_{k|k-1}H_k{}^T + R_k \tag{5.3.2.8}$$

Kalman gain

$$K_k = P_{k|k-1}H_k{}^T S_k{}^{-1} \tag{5.3.2.9}$$

Corrected state estimate

$$x_{k|k} = x_{k|k-1} + K_k y_k \tag{5.3.2.10}$$

Corrected covariance estimate

$$P_{k|k} = (I - K_k H_k) P_{k|k-1} \tag{5.3.2.11}$$

At each time step, the Jacobian is evaluated with current predicted states. These matrices can be used in the Kalman filter equations. This process essentially linearizes the non-linear function around the current estimated.

5.3.3. Load Estimator

In position and speed control a simple adjust of the control parameters could solve the disturbance of the load torque, although this is just possible considering it constant [20]. As it was observed before the load has effect in the performance and in the stationary error. To eliminate this effect of the load torque it is necessary to compensate the torque reference with the load torque value. With an EKF it is not only possible to estimate this load torque but also the speed and the position of the motor. This can be also used for failure detection of the position and speed sensor, resulting in a more robust system and being able for sensorless application.

Taking again the stator voltages in d-q frame

$$\begin{cases} V_d = R_s * I_d + \dfrac{d\lambda_d}{dt} - w_e \lambda_q \\ V_q = R_s * I_q + \dfrac{d\lambda_q}{dt} + w_e \lambda_d \end{cases} \tag{5.3.3.1}$$

and the flux expressions

$$\begin{cases} \lambda_d = L_d I_d + \lambda_{pm} \\ \lambda_q = L_q I_q \end{cases} \tag{5.3.3.2}$$

it is possible to get the following expression

$$\begin{cases} V_d = R_s * I_d + L_d * \dfrac{dI_d}{dt} - w_e L_q I_q \\ V_q = R_s * I_q + L_q * \dfrac{dI_q}{dt} + w_e L_d I_d + w_e \lambda_{pm} \end{cases} \tag{5.3.3.3}$$

Solving in order to the derivative of I_d and I_q it results:

$$\begin{cases} \dfrac{dI_d}{dt} = -\dfrac{R_s}{L_d} * I_d + p * w_r \dfrac{L_q}{L_d} I_q + \dfrac{V_d}{L_d} \\ \dfrac{dI_q}{dt} = -\dfrac{R_s}{L_q} * I_q - p * w_r \dfrac{L_d}{L_q} I_d - p * w_r \dfrac{\lambda_{pm}}{L_q} + \dfrac{V_q}{L_q} \end{cases} \tag{5.3.3.4}$$

From the equation of the electromagnetic torque and the mechanical equation

$$\begin{cases} T_e = \dfrac{3}{2} * p * (\lambda_{pm} * I_q + (L_d - L_q) * I_q * I_d) \\ T_e - T_L = J\dfrac{dw_r}{dt} + Bw_r \end{cases} \Rightarrow \dfrac{dw_r}{dt} = \dfrac{3}{2} * \dfrac{p}{J} * (\lambda_{pm} + (L_d - L_q) * i_d) * i_q - \dfrac{B}{J} w_r \tag{5.3.3.5}$$

At last assuming that the variation of the load torque is slower and so

$$\dfrac{dT_L}{dt} \approx 0 \tag{5.3.3.6}$$

These last 4 equations are the state equations, having the state defined has:

$$x = [I_d \quad I_q \quad \theta_r \quad \omega_r \quad T_L]^T \tag{5.3.3.7}$$

In the final system design it is pretended to measure both position and speed of the rotor through an incremental encoder, so the output matrix will be defined has:

$$H = \begin{bmatrix} 1 & 0 & 0 & 0 \\ 0 & 1 & 0 & 0 \\ 0 & 0 & 1 & 0 \\ 0 & 0 & 0 & 1 \end{bmatrix} \tag{5.3.3.8}$$

To complete the EKF the state matrix and the input matrix are:

$$A_{x_k} = \begin{bmatrix} -\dfrac{R_s}{L_d} & p*w_r\dfrac{L_q}{L_d} & 0 & 0 & 0 \\ -p*w_r\dfrac{L_d}{L_q} & -\dfrac{R_s}{L_q} & 0 & -p*\dfrac{\lambda_{pm}}{L_q} & 0 \\ 0 & 0 & 0 & 1 & 0 \\ 0 & \dfrac{3}{2}*\dfrac{p}{J}*\left(\lambda_{pm}+\left(L_d-L_q\right)*i_d\right) & 0 & -\dfrac{B}{J} & -\dfrac{1}{J} \\ 0 & 0 & 0 & 0 & 0 \end{bmatrix} \tag{5.3.3.9}$$

$$B = \begin{bmatrix} \dfrac{1}{L_d} & 0 \\ 0 & \dfrac{1}{L_q} \\ 0 & 0 \\ 0 & 0 \\ 0 & 0 \end{bmatrix} \tag{5.3.3.10}$$

Now it is necessary to discretize the equation of the EKF with a sample time T_s. To do that the state matrix should be:

$$F_{x_k} = I_5 + A_{x_k}*T_s \tag{5.3.3.11}$$

And the state prediction equation should be:

$$x_{k|k-1} = F_{x_k}*x_{k-1|k-1} + B*u_{k-1}*T_s \tag{5.3.3.12}$$

The EKF gain is obtained by iteration, and can change every cycle. Because there are many matrix calculations, and with big dimensions the computation takes a lot time. It is also necessary to adjust the Q_k and R_k to get good and fast estimation results [20]. By choosing these matrix diagonals, so by setting the initial covariance matrix, P also diagonal, then it is possible to know that all the predicted and corrected covariance matrixes are diagonal. This can simplify the calculations and also the computational cost of the inverse matrix of S_k.

To validate the developed EKF is used PSIM and the SIMCOUPLER to get all the data necessary to simulate the EKF in offline mode. Was used an block scheme from PSIM with the DTC working correctly and a Matlab script to first test the EKF and adjust the covariance noise matrix. The block diagram of Simulink to get the data is presented in the next picture.
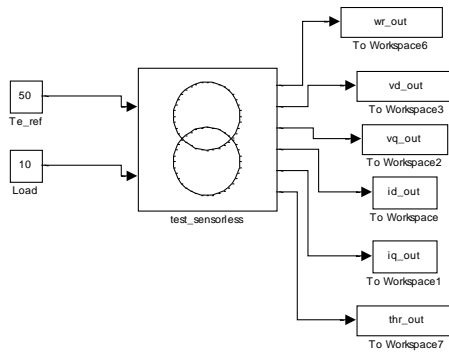
Figure 56 Simulink block scheme in order to get offline data to simulate the EKF in the Matlab script

The first obtained results are presented in figure 57. Firstly, the validation of the application of the EKF as a load estimator consists on the evaluation of the estimation time and in the correct estimation of the load value. So, if the EKF estimates correctly the load value and it has an estimation time smaller than the transportation time it can be applied as a load estimator. From the first simulation results it is possible to conclude that the EKF takes around 0.3 seconds to estimate the load torque. This way, the EKF can be used as a load estimator but it is still necessary to analyse the simulation results in closed loop in order to verify if the estimation is fast enough to reduce significantly the error in steady state.
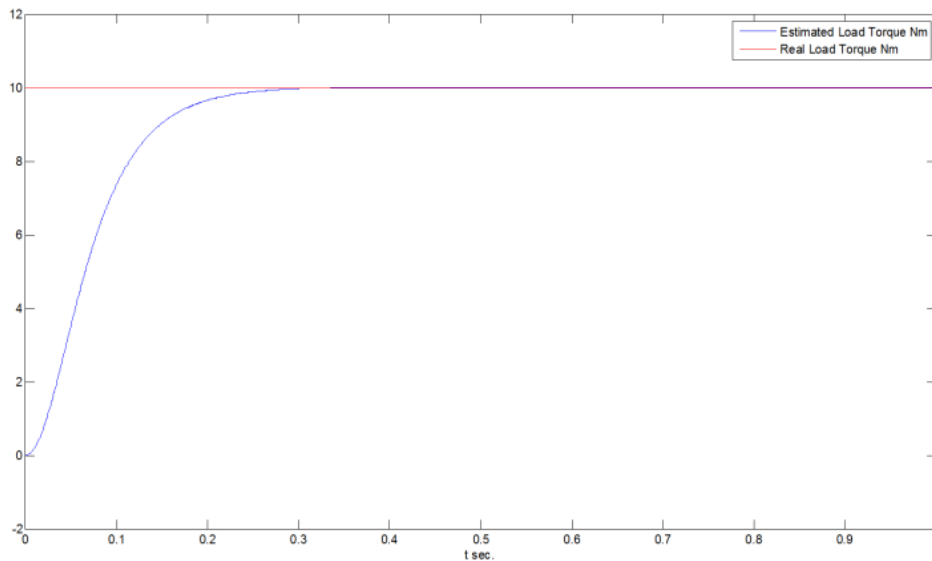
Figure 57 Load estimation results from the Matlab script for an real load of 10Nm

5.3.4. DTC-LQR with load compensation

So now using the PSIM ability of running a DLL file through the DLL Block, the estimator was programmed in C code and tested in PSIM in open-loop with all the designed control system. Below are presented the results.
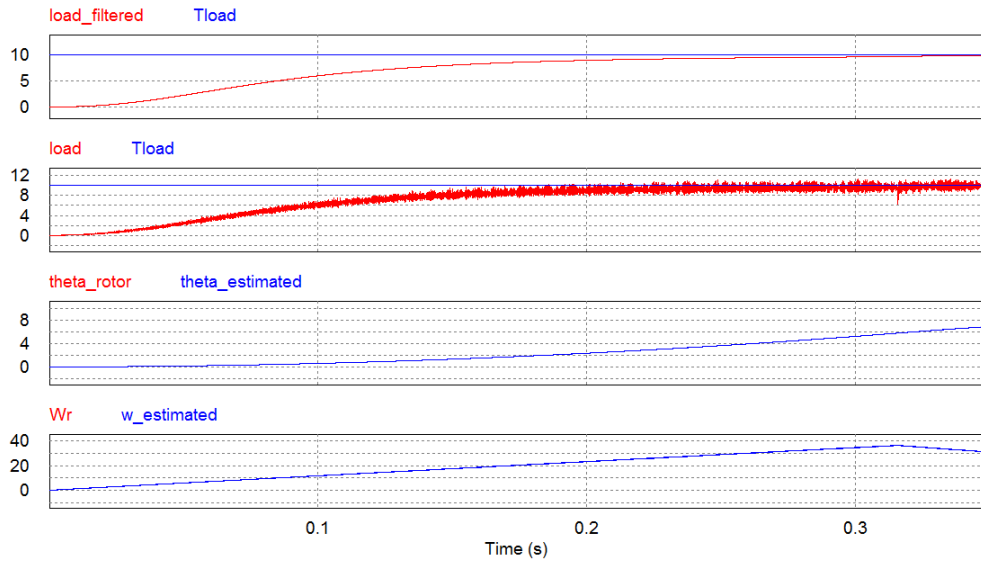
Figure 58 Estimation results of the EKF in PSIM

According with the obtained results is necessary to apply a second-order low-pass filter with a cut-off of 100 Hz to eliminate the oscillation present in the load estimation.   This variation present in the estimation can be seen in the second plot. The first plot presents the filtered estimation which has no variation and corresponds with the real value of the load. The estimation time is short enough because in the position control it is just necessary to compensate the load torque in steady state and it is expected to have transport times that have more than 2 seconds.

In the third and fourth plot are present both measured and estimate position and speed, as the curves are in overlap, the estimation results corresponds with the real values as it is expected.

Finally to verify the efficiency of the load compensation by the EKF is simulated the position and speed control, but now the estimated load is added to the LQR torque reference.

I.   Simulation of the position control with the EKF as torque compensator
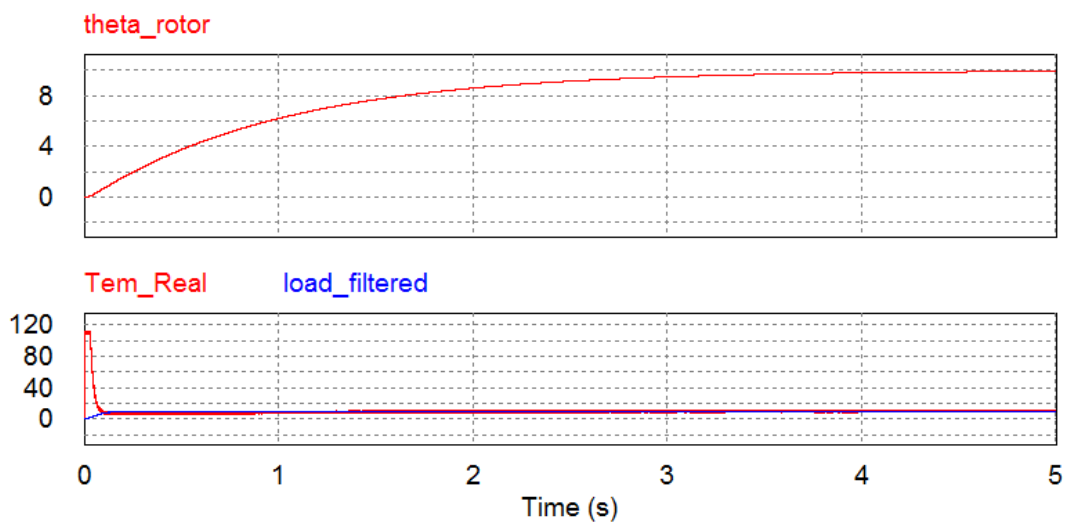
Figure 59 Position control with load compensation

Comparing with the result presented in the sub-chapter 5.2, for the same time instant there was an improvement of the steady state error around the 0.4%. In spite of this result is not too much significant but can be for larger positions reference. Looking at the figure 59 to the second plot, it is possible to observe that the time necessary to estimate the load is approximately the time of actuation by the LQR, concluding that for short movements is necessary a faster estimation. However for larger movements the actuation time is longer and so the load compensation can have significant effect and the estimation time can be neglected. It is also important to not forget that the final applications require really high precision and a gain of 0.4% on the precision of the system can be significant.

II. Simulation of the speed control with the EKF as torque compensator to eliminate the variation on the speed
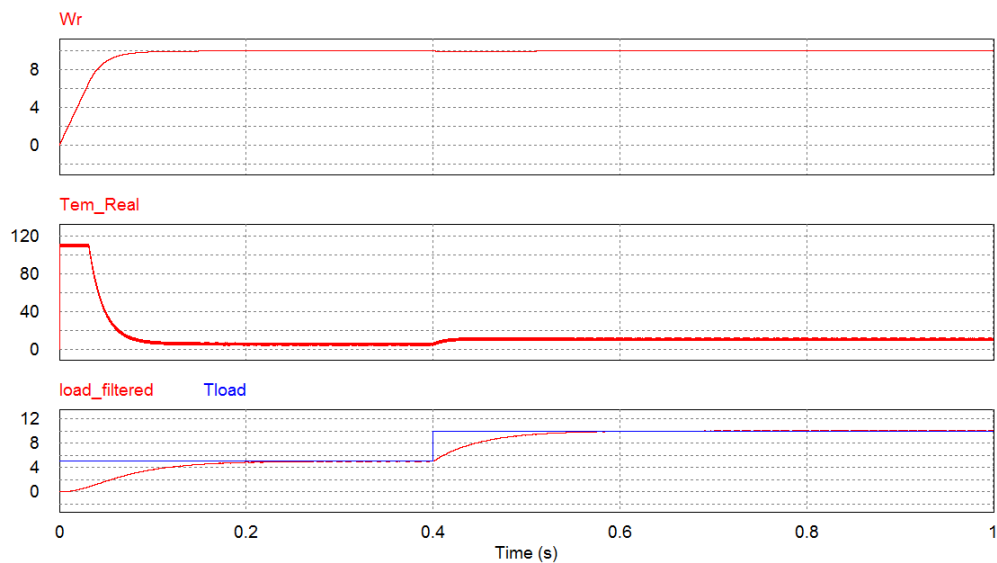
Figure 60 Speed control with load compensation

From the simulation result presented above it is possible to see a good performance in the speed control. At the beginning the applied load of 5Nm has no influence in the speed control, because the EKF is fast enough to compensate before the steady state of the controller. The estimation takes around 200ms, until it gets the final value the load has influence in the speed control, has can be observed at 0.4s when is applied an load change of 2 times the initial load. In spite of the load has influence on the speed while EKF is estimating the load change, this influence is around 2% of the total speed. Of course that this variation on the speed is proportional to the value of the load however the EKF start immediately to compensate the load change reducing its influence during dynamics period.

5.3.5. Conclusion

Using the electrical and mechanical equations of the PM motor it was possible to design an EKF as load estimator. It was developed two different simulations in order to evaluate the correction estimation of the load and also the improvements introduced by the load compensation.

In the first simulation it was verified the increase of precision in the position control introduced by the load compensation. The load compensation has also an important role in the control position, not only because, if there is a load applied to the rotor, it can preclude

the controller to reach the desired final position, but also because when the rotor reaches the final position the torque applied by the controller is null, so it is necessary to compensate the load, otherwise the applied load would move the rotor to a wrong position.

On the other side was verified that with the load compensation was possible to achieve a robust control of the motor speed, since the perturbations introduced by the load variation were compensated.

The only problem of the EKF is computational cost due to the matrix product with high dimensions, the inverse and transpose matrix calculations, among others. The time simulation has suffered 400% increase with the addition of the EKF as load compensator. Therefore it could be necessary, during the implementation phase, to have a dedicated microcontroller, just to implement the load estimator.

5.4. An optimal controller

5.4.1. Introduction

In the previous section it is concluded that the developed control system, has higher precision but longer transportation times comparing with the actual transportation system, which is not acceptable. Even though the controller was able to eliminate the steady state error the settling time was too long for the final application. Even that the new control design permits a high precision system, it could not ever be slower than the actual system, otherwise the production would fall which represents loss of money to the enterprise. So it is mandatory to develop a method that takes the precision advantage of the actual control system presented and accelerate it without affect the precision.

5.4.2. Model Predictive Control

The MPC, or Model Predictive Control, consists in a method of process control that has been in use in the process industries. Its objective is to optimize the forecasts of process behaviour that are based in the model of the system that it is the essential element of an MPC controller. Because models are not always a perfect representation of the real system, some undesired effects can occur, which are reduced introducing more details to the model.

The main advantage of this model is the time optimization. This is achieved by solving on-line, at each time instant, a finite horizon open-loop optimal control problem, using the current state of the plant and the optimization yields an optimal control sequence[24]. The components of MPC are:
- ✓ Prediction Model
- ✓ Objective function
- ✓ Obtaining the control law

The MPC is successful in industry because it can be used in multi-variable control problems, takes in account the actuator limitations and operation constraints, and it is easy to tune and handles structural changes[25].

So assuming a linear model:

$$\begin{cases} x_{k+1} = Ax_k + Bu_k + d \\ \quad\; y_k = Cx_k + v \end{cases}$$

(5.4.2.1)

Where d and v are the input and output disturbances, respectively. The output control law

$$u_k = f(x_k) \qquad (5.4.2.2)$$

Should be such that minimizes the cost function

$$\phi = \frac{1}{2}\sum_{k=0}^{\infty}(y_k - \bar{y})'Q(y_k - \bar{y}) + (u_k - \bar{u})'R(u_k - \bar{u} +) + \Delta u_k'S\Delta u_k \qquad (5.4.2.3)$$

Q, R and S are symmetric and positive definite matrix, $\bar{y}$ is a vector with the desired output target and $\bar{u}$ the desired input target. When is not measured the complete state of the plant, it is necessary to estimate it.

5.4.3. A new algorithm for optimal time position control

Empirically the optimal way to reach one position stopped and starting from another with zero speed is to accelerate the maximum that it is possible and starts breaking in the right instant that it will go to stop at the position that was pretended to reach.

But the problem is how to know the right time to start braking? Looking once more to the mechanical equation of the rotor and applying the unilateral Laplace transform two times. In the first it is considering a function of the rotor speed and in the second function of the rotor position. The equations get the next form.

$$\begin{cases} T_e = J * \omega(s) * s + B * \omega(s) \\ T_e = J * \theta(s) * s^2 + B * \theta(s) * s \end{cases} \qquad (5.4.3.1)$$

Solving in order to $\omega(s)$ and $\theta(s)$ respectively, it results

$$\begin{cases} \omega(s) = \dfrac{\dfrac{T_e}{J} + \omega_0 * s}{s * (s + \dfrac{B}{J})} \\ \theta(s) = \dfrac{T_e}{s^2(J + s + B)} + \dfrac{J * \theta_0}{J * s + B} + \dfrac{J * \omega_0 + B * \theta_0}{J * s^2 + B * s} \end{cases} \qquad (5.4.3.2)$$

Where ω_0 and θ_0 are the initial speed and position when it is applied a constant torque T_e. In order to get the expressions in the time domain, it is necessary to apply the inverse of the Laplace transform, the results are:

$$\begin{cases} \omega(t) = \dfrac{T_e}{B} - \dfrac{T_e}{B}e^{-\frac{B}{J}t} + \omega_0 e^{-\frac{B}{J}t} \\ \theta(t) = \dfrac{T_e}{J}\left(\dfrac{J}{B} + \dfrac{J^2}{B^2}e^{-\frac{B}{J}t} - \dfrac{J^2}{B^2}\right) + \theta_0 e^{-\frac{B}{J}t} + \dfrac{J * \omega_0 + B * \theta_0}{J}\left(\dfrac{J}{B} - \dfrac{J}{B}e^{-\frac{B}{J}t}\right) \end{cases} \qquad (5.4.3.3)$$

Replacing T_e for the constant maximum brake, T_{brake}, and equating the speed equation to zero, it is possible to obtain the time instant that the rotor would stop if the rotor was moving with a speed ω_0 and it was at position θ_0 when the brake was starting to be applied.

$$t_{stop} = -\frac{J}{B}\ln\frac{-\dfrac{T_{brake}}{B}}{-\dfrac{T_{brake}}{B} + \omega_0} \qquad (5.4.3.4)$$

With the time instant and using the time position equation, it is possible to know where the rotor would stop. With this it is possible to build an algorithm that will control the position reference given to the LQR controller. Considering $\theta_{controlled}$ as the generated position reference by the algorithm, θ_{ref} the desired final position to the rotor, the steps of the algorithm are presented:

1. At beginning $\theta_{controlled} = k_{control} * \theta_{ref}$, with $k_{control} > 1$ such that LQR will apply the maximum available torque to accelerate the rotor;
2. At each time step calculates t_{stop}, using the equation 5.4.3.4 based on the information of the actual speed and position from the encoder;
3. Using the equation 5.4.3.3 calculates the predicted stop position, $\theta_{predict}$;
4. Finally if $\theta_{predict} > k_{threshold} * \theta_{ref}$ with $k_{threshold} \approx 1$, $\theta_{controlled} = \theta_{ref}$.

This is a kind of predictive controller because it is iterative. At each time step, the information from the system is read and it is based on the model system equations to predict the possible futures scenarios of the system. Although it does not try to minimize a cost function, instead when the predict position is closed to the desired final position, it changes the position given to the LQR to the real final position. When the given position reference given to the LQR is changed, the system is being moved to an exaggerated position, so it is moving too fast to stop in this new position reference. Because the LQR is able to control the position without overshoot, when it sees the change of reference it will be obliged to give a negative torque reference to the DTC in order to brake the rotor and stop it before it passes through the final position.

5.4.4. Optimal controller simulation

The predictive controller is the final component of the controller designed. It is also implemented in the simulation platform in C using PSIM. To integrate it is necessary to change the last block scheme. The position reference is given to the predictive controller, this generates the position reference to the LQR, which also receives the information about the existing load from the EKF and finally the LQR generates the torque reference to the DTC resulting in the next block diagram present in the following figure.
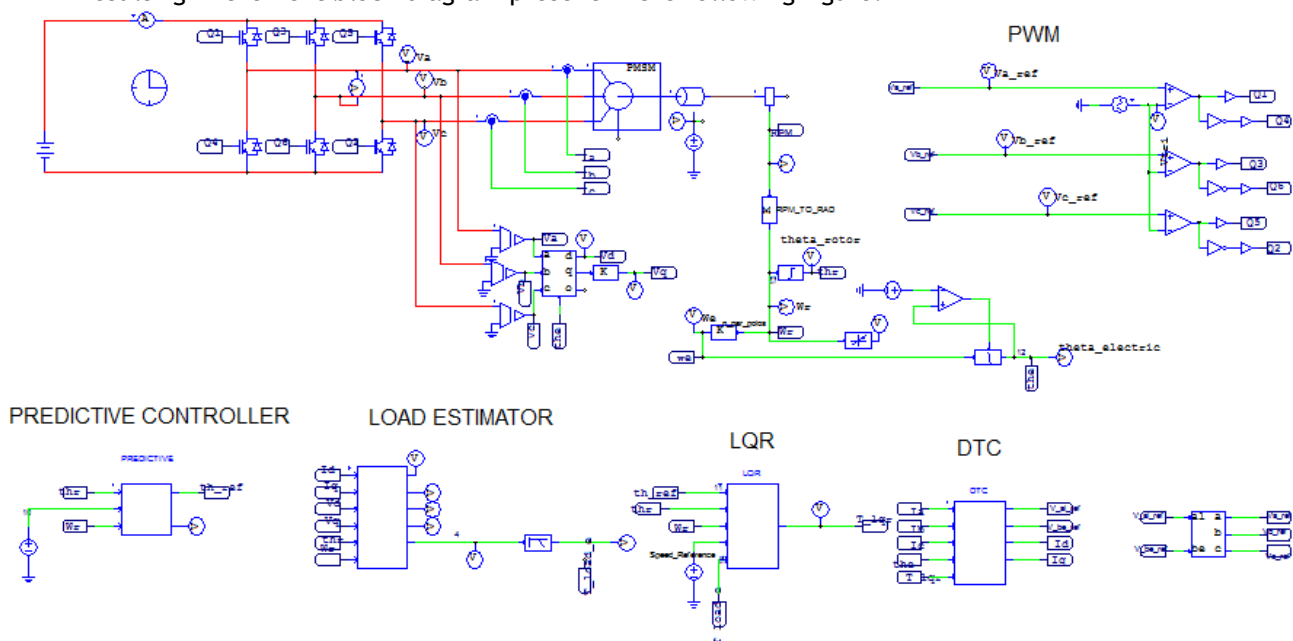

Figure 61 Introduction of the optimal controller in the simulation block scheme

The behaviour of the designed controller can be analysed through results carried on in similar conditions as defined in the previous chapter. Figure 62 shows the simulations results and in order to make comparison with the results obtained before is given the same position reference, using a limited acceleration and braking torque of 70Nm. The control parameters have to be adjusted until the steady state position error and speed transport is inside the tolerance values. The best parameterization of the system with a constant $k_{threshold}$ of 1.06 and $k_{control} = 5$, which can be different according with the conditions of the control application. The value of $k_{control}$ should be chosen with a high value such that it forces the LQR to have a step response between acceleration and braking, ensuring the minimum time. On the other hand $k_{threshold}$ should be adjusted until the position error is inside of the tolerance values.
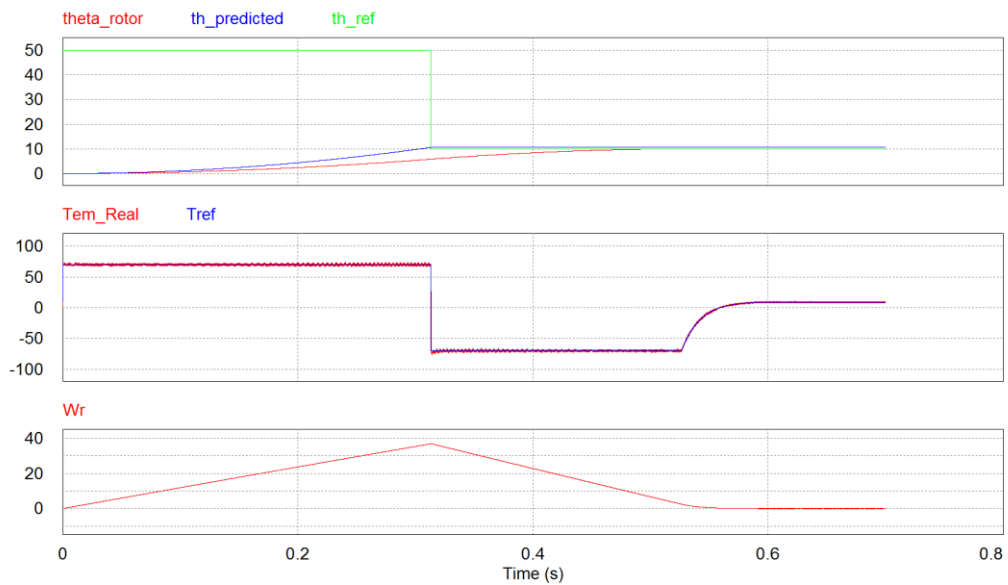
Figure 62 Simulation results of the optimal position control

In the first plot at green is represented the position reference generated by the predictive controller, with red the real position of the rotor and with blue position predicted. It is possible to observe that the position reference changes, when the predicted position is higher than the threshold. This change in the generated position reference will actuate the change of the torque reference given by the LQR as it is possible to see in the second plot of the figure 62. When the LQR receives the new position reference and states that it is near to the new final position, it generates a negative torque reference to the DTC, to reduce the rotor speed and do no overshoot the final position. In this way it is possible that the LQR uses the capability to brake, having the same transient response during the approach to the final position, that is smooth which avoids the slippage.

The rotor reaches the desired position in steady state in less than 0.6s, without overshoot. Comparing these results with the ones obtained without this estimation process, it is concluded that the system has a time performance improvement of about 85%.

5.4.5. Conclusion

A new algorithm for optimal time position control was developed in order to increase the operation efficiency, without prejudicing the already obtained position accuracy due to its significance in the process.

The maximum acceleration, the braking capability of the motor and the maximum applicable torque to avoid drift during the transportation are identified as the limitations to the control system. These should be controlled in order to also control the steady state error and to reduce the variance in the final position. In this way, the algorithm also allows the adaptation of the threshold and control gains that concede the opportunity to smooth the movement, allowing adjustment the control to the final conditions of the system application.

On the other hand it is easy to implement, has low cost on the computational level, since it is just necessary to calculate two expressions. The calculus can be made at low frequency when comparing with the necessary calculation frequency of DTC because the dynamics of the movement is much slower.

Finally it must be remarked this control system that in this chapter is developed a new algorithm for optimal time control, which can be applied not just to transport of material system, but also in other applications where it is necessary to get the minimum time to reach one position taking in account the system limitations. Since the role of this algorithm is to generate the positions references, it can be used in other control architectures and also in another type of motors.

Chapter 6

System Validation and Implementation

6.1. Introduction

Presently will be discussed the diverse implementation phases of the developed control scheme and the final simulations. In the final simulation is tried to include all the real conditions of the system to be implemented, as the processing time that the MCU takes to run the entire algorithm, the error from the current measurement, etc. From this first final simulation results was decided to change the DTC control scheme to achieve lower torque ripple. The simulations of the final design control and also the production line simulation with the new control scheme are presented.

Finally, because it was proposed implementing the designed controller, this chapter will discuss about the design of electronics components, simulation and implementation. Unfortunately it was not possible to present the practical results of the implemented controller since was not possible to connect the rotor to the measurement system.

6.2. Brief comparison between the controller platforms

As embedded technology proliferates in electronic devices, the selection of the right technology for a specific design is becoming a hard task. In general, a closed-loop control system consists of three main parts: the measurements from the sensors, the processing of those signals and finally the output that will actuate over the process. Having in mind the requirements of the system and its final propose, that in this case is the industrial environment, there are three main classes of controller platforms that should be taken in account: DSPs, MCUs and FPGAs. They are all used in control being each device suited for a specific role having a variety of specific tools for developing applications[26].

Digital signal processors or DSPs hard-wire the basic functions for signal processing, optimizing these operations but with loss of flexibility. They are easily programmable usually trough C language and are able to perform fixed and floating-point processing, being low-cost and low power devices. In some cases a DSP is the optimal solution for some functions but not for all. Because MCUs can include basic DSP operations in their instruction set, allowing

simple signal processing, there are industrial microcontrollers they are preferable in the most applications[27].

Microcontrollers Units or MCUs are general propose processors being used in a wide range of applications, as signal processing and control. They are designed to handle multiple asynchronous tasks efficiently, using saving methods and program stacks for each processor to facilitate the switching back. In real-time control applications it is necessary to perform multiple tasks asynchronously. Therefore, microcontrollers are the most common choice for this kind of applications.

FPGAs or Field Programmable Gate Arrays run the logic in hardware and are reprogrammable, being popular because of their speed and flexibility, with the disadvantage of their high unit cost. When this device is programmed, the gates are configured and connected in such way that the software application is hardware implemented. However the programming language VHDL, or VERILOG, it is complex and takes a long time for application development.

According to design requirements and the final propose of the project the MCUs are the most suitable choice. With the advent of the ARM processors many of dedicated MCUs appear for dedicated industrial solutions as real-time controllers, motor drives and critical systems. The ARM has allowed these MCUs to be really low-cost and low-power consumption and at same-time real-time processing and a dedicated programming library to increase the code performance.

6.3. The microcontroller

The Infineon has launched recently the family XMC microcontroller based on ARM Cortex-M Cores. Designed for real-time critical applications and with all the benefits of an industry-standard processor, it is dedicated to applications such as renewable energy, factory and automation, etc.

From all the range of products that this family offers, it has been chosen the XMC4500 that it is best suited for supporting motor control applications such as servo drives, as it is the final propose of all the developed work.
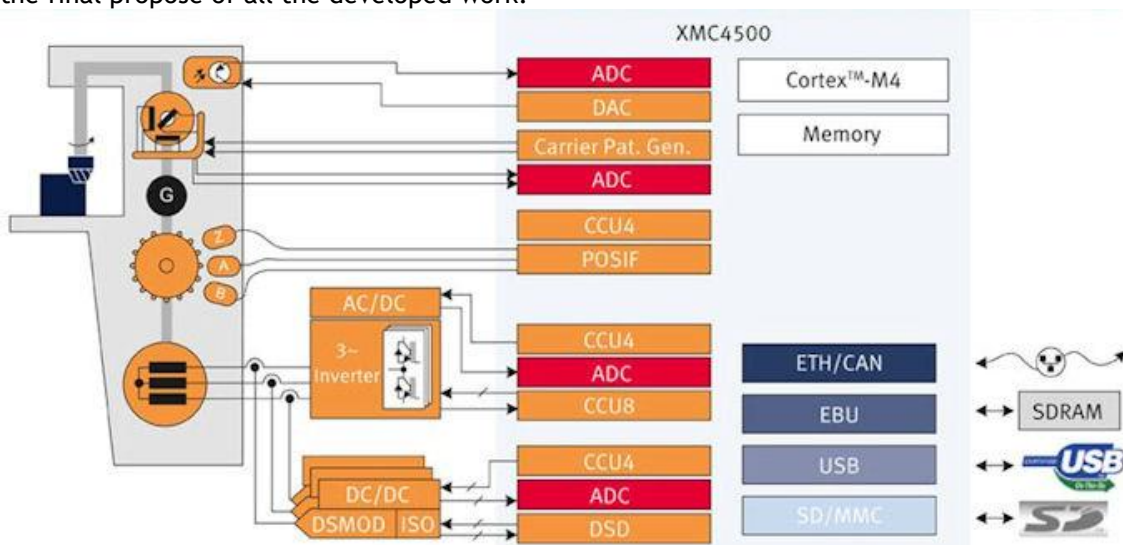

Figure 63 XMC4500 hardware applications example

It is also equipped with a wide range of dedicated applications for motor control. A resume of these applications can be found in the next table.

Table 6 Hardware applications of the microcontroller

Application Requirement	Used Device Feature
Quadrature Encoder position detection	POSIF interface together with Capture Compare Unit CCU4
Rotary angle detection with Resolver	Carrier pattern generator for primary coil excitation and resolver feedback signal measurement via Analog to Digital Converter (ADC)
Motor control inverter	Capture Compare Unit CCU8
In-phase current measurement via galvanic isolated Delta Sigma Modulator	Delta Sigma Demodulator (DSD)
Main and auxiliary power supply generation with Power Factor Correction (PFC)	Pulse generation via Capture Compare Unit CCU4 and current/voltage measurement via Analog to Digital Converter (ADC)
Sensor calibration, offset and gain adjustment	Digital to Analog Converter (DAC)
Fieldbus interface	Via Ethernet MAC with IEEE1588 timestamping and/or CAN
External memory extension for process data image and code	External Bus Unit EBU supporting synchronous and asynchronous protocols for e. g. SDRAM and NAND- or NOR-flash
Service access via plug and play interface	USB 2.0 OTG interface
User access for machine configuration	SD/MMC interface

Concluding for all the reasons presented about, with a frequency clock of 120 MHz and for just 10€, the XMC4500 was at this time the best choice for controller platform.

6.4. Currents Measurement

For the current measurement it is used the current transducer LF305-S. Considering that the motor used to test the control system has maximal current of 240Arms, which represents a measuring range of [-340,340] A it was chosen a current sensor with a measuring range of [-500,500] A. Also, as the output signal is a current signal, there is no influence of electromagnetic noise in the signal, allowing excellent accuracy and a wide frequency bandwidth.

The next step it to adapt the current signal into a voltage signal in a range of [0, 3.3] V, that it is the measuring range of the ADC inputs of the microcontroller. The conditioning circuit should do three basic operations:
- ✓ Convert the current signal into a voltage signal;
- ✓ Filter the signal;
- ✓ Add an voltage offset;

The signal conversion is made using a precision resistance in order to prevent affecting the accuracy of the measurement. It is used an active low-pass filter with a cut-off frequency of 10 kHz just to stabilize the voltage at the ADC input, being also recommended by the

Infineon application examples. Finally analyzing the datasheet of the current transducer it has a conversion ratio of 1:2000. It means that the output signal range will be [-250,250] mA for full range measurement of the sensor, but as the maximal current of the motor is

340A, the output of the sensor will have a range of [-170,170] mA. Using also the full range measurement of the ADC that is of 1.65V for a signal of 170 mA, it means that the value of the precision resistor will be:

$$R_{precision} = \frac{1.65}{0.17} \approx 9.7 \ \Omega \tag{6.4.1}$$

The power of the resistor should be

$$P_{resistor} > 1.65 * 0.17 = 280mW \tag{6.4.2}$$

The designed active low-pass filter has an inverting topology, which cut-off frequency is given by:

$$f_{cut-off} = \frac{1}{2*\pi*R_1*C_1} \ hz \ [28] \tag{6.4.3}$$

And the voltage gain

$$A_{v0} = -\frac{R_1}{R_2} \ V/V \tag{6.4.4}$$

To avoid the current division between the precision resistance and the filter, it was chosen a $R_2 = 100 \ k\Omega$, to have unitary gain $R_1 = R_2$ and finally to have the desired cut-off frequency has been chosen $C_1 = 10 \ pF$. In cascade it is added a subtractor circuit that will invert again the signal, nulling the first inversion and add the reference voltage of 1.65V. To generate an adjustable reference it is used the DAC of the MCU to generate this reference. The voltage gain associated to the addition of the offset signal is given in the expression 6.4.5 being necessary that the DAC generate a 0.75V signal to obtain the desired offset.

$$A_{v0} = 1 + \frac{R_5}{R_4} = 2 \ V/V \tag{6.4.5}$$

The designed circuit was simulated using a simulation tool from the National Instruments, Multisim 11.0, since it is a simulation tool dedicated for low-power, circuit conditioning simulation tool. The obtained simulation results are presented in figure 65.

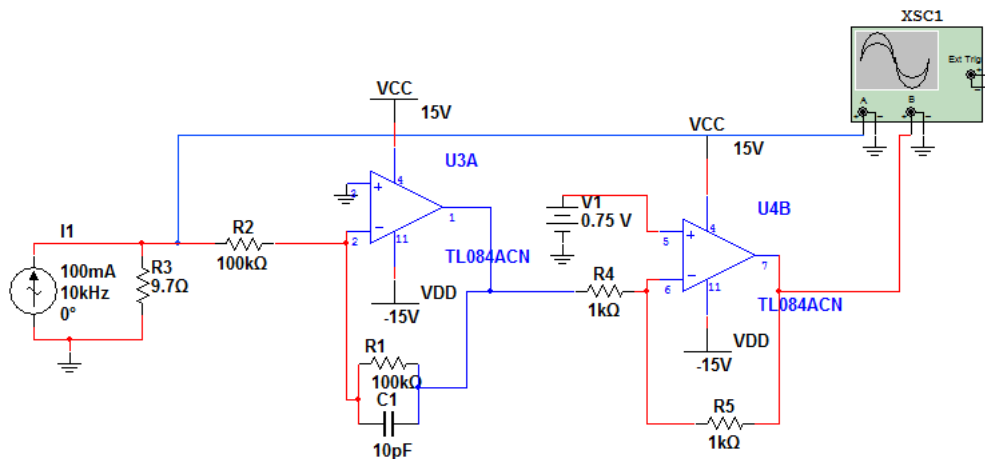$$A_{v0} = -\frac{R_1}{R_2} \ V/V \tag{6.4.4}$$

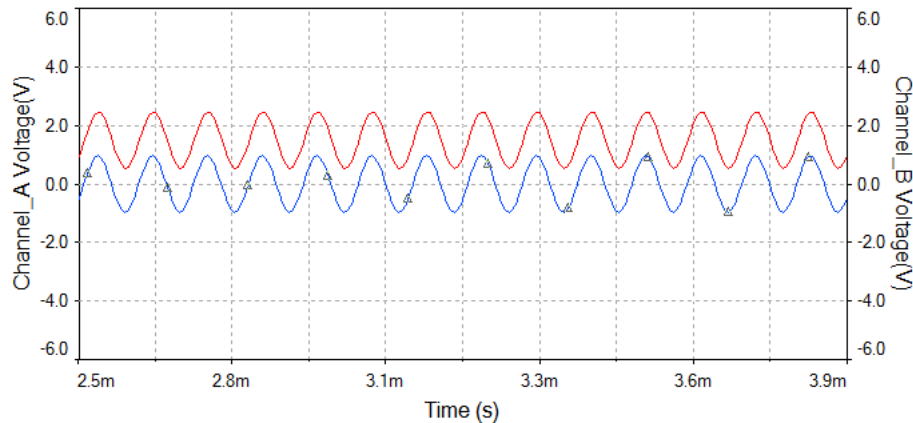**Figure 64 Current conditioning circuit simulation**

Figure 65 Simulation results of the conditioning current circuit. The blue signal is the voltage in the precision resistance, the red signal the output of the conditioning circuit.

After verifying the correct conditioning of the signals, the circuit design was implemented in a breadboard and using the operational amplifier TL084. Through a AC voltage source of 50Hz and a potentiometer was measured the current on the cables of this circuit using the indicated sensor.
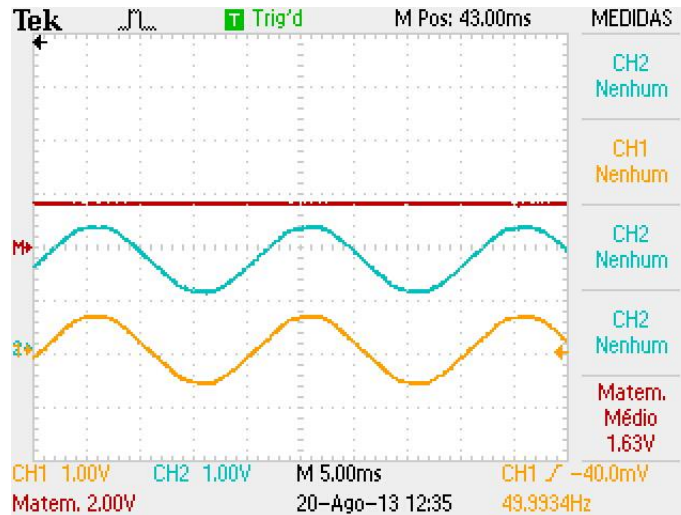
Figure 66 Implementation results of the conditioning current circuit. The yellow signal is the voltage in the precision resistance, the blue signal the output of the conditioning circuit and finally the red signal the subtraction of the blue signal with the yellow.

From the mathematical operation, represented in red, it is concluded that the input and the output signal are exactly except the introduced offset. The offset mean offset value is presented on the right bottom side of the picture. The signals are not lagged since the frequency is under the 10 kHz defined as the cut-off frequency, so the circuit is working properly.

The MCU is equipped with 12 bits ADC, having a total unadjusted error, TUE, of ±4LSB. This error is a sum of the differential non-linearity error, the gain error, integral non-linearity and offset error. This error will be convert in terms of the current measurement, for later be used in the final simulation.

$$1\text{LSB} \Leftrightarrow \frac{3.3}{2^{12}} \approx 0.8\text{mV} \tag{6.4.5}$$

Because 1.65V corresponds to a measurement of 340A, 1A measurement corresponds to $\frac{1.65}{340} = 4.9$mV. This way an error of 4LSB corresponds to $\pm\frac{4*0.8}{4.9} = \pm0.6531$A error in the current measurement.

Finally the ADC readings in the program are in a range of $[0, 2^{12}]$, being necessary to convert this values in the real value of the current. The designed circuit generates 1.65V for 340 A of measurement plus the offset. It means that for 340A we have half of the full-scale of the 12 bits ADC, which is equivalent to a conversion ratio of $k_{ADC} = \frac{340}{2^{11}} = 0.166 \, A/dec$.

6.5. Position Measurement

As sensor for position measurement it was used an incremental encoder from SEW for the rotor position measurement. In order to know the absolute position of the rotor it is necessary at the beginning of the application to make the rotor spin one time, as for this application should be used an absolute encoder. Because usage of synchronous drives it was necessary to align the rotor with one phase voltage and define this position as the zero position of the incremental encoder. This process was made by feeding two phases to a 40V battery, with a resistance in series. Otherwise we would short-circuit the stator. Defining one phase as the phase A, when the motor is fed it aligns to one pole pair, defining in this way the zero position of phase A .

The encoder generates 1024 pulses per revolution, so it has a resolution on the position measurement of

$$\frac{360}{1024} = 0.3526º \tag{6.5.1}$$

which is enough for this application.

On the electronic level, the supply voltage of the encoder was 15V, which means that the output pulses from the encoder has to be converted in pulses from 0 to 3.3V, that is the maximum voltage that can be applied to the inputs of the MCU. For this propose was used the integrated circuit AM26LV32E, that it is basically a logic circuit with three states, represented in the next table, that it is able to receive differential input of $\pm15V$ and convert this signal to 0 or the supply voltage, that in this case will be 3.3V. The outputs of the encoder are also 6 signals represented in the next figure.
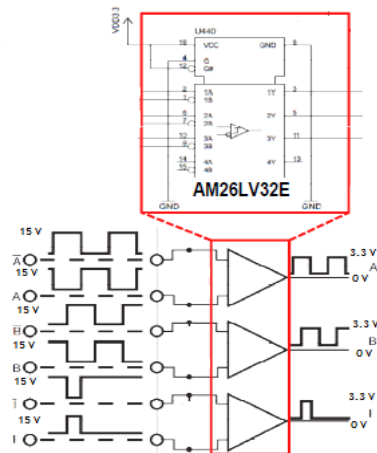

Figure 67 Integrated circuit for voltage level conversion
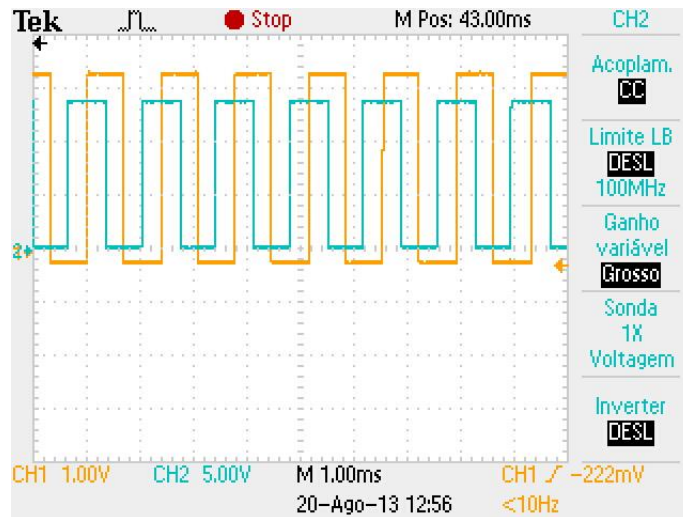
Figure 68 Implementation results of the voltage level conversion circuit

Looking at the figure presented above it is possible to see in blue the input signal from the encoder and in orange the signal converted a scale from 0 to 3.3 V.

The MCU has incorporated a high level application, POSEQ, dedicated to the encoder, being the position and the speed determined by the next expressions for this application.

$$POSITION = \frac{N^\circ \; PULSES}{1024} * 360^\circ$$

(6.5.2)

$$SPEED = \frac{N^\circ \; PULSES * 60}{1024 * TIME\_WINDOW} \; RPM$$

(6.5.3)

Where the time-window is a time period that can be defined by the user to count pulses, using the generated 3 signals namely Phase A, Phase B and Index. The signals are shown in the diagram below.
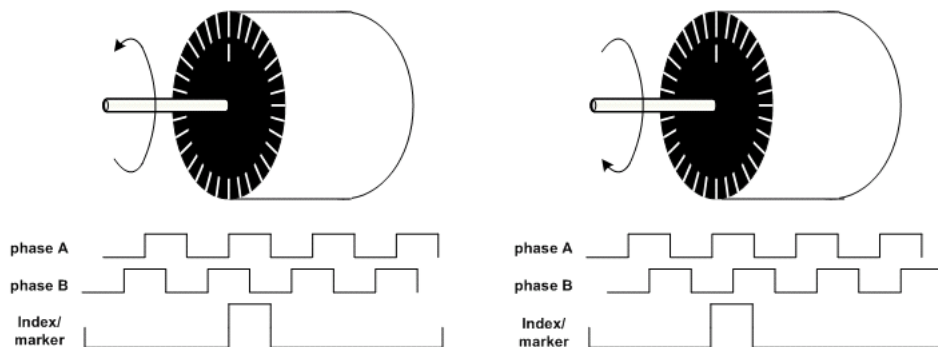
Figure 69 Encoder signals, retired from DAVE help software

As seen in the picture above the Phase A and Phase B signals are 90 degrees apart, hence the name Quadrature Encoder. The above diagram shows the encoder signals for anticlockwise and clockwise rotation. In Clockwise direction the Phase A is leading and vice versa. The Index signal is generated once per rotation being used to find out the absolute position and it can also be used to count the number of revolutions.

The absolute motor position is a demanded characteristic for vector control and can be chosen as the zero position of an electrical phase. In order to know the absolute position of the motor it is necessary to choose an electrical phase of the motor as reference and synchronise the zero of this phase with the Index signal of the absolute encoder. Once all the control is based on the motor position, the determination of the absolute motor position represents an important step that should be done with precision. The control response consists in the generation of phase voltages according with the position of the motor. The loss of synchronism or the no knowledge of the motor position leads to destabilization of the control system, resulting in the instability of the transport system.

The used method consists in the measurement of the back electromotive force generated in one phase of the motor and in the synchronization of the pulse index with the zero crossing of the phase. Using a differential probe and an oscilloscope it is possible to measure both signals. Because the used motor for implementation presents a delta connection, it is just possible to measure the compound voltage, which means that the Index pulse is synchronised 30 degrees in advance of the phase voltage. Therefore it is necessary to compensate the position read from the encoder in 30 degrees. The trigger signal of the oscilloscope is synchronized with the Index pulse being obtained the results presented in figure 70.
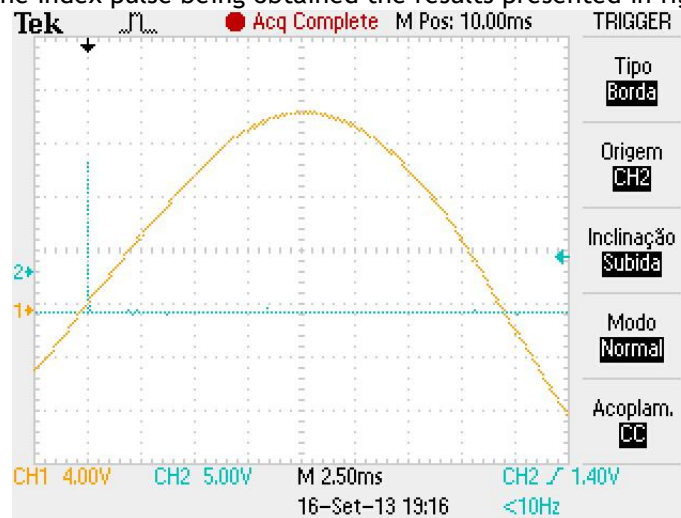
Figure 70 Determination of the zero position of the motor. In orange the back electromotive force and in blue the Index signal from the encoder.

Analyzing the figure 71, where it is shown the zero crossing instant, it can be observed that the index signal is in advance 250us, representing an advance of 2.25 degrees. As it is referred it is necessary to subtract 30 degrees to the read position from the encoder, being in this case compensated 27.75 degrees.

Due to human error it was not possible to eliminate the advance of the pulse index, which leads to an introduction of uncertainty in the motor position. To avoid that the system becomes unstable due to this uncertainty, the control angle of the motor is limited to 80 degrees in the control algorithm. Once it is not a requirement for this application it could be for others that require full control of the torque angle. In this case the encoder could be calibrated, being the position error just limited to the encoder resolution.
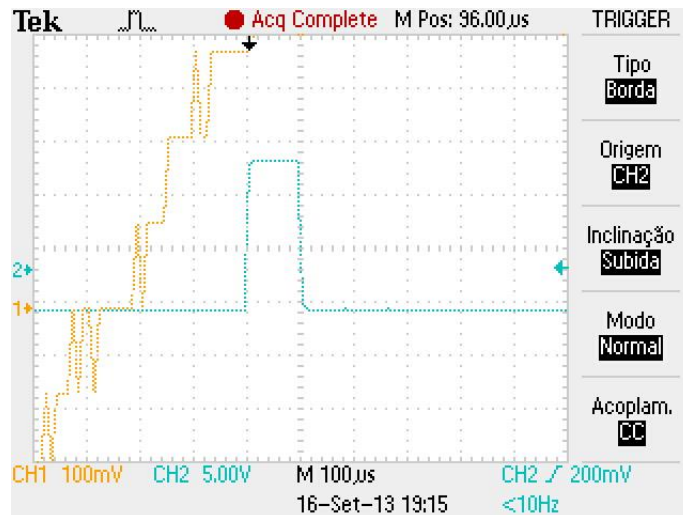
Figure 71 Zero crossing of the compound back electromotive force and the Index pulse.

6.6. The output circuit

The output circuit is composed by:
1. The PWM signals from the MCU;
2. The protection circuit of the IGBT drivers;
3. The drivers;
4. The inverter.

The XMC4500 is equipped with an application dedicated the PWM generation. The application method is the same as described before, through the comparison of a triangular wave with the reference value. The application provide the two signals for each leg, the non-inverted and the inverted signal, being possible to add and configure the dead-time to never shot-circuit the inverter. The measured results from the oscilloscope are in the next two pictures, figure 72 and 73.
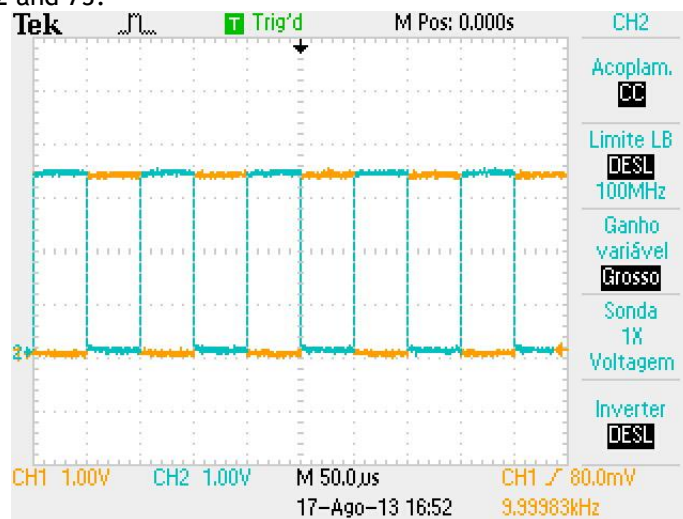
Figure 72 PWM signal generated by the microcontroller
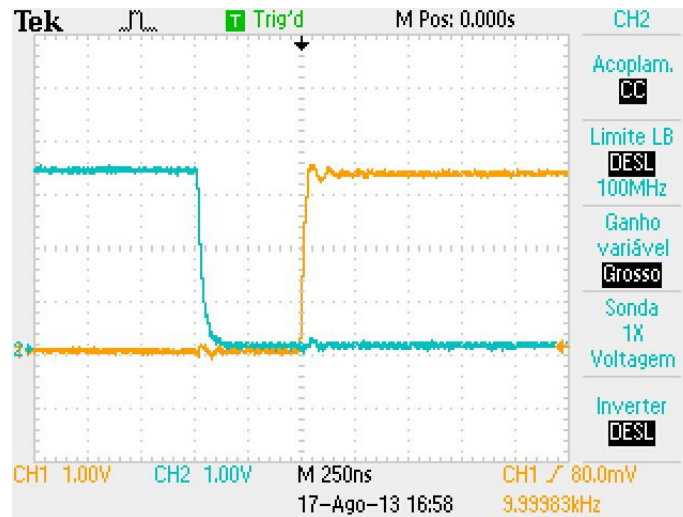
Figure 73 Dead time of the generated PWM signal

In the first picture it is possible to observe the signals for each IGBT of one leg of the inverter. The blue signal is the inverted of the orange signal. On the second picture that is basically a zoom in the time domain of the first signal if possible to observe defined dead-time of 500ns.

6.6.1. The protection circuit

In order to avoid the short-circuit of the inverter it was designed a simple logic circuit that force the low level in the command gates if in any case is given a high level command signal for both switches of one leg. Notwithstanding the defined dead time in the PWM signal is already protecting that is happens this circuit is just a replication of the protection of the inverter.

To do it is done a AND logic with both command signals of each arm and it is done a OR operation with all the results.

$$Y = A \cdot \overline{A} + B \cdot \overline{B} + C \cdot \overline{C} \tag{6.6.1.1}$$

Where with A and $\overline{A}$ are the non-inverted and the inverted signal for the phase A. The same happens for B and C. The output Y is negated and it is done a AND logic operation with the negated signal with all the command signals. So if in any time are given to high logic signals for the same leg, the command signals if forced to have low level.

The integrated circuit used for the logic operation AND was the 74LS08N and the OR was the 74LS32N.

6.6.2. Signal Amplification

The IGBT inverter module used is the FS200R07A1E3 from Infineon having the resumed characteristics presented in table 7.

Table 7 IGBT main characteristics

Collector Emitter Voltage	650 V
DC- collector current	250 A
Gate-emitter peak voltage	±20 V
Gate threshold voltage	5.8 V
Turn-On Time	0.06 us
Turn-Off Time	0.39 us

According with inverter characteristics, it is necessary to find a driver module solution compatible. A low-cost solution based on the Base Board 2BB0108T and the drive core 2SC0108T from Concept has been chosen, having the plug-and-play capability, being ready to operate immediately after mounting.

Table 8 Drivers main characteristics

DC-link Voltage	800 V
Turn-on threshold	2.6 V
Turn-off threshold	1.3 V
Recommended Supply Voltage (Vcc)	15 V
Min. Logic input	-0.5V
Max. Logic input	Vcc+0.5
Max. frequency	50 kHz

Although the drive input voltage is from 3.3V to 15V, which means that the PWM signal could be used directly, it is decided to use a PWM signal with 15V of amplitude to ensure the good operation of the driver and to reduce the effect of the EMI.

The analog multiplexer-demultiplexer HCF4053B was used as the voltage level converter, converting the PWM signal with 3.3V in the input to a PWM signal of 15V of amplitude and working also as a current buffer, ensuring the necessary current to activate the gates.
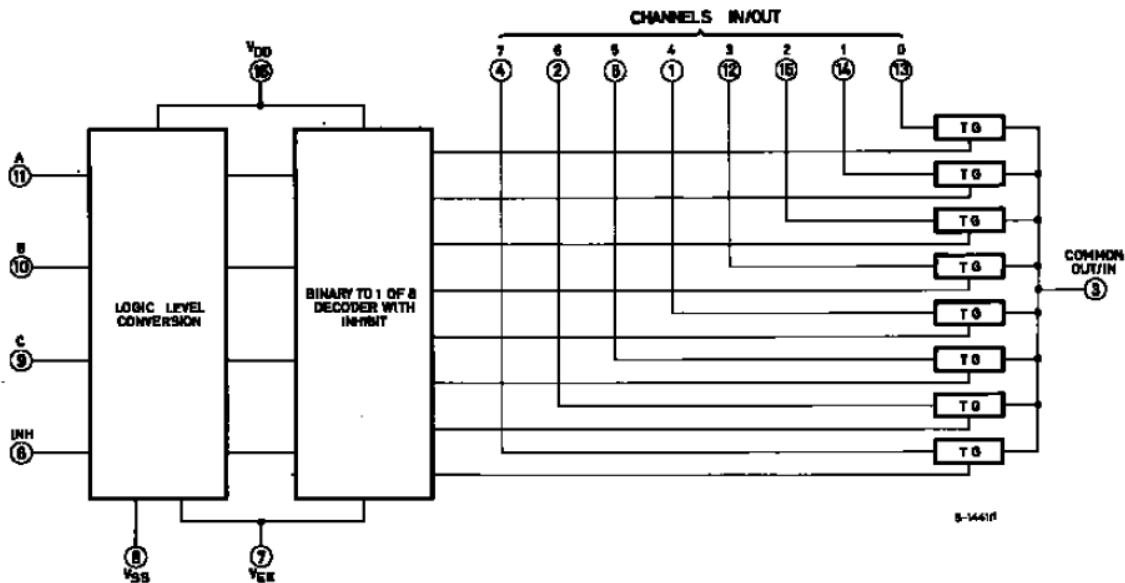
Figure 74 Function diagram and truth table of HCF4053B

Table 9 Truth table of HCF4053B

Inhibit	A or B or C	Output
0	0	ax or bx or cx
0	1	ay or by or cy
1	X	None

Looking at the diagram presented in the figure 74 and according with the logic presented in Table 9, at each input A, B and C will be connected a PWM signal, used to select the input that appears in the common output. On the other side ax, bx and cx will be connected to 0 V and ay, by and cy to Vdd. In this way when the input signal is low, it is selected to the output one input with low level and when the input is high one input with high level, Vdd, obtaining in the output the same PWM signal but will the voltage level desired.

In order to test the electronic circuit, it is implemented using a breadboard and it is applied a square wave of 10kHz and 3.3V of amplitude using a signal generator. The oscilloscope measurements of the input and output of the system are presented in figure 75, where it is verified that the output signal has 15V of amplitude as expected.
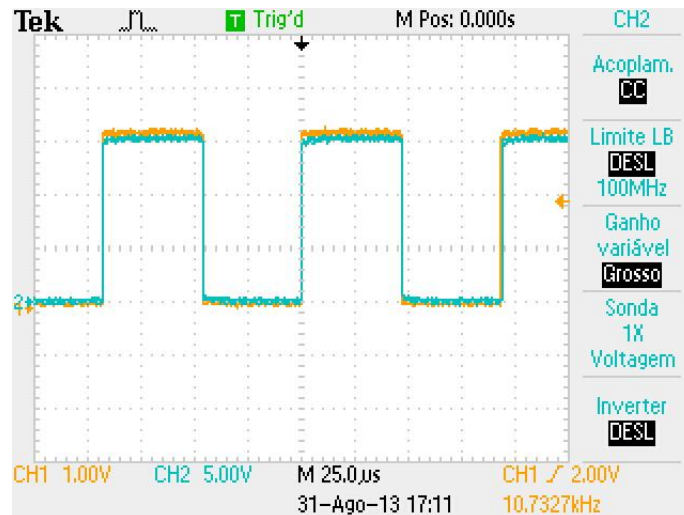
Figure 75 Oscilloscope results of the PWM voltage level conversion. On yellow it can be seen the input signal and on blue the output signal.

However it is necessary to use two of these integrated circuits in series to obtain the 15V of amplitude in the output. It is verified during the test of the circuit that the signal for channel selection should have 6V of amplitude to have 15V of amplitude in the output. Because as it is referred before, the PWM signal has 3.3V of amplitude, in this way it is used the presented scheme to convert this signal first to Vdd/2 being applied the same logic to this last signal to obtain the desired 15V. The designed output circuit introduces a delay around 250ns in the PWM, as can be observed in figure 76. The introduction of a time delay in the PWM signal generation represents an increase of the time response of the controller representing a reduction of the system phase margin. So the system stability is reduced and that is why this effect of the output circuit is later included in the simulations conditions of the controller.

Figure 76 Input and output of the output circuit. In orange is represented the output signal which is delayed from the input signal in blue.

6.7. MCU code optimization and performance evaluation

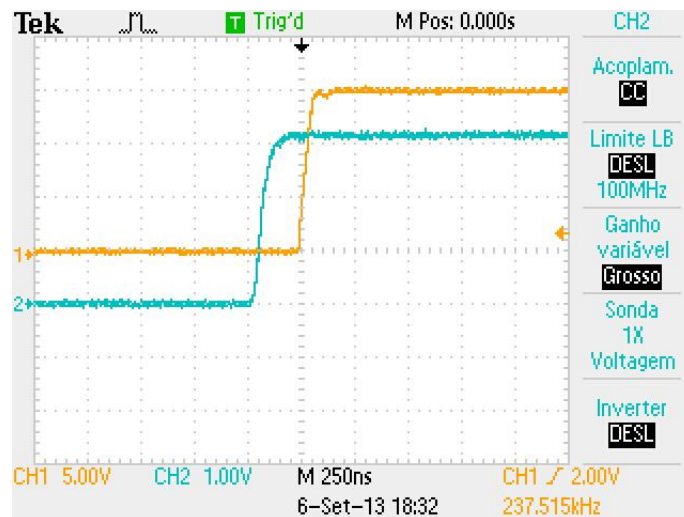A first analysis step of evaluation of the computational capacity is done, since it can affect the algorithm dynamics and stability that are critical in the control operation. The obtained performance results are later introduced in the control system simulation, allowing the knowledge of the control system performance with the application of this MCU.

The programming platform used is from Infineon, DAVE 3, and it is dedicated to the XMC series programming and debugging

The chosen MCU is just able to process one basic instruction at each cycle time, because it is a sequential processing unit and does not allow to process in parallel.

As it was referred before, the DTC was simulated with a simulation step of 1us, so in the simulation it is assumed that at 1us is done one calculation of the DTC algorithm. However, in reality the time that the MCU takes to make of calculation of the DTC algorithm is unknown. So the first step was to program the essential component of all the designed control, the DTC, in order to measure the cycle time that the MCU takes to make all the necessary calculations. This is done, because DTC is the control component which the cycle time can affect the stability of the system. To do it, it was turned on a digital output at the beginning of the processing cycle and turned off at end of the cycle, being in this way possible to measure the cycle time through an oscilloscope. In the first simulation results was got a cycle time of more than 100us, which invalidates the 10 kHz for the PWM or necessity of a faster MCU. It is known by the Nyquist sampling theorem that it is necessary to have the DTC running at least 2 times the frequency of the PWM. This means that it was necessary to get a cycle time smaller than 50us. To get this it was done a performance study of each function and a search for methods that can optimize it. The DTC algorithm basically consists in the next basic functions:

- ✓ Clarke Transformation;
- ✓ Sine and cosine;
- ✓ Park Transformation;
- ✓ Torque estimation;
- ✓ Inverse Park transformation;
- ✓ PI controller;
- ✓ Arctangent function;

For each basic function was measured the calculation time of the MCU and made a comparison between the same function from different libraries. For the example the C math library, the Cortex Microcontroller Software Interface Standard (CMSIS) library or another searched method and the developed function in this project. The CMSIS is an optimized library created for the ARM processors. On the next table are present the measured times for each function from each library or method.

Table 10 Function running time of XMC4500

Function	Library/Method	Time us
Sine & Cosine	C Math	38
	CMSIS	1,1
Clarke Transform	CMSIS	1
	Developed	0,73
Park Transform	CMSIS	1
	Developed	3,5
PI Controller	CMSIS	1
	Developed	1,5
Arctangent	Kordic Method	2,1
	C Math	12
Inverse Park Transform	CMSIS	3
	Developed	7
Square Root	CMSIS	1
	C Math	10
Sum of Square	CMSIS	1
	Developed	0,5

Based on this time comparison it was possible to optimize the code and get a cycle time less than 50us. There was times associated to the cycle, like the conversion times of the ADC, of the app for the encoder that was not possible to improve, but it was possible to measure and evaluate and can be used for a comparison of performance with another MCU.

Table 11 Routines running time

Routines	Calculation Time us
LQR Speed Control	2,5
LQR Position Control	5
DTC-SPWM	23,2
DTC Modified	27,6
DTC-SVM	
Read Current	3,5
Read Position	4,5
SVM Update	
PWM Update	6

This time results were also used to define the frequency that each routine will run. The idea is based on the Time Division Multiplexing (TDM) algorithm. It will be defined a time-slot where each routine can access to the processor. Each routine has one priority number and

the routine with the lower number will be the one with high priority. At each time slot the processor processes by order of priority each routine that the interrupt was enabled. If the time-slot is not enough and the processor could not answer to all requests, the routine has to request again to be processed. By defining a main routine, which include the current reading, position reading, DTC and PWM update, with high priority it is possible to be sure that this routine will run periodically, with a defined cycle time. This is important to ensure in order to guarantee the stability of the system. The other routines as LQR, stop buttons, etc. are not critical, so can be run in lower frequencies and the effect that the routine do not run in every cycle is negligible.

Figure 77 TDM used in the microcontroller
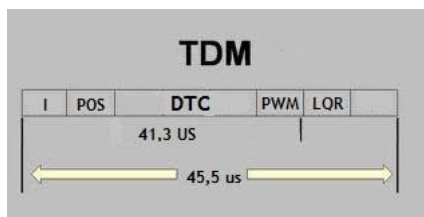
As represented in figure 77, the main routine was defined to run at 22 kHz what is equivalent to a cycle time of 45.5 us. In spite of it could run at higher frequency but with this would not be possible to run the rest of the control routines. The LQR was defined to run at 5 kHz resulting in the next software/hardware structure.
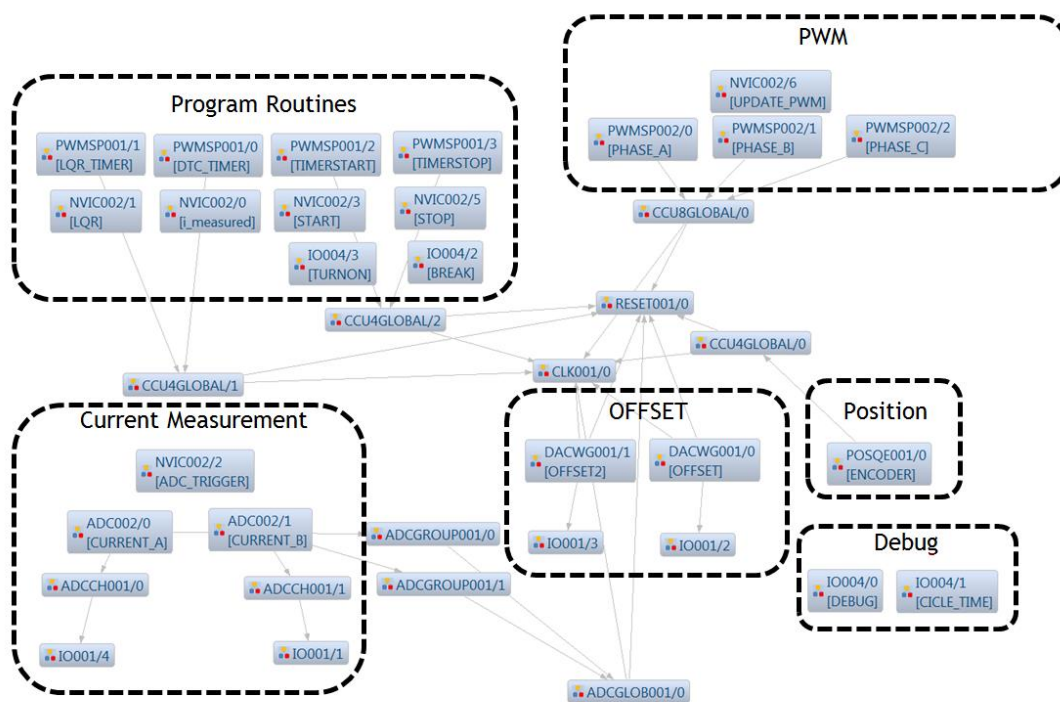

Figure 78 Final hardware applications structure

6.8. Improving DTC scheme

An improved DTC scheme is developed in this section in order to improve the system performance that can be obtained with the actual presented control structure, which presents results outside the permissible tolerance.

Firstly in order to evaluate the performance of the developed control system based on DTC with the presented hardware architecture, it is pretended to develop a simulation scheme, where are included all the real conditions where the system. So can be tested and also certified that the designed control achieves the desire performance considering the system application conditions.

Until now it was referred that the current measurement will be done using the ADC of the microcontroller, which has a finite resolution of 12 bits and also a TUE less than 1A. The TUE was modulated adding to the current measurements a Gaussian random noise signal with 1A of peak amplitude. To simulate the ADC readings were used a worse case. It was decided to use a 10bits ADC with a sample frequency of 1MHz since each reading in the MCU takes 1 us.
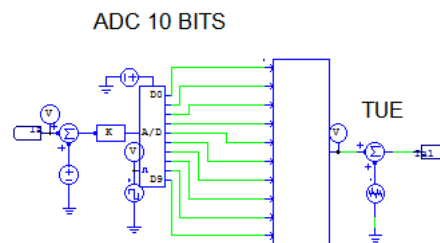

Figure 79 ADC block scheme simulation

The second step was to define the frequency routine of the DTC to 22 kHz, the LQR to 5 kHz and finally the Predictive controller to 1kHz, in order to simulate the interrupt routines that run each component of the control system. To do it, it was added in the code of each routine a variable that is incremented at each simulation step and when this variable reaches the necessary number of simulation steps corresponding with the period of the interrupts, the variable is reset and the code runs once.

On the power side, because the DC Bus is linked to the DC generated by cables, it was necessary to introduce the cable inductance. The expression for the voltage in the inductance is given by $V_L = L \frac{di_L}{dt}$, so the high current variation in the line due to the fast commutations in the inverter can introduce overvoltage in the inverter and damage it. To avoid this effect it was added near the inverter a capacitance that will stabilize the voltage in the inverter terminals and will also give to the motor the current that it needs at each instant.

The simulation step was reduced to 0.1us. Finally are presented the first final simulation results in the figure 80.
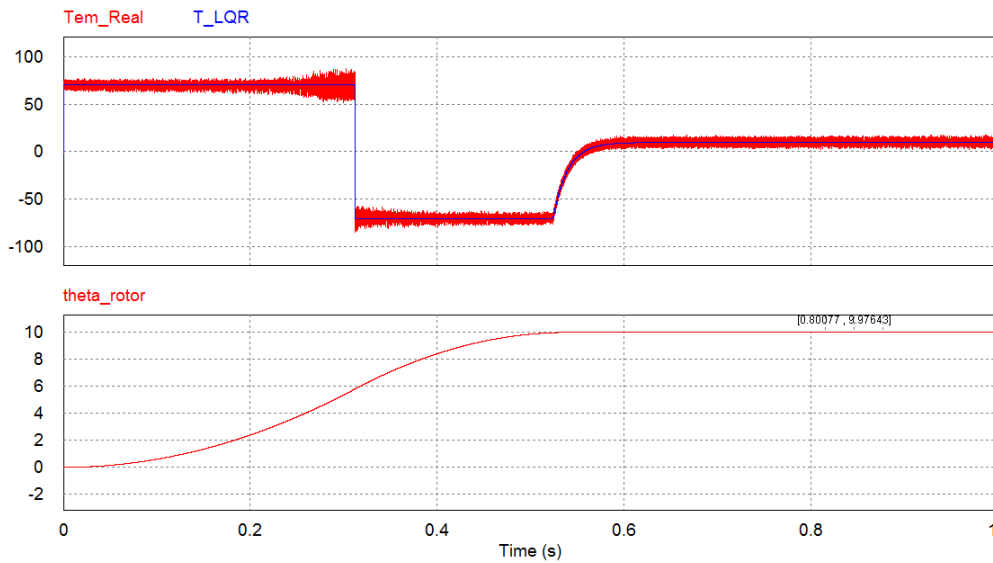
Figure 80 Final simulation of the control position including the implementation conditions

The first conclusion that can be taken is that the torque response has high oscillation of almost 15Nm from the torque reference, which can introduce high frequency vibrations in the final transport structure and also uncertainties in the position control. This can be better observed in the next figure.
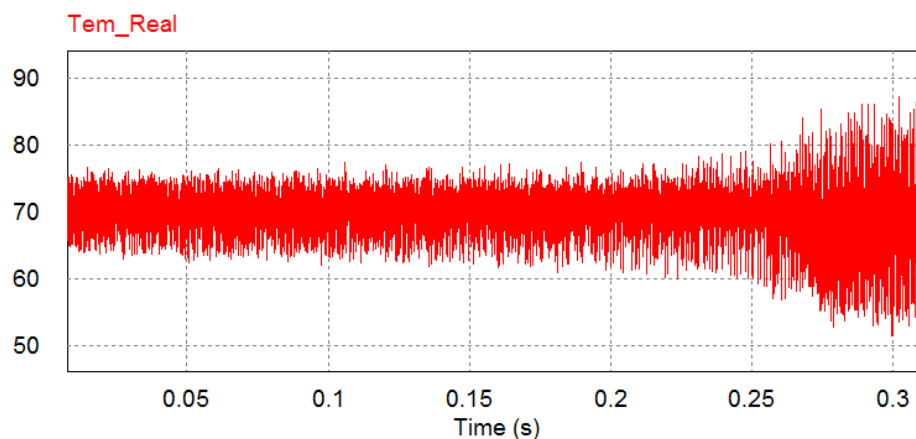
Figure 81 Torque ripple when then implementation conditions are included

6.8.1. An improved DTC scheme

To solve the presented problem, a solution to reduce the torque response variation was developed. Looking at the phase voltage references generated it is possible to observe the same high variation. This means that the problem of the high ripple value of the torque response is caused by the voltage references generated by the DTC-SPWM algorithm. At first it is assumed that it is possible to run the DTC algorithm at 1 MHz, but when the real conditions and the real processing time is introduced, which leads to reduce the frequency of the DTC to 22 kHz, the control becomes near the instability, producing the high torque ripple results.

Figure 82 Generated phase voltage when then implementation conditions are included

The increase of the running time of the control scheme means an increase of delay in the response of the controller, which causes major instability of the system. Analyzing the expression 4.3.3.5, it is clear that the voltage 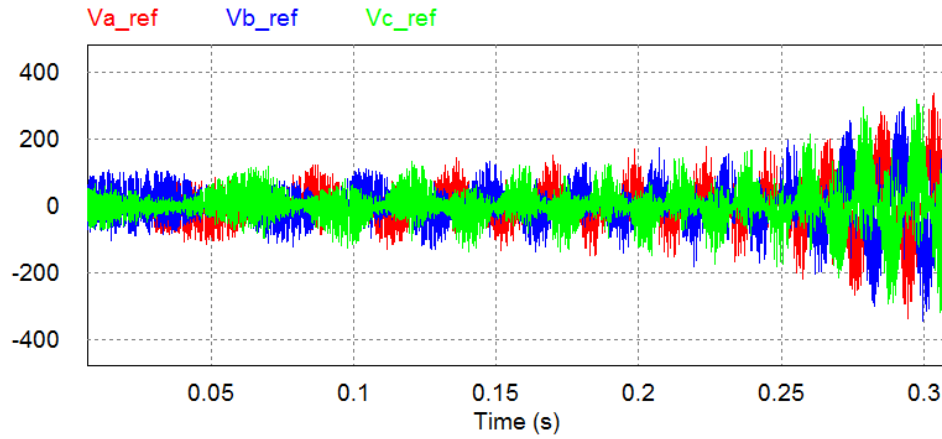references are calculated using the discrete approximation of flux derivatives. As shorter as the sampling period, T_s, more precise this approximation becomes. It is this introduced error that causes the high variation in the generated reference.

In order to smooth the controller response and to get a continuous voltage signal, different solutions were simulated, like the introduction of a low-pass or moving average filter in the voltage reference generator.

The introduction of the low-pass filter just solved the problem in a limited range of speed, since the cut-off frequency of the low-pass filter limits the control bandwidth.

The tuning of the moving-average filter is a hard task to do, becoming even harder as length of the average window increases. Therefore it was designed with a proportional component but with the integrative component replaced for a limited time window average weighted, but it wasn't also found a good parameterization of this filter that guarantees the required performance.

So the developed solution was carried out through the application of two PI controllers to V_α and V_β, being now possible to stabilize the controller response and to smooth the generated voltage reducing the torque ripple. Defining the proportional gain, smaller than one, it was reduced the high variation of the controller response. Defining sample time of the integrative component, at least, two times faster than the controller's frequency, increases the gain margin of the system without affecting the stability and the bandwidth of the controller. The new expression of the voltage references using a discrete PI controller will be presented   on   6.8.1.1.

$$
\begin{cases}
V_{\alpha_{ref}} = k_p * V_{\alpha_{ref}} + T_i \sum_{k=0}^{n} V_{\beta_{ref}} \\
V_{\beta_{ref}} = k_p * V_{\beta_{ref}} + T_i \sum_{k=0}^{n} V_{\beta_{ref}}
\end{cases}
\tag{6.8.1.1}
$$

where T_i is the time integration and K_p the proportional gain.

Defining $k_p = 0.1$ and $T_i = 2 \times 10^{-5}$ the ripple is reduced from the ±15Nm in the worst case to ±2Nm. The simulation results and the final block scheme of the DTC are presented in the   next   figures.

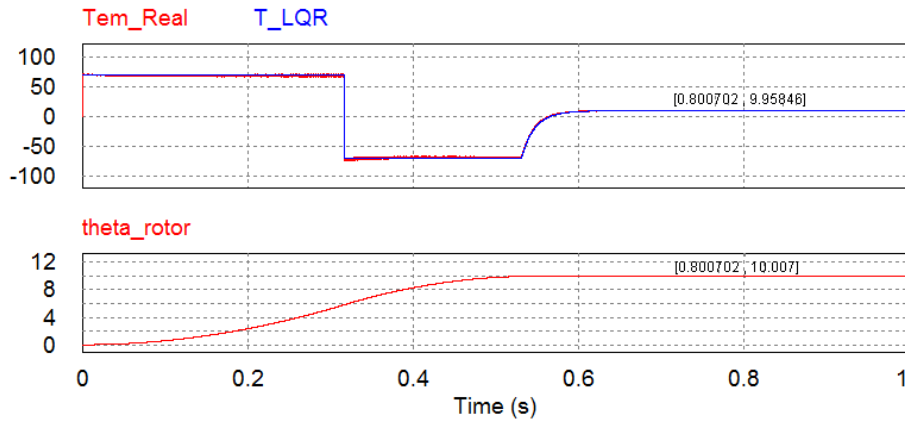**Figure 83 Simulation results with the improved DTC scheme and considering the implementation conditions**

For the same time instant, the steady state error is eliminated. Zooming the first 0.3 seconds of the torque response it is also possible to check the reduction of the torque ripple to less than ±2Nm.
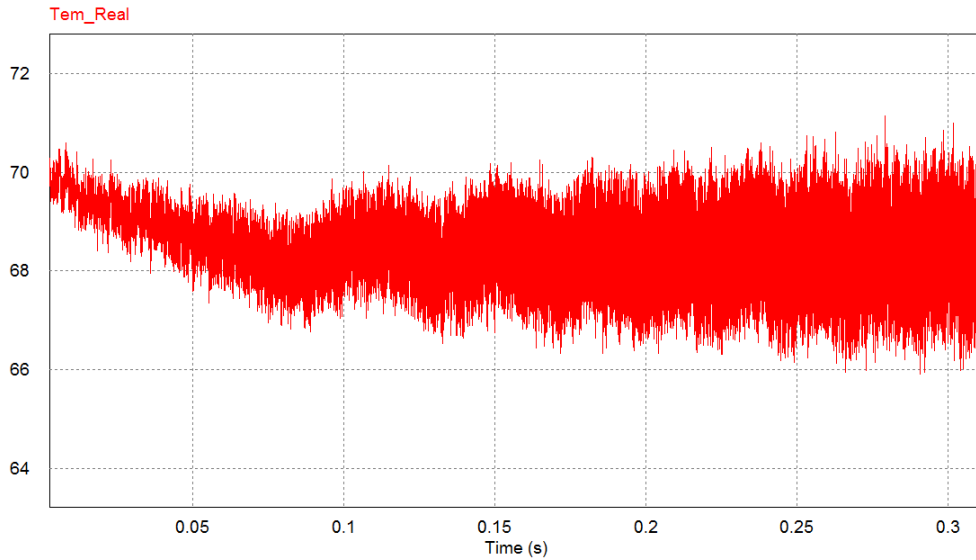

Figure 84 Torque ripple with the improved DTC scheme and considering the implementation conditions
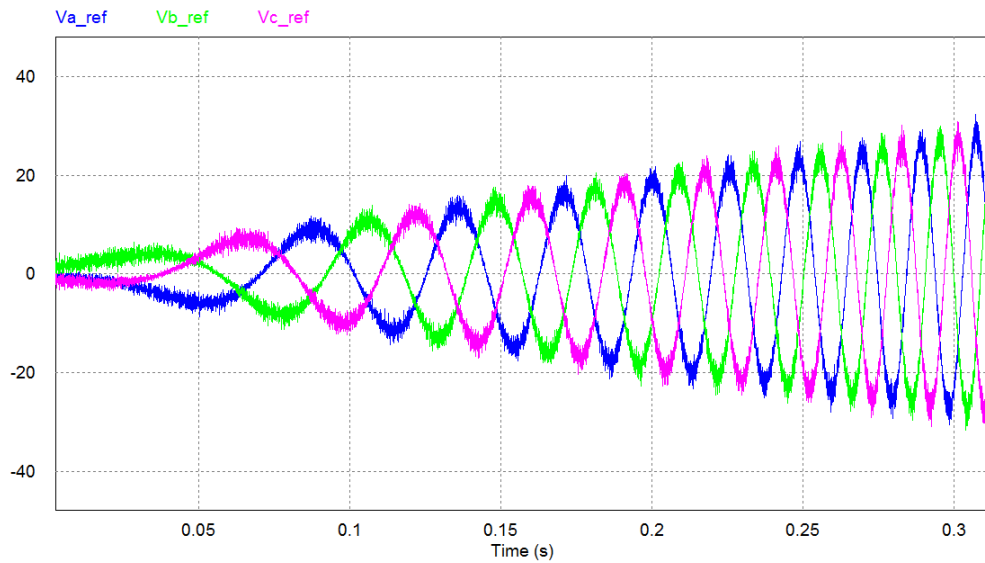
Figure 85 Generated phase voltage with the improved DTC scheme and considering the implementation conditions

Finally looking for the figure 85 it is possible to conclude that the controlled reference does not have the same oscillating behaviour, presenting a sinusoidal form as expected since the beginning. The achieved results represent the high value obtained with the presented solution. With the simple introduction of two PI controllers it is possible to reduce the time requirements of the controller, which means the possibility to use simpler and slower clock frequency, in the controller platforms, achieving the same performance as the obtained with computational platforms of high speed. The concept can be applied to other control schemes in order to reduce the speed requirements of computational side, allowing the use of lower-cost platforms which is an advantage for the final application.

6.8.2. Line behaviour with the new transport control system

To complete the analysis of the developed control system, in fact constituting a new transportation of material system, it becomes necessary to evaluate the production line behaviour integrated with the new transport system.

The evaluation process is based on the architecture already analysed, considering as key factors the precision of the cut-length and transportation time, which determines the production capacity and production efficiency.

The simulation model of the extrusion was not just developed in order to evaluate the actual performance of the production line but also to evaluate in simulation environment the effect of the replacement of the actual transport system for the new one. The developed transport system can have the advantage of higher precision but beyond that it is necessary to ensure that the actual production is guaranteed or even enhanced.

The first approach is based on the comparison of the production capacity considering a limited time period for each transport systems. To do this comparison, was simulated one of the fastest receipts, with a line speed defined as 37 m/s, knowing that the actual limit speed is 40 m/s. From the receipt was possible to know the desired cut-length for each tread, knowing the rotation radius it is possible to convert the cut-length in angle rotor position.

$$\theta = \frac{cut\_length}{radius} \qquad (6.8.2.1)$$

The cut-length of this receipt was 1.784 m and the radius of the transport conveyor was 0.07m it means $\theta = 25.5143 \, rad$. The position of the rotor was simulated in PSIM and was imported to Matlab using the SimCoupler to be simulated in the line model. The same cut-time of the actual cut machine is considered and the loop control is not integrated in the control of the new transport system, being necessary to adjust the line speed in order to guarantee the stability of the production line.
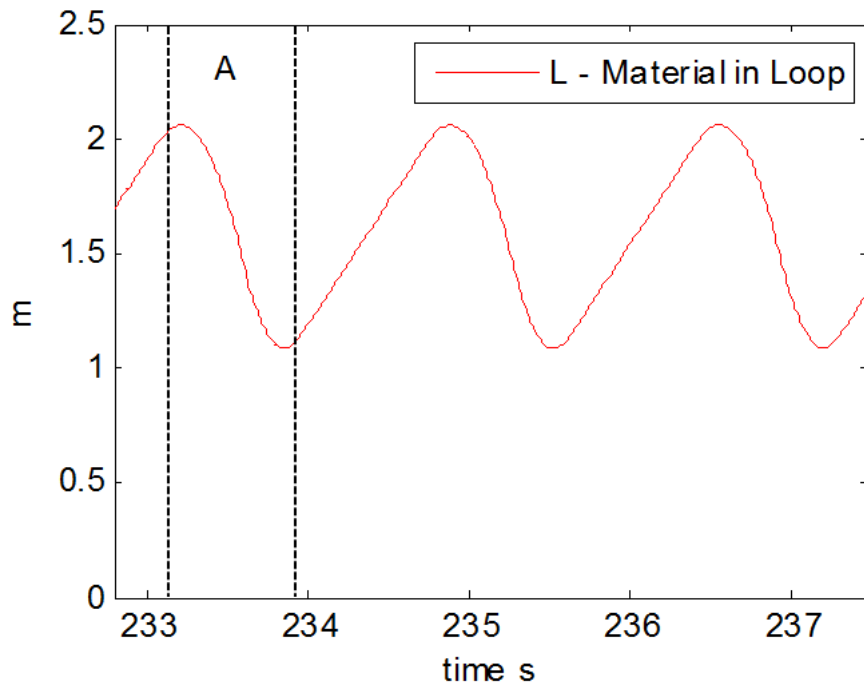
Figure 86 Material inside the loop using the new transport algorithm

In order to guarantee the continuous flow of the line it was necessary to increase the line speed to approximately 68 m/s. This is a really high value that is not realistically practicable. But by setting a lower torque limits it is possible to get a lower value of the line speed, that way avoiding the slip of the material and ensuring always that the transport time is optimal with high precision. The delimited zone in the picture represents the new behaviour of the transport conveyor followed a region where the material in the loop increases because the transport is stopped for transversal cut of the material. The behaviour is periodic as expected. Finally are presented the expected production results, in number of treads for each transport system for a period of 400 seconds.

Figure 87 Comparison of the number of the produced treads with both transport algorithm

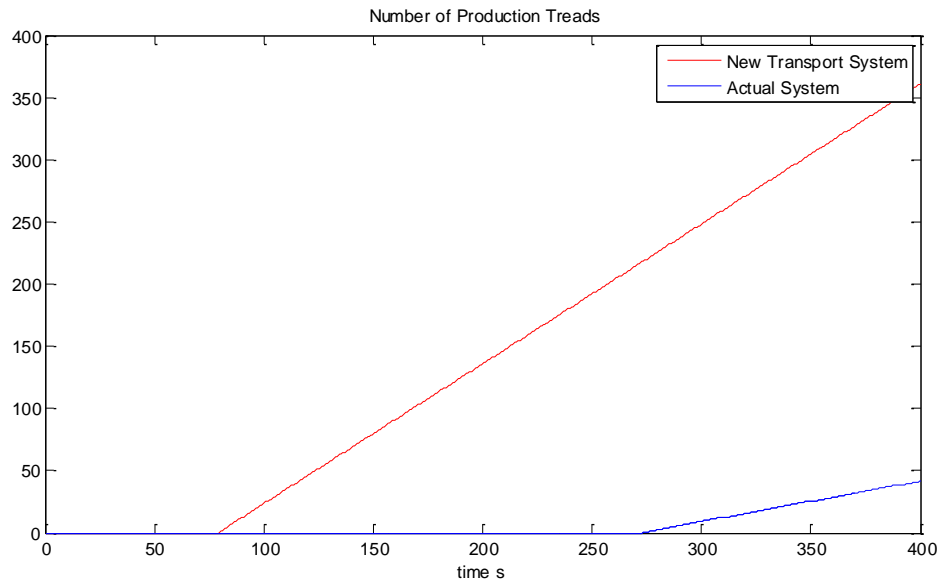The period in which the number of treads remains in zero represents the time that the continuous flow of material takes to arrive from the extruder to the cut-machine.

Ideally, it would be possible to increase the rate production, approximately 1.8 times, neglecting the necessary time that the materials takes in the path from the extruder to the cut-machine. However, it is important to refer that this results consider that there is no drift of the material during the transport, even with the defined maximum acceleration and torque break. Adjustment of the transport system will possibly be necessary to achieve the precision that allows the length of the material to be according with the tolerance values. Although, real implementation can produce worse results, but the new transport system ensures always the optimal time transport for the requested precision and so, the optimal production for the actual structure of the extrusion line.

On the other hand, the stability of the line is guaranteed by the increase of the speed, but quality requirements of the material in production can reduce the maximum speed limits. So it is necessary to control the transport system according with the accumulated length of material in the loop, achieving the line stability with the application of the developed transport system for lower speeds. When the characteristic of the material does not allow the increase of line speed, it is necessary the introduction of one trigger system that indicates the moment when the developed system should start the transportation of the material.

As it is referred in section 3.2, using the catenary equation it is possible to determine the material length in the loop from the minimum height of the curve that can be determined using an ultrasonic sensor. Using this variable to calculate the length of material at each moment, the signal to initiate the movement should be triggered when this reaches the position that corresponds to longer length of material than the cut one. This ensures the stability of the loop for lower and stable line speeds.

Therefore the necessary condition to ensure the stability of the process is the maintenance of the average length of accumulated material in the loop constant.

6.9. Conclusion

In this chapter firstly it is presented the discussion where are compared the principal control platforms in order to choose the most suitable to implement this control architecture. The main requirements are the price of the unit, the necessary time for application development which represents two main factors that will determine the final cost of the project. On the other hand at the hardware level it is required that the control platform is able for real time control and also discrete and analog input and outputs.

About the implementation of the drive system, it is presented the designed electronic circuits for signal acquisition, current and position, its implementation and tests, being the presented practical results according with the simulation results of these circuits.

It is done also an analysis of the chosen MCU, evaluating the performance and it is discussed the computation time necessary to implement the same function with different libraries. These results can be used in further comparisons of MCU as well as to evaluate the possibility of application of this MCU in other projects, by the knowledge of its performance values.

According with the designed hardware structure and with the knowledge it is possible to have previous results of the control system and predict the performance and stability of the designed control system before start the real tests of the system. To do it is developed a simulation scheme where the real conditions are included. From the first simulation results of the control system it is found a high ripple in the torque response, which reduces the precision of the control algorithm in comparison with the simulations results in ideal conditions. So it is carried a research to improve the obtained results that permit to use the designed hardware structure and more flexible real time control requirements. It is remarkable that the designed modified structure of the DTC scheme present, achieving better results and allowing the use of a low-cost MCU, representing the possibility to implement a high precision and time optimal application in a low-cost architecture.

Finally it is evaluate the behaviour of the production line considering the application of the new transport system, through its introduction in the line model. When it is consider the same line speed has used in the simulation of the actual transport system, it results in destabilization of the production line and on the break the continuous flow of material. This happens because the transportation times were reduced with the developed transport system and because it is not considered the material present on the loop. It results in the need to take in account the loop in the control system, being designed a possible control structure to stabilize the line with the designed transport system.

Concluding all conditions are gathered in order to implement the developed transport system in the E03 extrusion line.

Chapter 7

Conclusions

7.1. Epilogue

This dissertation deals with two main subjects: the modelling of the extrusion line and the design of an optimal solution for high precision and transportation time of the material.

Initially, a research about the extrusion process is presented, directed to the tires tread production. Electrical and mechanical structures were focused, as the quality and control systems. This allowed the system knowledge to elaborate the system breakdown structure of the second chapter.

System requirements were identified through the knowledge of the product specifications and the bottleneck of the production through the analysis of the production process. This resulted in the main topic of this dissertation: the research and development of a new algorithm to control the actuation of the transport conveyor.

Empirical knowledge of the process shows that the cutting machine is the limiting factor of the maximum speed production, so it was designed a simplified model of the system to prove it and also to determine possible improvements. This was the first developed model for this extrusion line and is the first main topic of this document.

After comparison with reality, good time correlation was achieved, and this allows the improvement of existing applications such as RMEA system, and the design of new ones for material tracking or production time prevision for better scheduling.

The design of the control solution begins with the research of Permanent Magnet motor modelling, the Park and Clark transformations and finally the modulation methods. Two modern and effective control methods (FOC and DTC) were studied and the benchmark between them resulted in the choice for the DTC method. Modulation methods were also compared through simulation. Despite the advantages of SVM such lower harmonic distortion or less semiconductor commutations, PWM technique adapted form SVM was chosen due to less ripple in torque response since it is the main requirement for the purpose of this application. .

Linear Quadratic Regulator is used as position and speed controller. Through the minimization of the square error high precision controller is obtained, without overshoot but without optimal performance.

Looking at the mechanical equation of the motor, it is concluded that controlling the applied torque it is possible to control simultaneously position and speed, and so, this controller was used as torque reference generator. On the other hand because of the linear characteristic of the controller brake capability was not being used, representing the main reason of the sub-optimal time movement. At this stage, transportation times were relatively larger than the actual ones therefore the designed control would have no interest for implementation even with higher precision.

According to this, system evolved in order to optimize the transportation time that is critical in this application. The idea is based on the predictive control, where the actuation over the system takes into account the prediction of the future states, being the system's model now crucial. Differential equations characterize the mechanical movement of the motor and it is possible to determine the one that gives the final position of the rotor if brake is applied starting from initial position with chosen rotating speed. This algorithm is used as on time position reference generator to the LQR, which allows the generation of optimal torque reference to the DTC and with this, transport time reduction.

Estimation of the applied load to the motor is necessary to keep the material static in the final position. Accumulated material in the loop applies force to itself, and so it is imperative the estimation of this tension and the compensation in the reference for torque.. To achieve this, an Extended Kalman Filter was designed, which presents also the capability of load compensation in the speed controller. This represents also an advantage for other applications which require stable speed even if load variations are applied in the motor.

The integration of all this systems results in the total control of the PM motor. This is a robust control solution for the torque, speed and the optimal positioning of the motor, using load compensation. The designed controller is a flexible and general solution for several different applications. The final structure scheme of the controller is presented in the next picture.
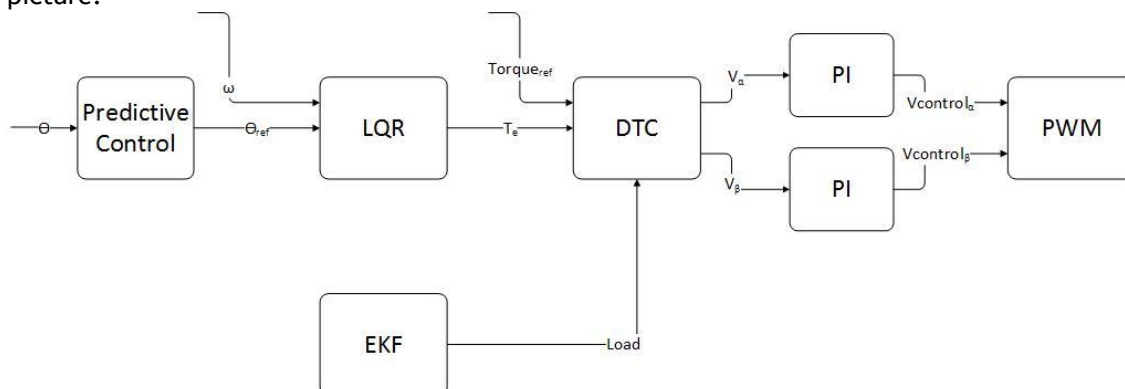

Figure 88 Final control design

This system is implemented in the XMX4500 industrial microcontroller that incorporates recent technology with high prospection in the market, low-cost and easy programing based on C language and already existent hardware applications that generate code automatically. All the designed electronic components were successfully tested.

Due to the hardware limitations introduced in simulation it was verified high overshoot in torque control response that leads to the introduction of PI controller in the DTC voltage

reference generator This modified DTC scheme results in the lowering of maximum torque overshoot to 2Nm which represents the high precision that, ensures the required accuracy in position control.

Motor and encoder support structure were also designed and technical draws can be found in appendix I. Final circuit and system test structure is presented in picture bellow.
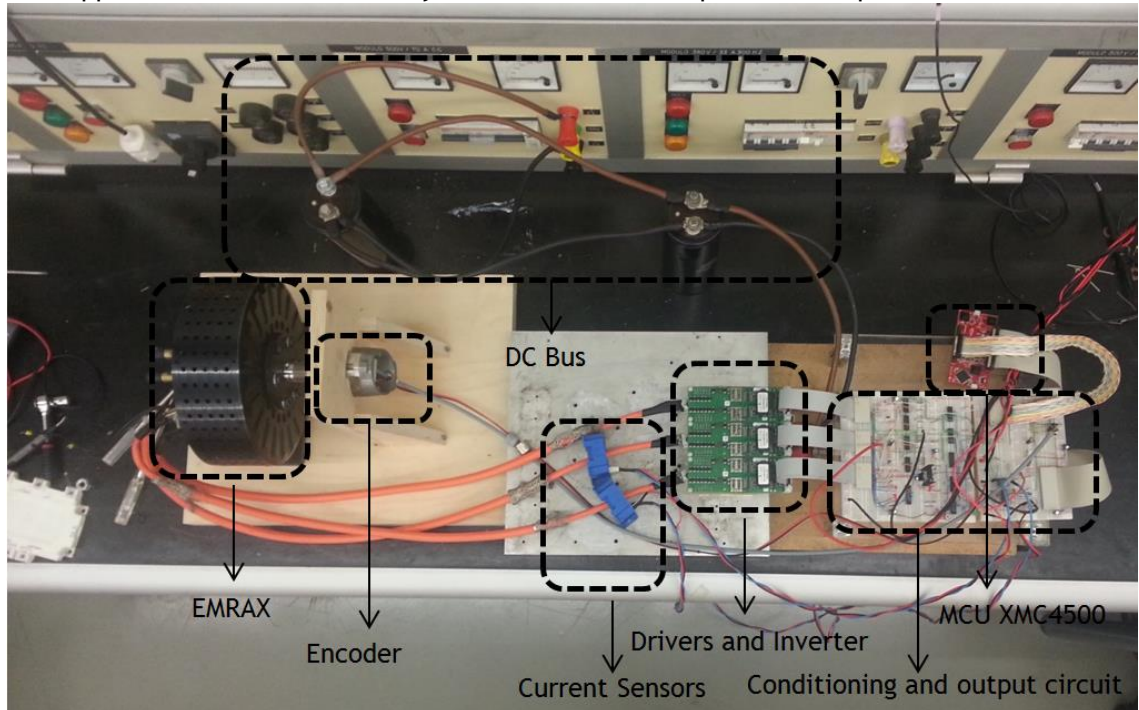

Figure 89 Implementation of the final circuit

As resume of the work performed:
- ✓ Development of the model of the production line;
- ✓ Design of DTC scheme simulation and implementation;
- ✓ Design of LQR to control the speed and the position of the motor with high precision;
- ✓ Development and validation in simulation of EKF for load estimation and compensation.
- ✓ New algorithm for optimal position control ;
- ✓ Improved DTC scheme for solving the high torque ripple problems of the controller as well as reduction of the computational cycle time;
- ✓ Design and implementation of all the electronic circuits for signal conditioning;
- ✓ Programming and optimization of the developed code;
- ✓ System testing for validation

This new transport system was simulated using the line model that predicts an increase of 28 m/s from the current maximum speed of 40 m/s, representing an increase of the production around 70%.

7.2. Future Work

There is still work to do for full implementation of the entire designed controller. In this section several suggestions of possible expansions are described:

- The EKF programming in another microcontroller and offline implementation in order to validate the estimated values;
- Implementation of all design controller;
- Implementation using an absolute position encoder;
- PCB design of the conditional signal circuits;
- Shaft design in order to get real measurements of the real torque and speed of the motor;
- Establish the communication system between the microcontroller and the automata system Siemens S7 for further integration of the system in the enterprise;
  Using the Ethernet capability of the XMC4500 Create an interface for online configuration of the controllers parameters
- Create microcontroller design with two levels of control, one platform dedicated to the motor control and another to the communications with the external system, system failures and errors that should communicate with each other;
- Development and simulation of the referred trigger system in section 6.9;
- The actual mechanical system can also be improved. In addition to the new transport system presented in this document, a new cut system can also be developed. The actual system is just able to cut in one direction, so the development of a new system with two knifes, that is able to cut forward and backward, would reduce the cut time.

References & Bibliography

[1]   E. Gebennini, A. Grassi, C. Secchi, and C. Fantuzzi, "An analytical model for automated packaging lines design," in *American Control Conference, 2008*, 2008, pp. 89-94.

[2]   "Ford's assembly line starts rolling — History.com This Day in History — 12/1/1913," *History* Retrieved 30 November 2011.

[3]   T. Chang Yan and C. K. W. Eric, "A simulation model for a 4 phase switched reluctance motor for PSIM," in *Power Electronics Systems and Applications (PESA), 2011 4th International Conference on*, 2011, pp. 1-5.

[4]   Bogdan M. Wilamowski, J. David Irwin, *Power electronics and motor drives* vol. 2nd ed. Boca Raton: CRC Press, 2011.

[5]   Y. Haisheng, H. Jun, and Z. Zongwei, "Position control of PMSM based on energy-shaping and MTPA principle," in *Intelligent Control and Automation, 2008. WCICA 2008. 7th World Congress on*, 2008, pp. 6532-6536.

[6]   J. Singh, B. Singh, S. P. Singh, and M. Naim, "Investigation of performance parameters of PMSM drives using DTC-SVPWM technique," in *Engineering and Systems (SCES), 2012 Students Conference on*, 2012, pp. 1-6.

[7]   Tiago Sá, "*Traction control in electric vehicles. Porto*", Master Dissertation, 2012.

[8]   (2012). *Field Oriented Control (FOC) of PMSM Motor with Encoder*.

[9]   R. Krishnan, *Electric motor drives: modeling, analysis and control*: Prentice Hall, 2011.

[10]   R. C. Garcia and J. O. P. Pinto, "Position control of a PMSM using a filterbank-ADALINE load torque estimator," in *Power Electronics Conference, 2009. COBEP '09. Brazilian*, 2009, pp. 1149-1154.

[11]   Tore M. Undeland, Ned Mohan, William P. Robbins, *Power Electronics*, 2° ed.

[12]   D. O. Neacsu, "SPACE VECTOR MODULATION –An Introduction," presented at the IECON2001, 2001.

[13]   José Ricardo S. Soares, "Traction Control for Hybrid Electric Vehicles," Master, FEUP.

[14]   D. Świerczyński, "Direct Torque Control with Space Vector Modulation (DTC-SVM) of Inverter-Fed Permanent Magnet Synchronous Motor Drive," WARSAW UNIVERSITY OF TECHNOLOGY, 2005.

[15]   a. F. N. M. S. Merzoug, "Comparison of Field-Oriented Control and Direct Torque Control for Permanent Magnet Synchronous Motor (PMSM)," *World Academy of Science, Engineering and Technology*, 2008.

[16]   Adriano Silva Carvalho, Carlos A. Martins, "Technological Trends in Induction Motor Electrical Drives," presented at the IEEE Porto Power Tech Conference, Porto.

[17]   D. Swierczynski and M. P. Kazmierkowski, "Direct torque control of permanent magnet synchronous motor (PMSM) using space vector modulation (DTC-SVM)-simulation and experimental results," in *IECON 02 [Industrial Electronics Society, IEEE 2002 28th Annual Conference of the]*, 2002, pp. 751-755 vol.1.

[18]   P. Hai-Ping and Y. Qing, "Robust LQR tracking control for a class of affine nonlinear uncertain systems," in *Control and Decision Conference (CCDC), 2012 24th Chinese*, 2012, pp. 1197-1202.

[19]   G. F. Franklin, J. D. Powell, and M. Workman, *Digital control of dynamic systems* vol. 3rd ed. Menlo Park, CA: Addison Wesley, 1997.

[20]   Z. Zedong, M. Fadel, and L. Yongdong, "High Performance PMSM Sensorless Control with Load Torque Observation," in *EUROCON, 2007. The International Conference on "Computer as a Tool"*, 2007, pp. 1851-1855.

[21]   D. Simon. (2011) Kalman Filtering. *Embedded Systems Programming*.

[22]   S. Praesomboon, S. Athaphaisal, S. Yimman, R. Boontawan, and K. Dejhan, "Sensorless speed control of DC servo motor using Kalman filter," in *Information, Communications and Signal Processing, 2009. ICICS 2009. 7th International Conference on*, 2009, pp. 1-5.

[23]   S. J. Julier and J. K. Uhlmann, "Unscented filtering and nonlinear estimation," *Proceedings of the IEEE,* vol. 92, pp. 401-422, 2004.

[24]   J. B. Rawlings, "Tutorial overview of model predictive control," *Control Systems, IEEE,* vol. 20, pp. 38-52, 2000.

[25]   P. E. Orukpe, "Basics of MPC",EBook, 2005.

[26]   G. G. A. J. S. SHELLEY GRETLEIN. (2006, DSPs, Microprocessors and FPGAs in Control.

[27]   P. Bishop. (2009, A tradeoff between microcontroller, DSP, FPGA and ASIC technologies.

[28]   M. d. M. Silva, *Introdução aos circuitos eléctricos e electrónicos*. Lisboa: Fundação Calouste Gulbenkian, 1996.

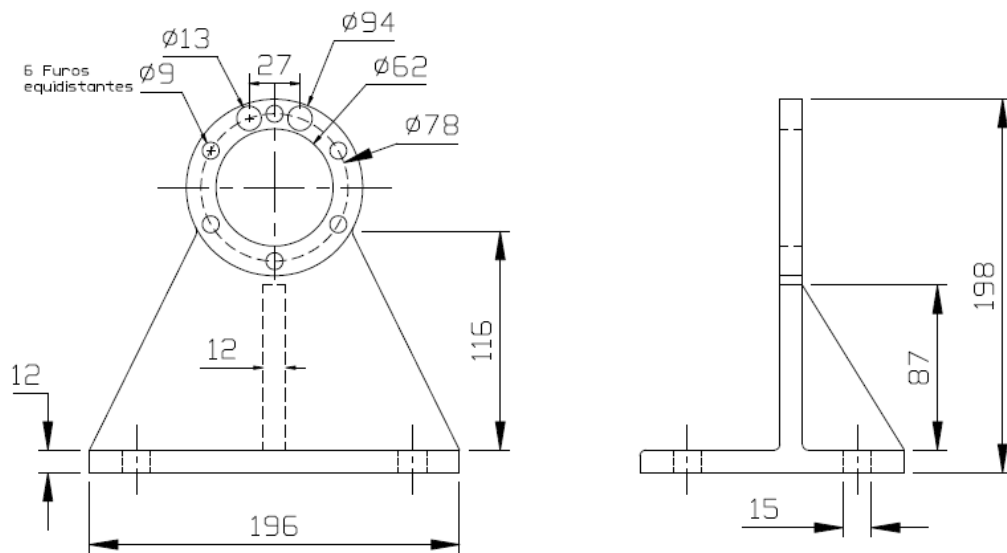# Appendix

I – Mechanical drawing of the support

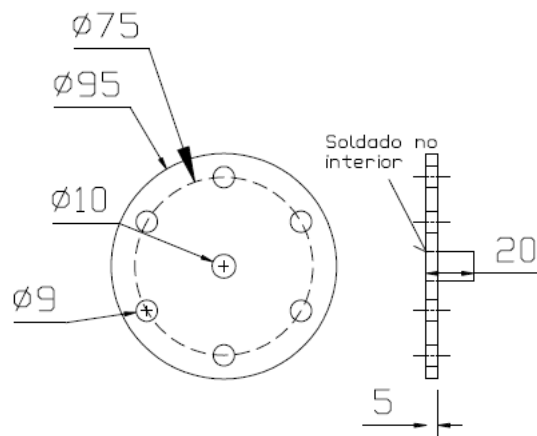**Figure 90 Mechanical dimensions of the designed mechanical support**

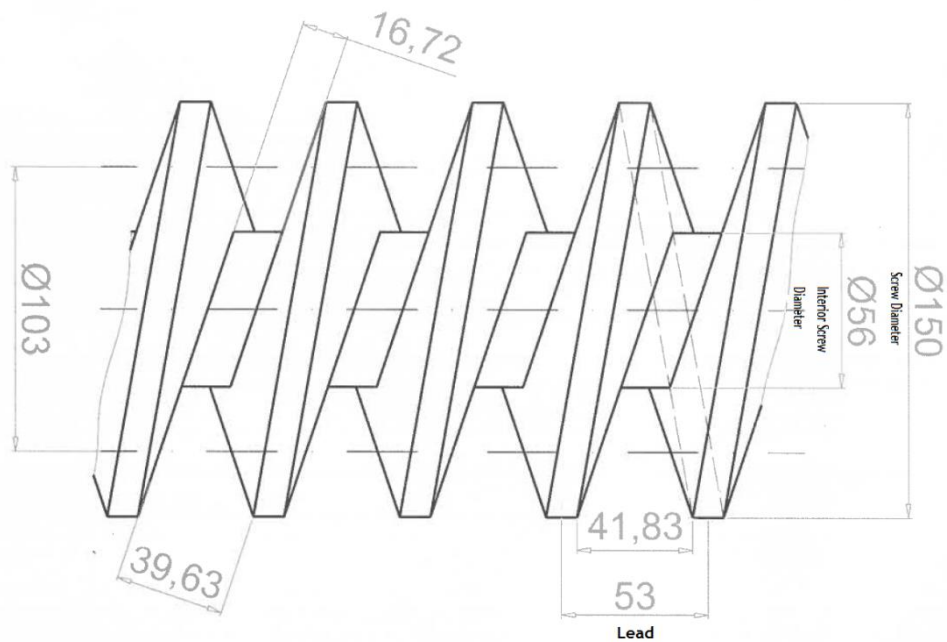**Figure 91 Frontal support for the encoder connection**

II – Mechanical Draw of the 150mm extruder screw

Figure 92 Screw from the extruder 150